NIST Technical Note
NIST TN 2341

Eave and Vent Experiments (EaVE)

Phase A

Christopher U. Brown
Alexander Maranghides
Shonali Nazare
Giovanni Di Cristina
D. Michelle Bailey
Lucy Fox
Eric D. Link
Selvarajah Ramesh
J. Houston Miller
Erin E. McCaughey
Monica M. Flores

This publication is available free of charge from:
https://doi.org/10.6028/NIST.TN.2341

NIST NATIONAL INSTITUTE OF STANDARDS AND TECHNOLOGY
U.S. DEPARTMENT OF COMMERCE

NIST Technical Note
NIST TN 2341

Eave and Vent Experiments (EaVE)

Phase A

Christopher U. Brown
Alexander Maranghides
Giovanni Di Cristina
Lucy Fox
Eric D. Link
Selvarajah Ramesh
Fire Research Division
Engineering Laboratory

D. Michelle Bailey
Chemical Sciences Division
Material Measurement Laboratory

Shonali Nazare
Directorate for Laboratory Sciences
U.S. Consumer Product Safety Commission

J. Houston Miller
Erin E. McCaughey
Monica M. Flores
Department of Chemistry
George Washington University

This publication is available free of charge from:
https://doi.org/10.6028/NIST.TN.2341

June 2025

U.S. Department of Commerce
Howard Lutnick, Secretary

National Institute of Standards and Technology
Craig Burkhardt, Acting Under Secretary of Commerce for Standards and Technology and Acting NIST Director

Certain equipment, instruments, software, or materials, commercial or non-commercial, are identified in this paper in order to specify the experimental procedure adequately. Such identification does not imply recommendation or endorsement of any product or service by NIST or CPSC, nor does it imply that the materials or equipment identified are necessarily the best available for the purpose.

The policy of the National Institute of Standards and Technology is to use metric units in all its published materials. Because this report is intended for the U.S. building construction industry, which uses inch-pound units, it is more practical and less confusing to use inch-pound units, in some cases, rather than metric units. However, in most cases, units are presented in both metric and the inch-pound system.

Another policy of the National Institute of Standards and Technology is to include statements of uncertainty with all NIST measurements. In this document, however, some measurements of authors outside of NIST are presented, for which uncertainties were not reported and are unknown.

The contribution to this report by the U.S. Consumer Product Safety Commission (CPSC) staff has not been reviewed or approved by, and may not represent the views of, the Commission.

NIST Technical Series Policies
Copyright, Use, and Licensing Statements
NIST Technical Series Publication Identifier Syntax

Publication History
Approved by the NIST Editorial Review Board on 2025-06-04

How to Cite this NIST Technical Series Publication
Brown CU, Maranghides A, Nazare S, Di Cristina G, Bailey DM, Fox L, Link ED, Ramesh S, Miller JH, McCaughey EE, Flores MM (2025) Eave and Vent Experiments (EaVE): Phase A. (National Institute of Standards and Technology, Gaithersburg, MD), NIST Technical Note (TN) NIST TN 2341. https://doi.org/10.6028/NIST.TN.2341

Author ORCID iDs
Christopher U. Brown: 0000-0002-0426-2249
Alexander Maranghides: 0000-0002-3545-2475
Shonali Nazare: 0000-0002-0407-5849
Giovanni Di Cristina Torres: 0000-0002-0799-3418
D. Michelle Bailey: 0000-0001-6273-3830
Lucy Fox: 0009-0004-7725-708X
Eric D. Link: 0000-0002-7784-5023
Selvarajah Ramesh: 0000-0002-9525-6767
J. Houston Miller: 0000-0002-6686-1976
Erin E. McCaughey: 0009-0004-3757-6238
Monica M. Flores: 0009-0003-1101-5961

Contact Information
christopher.brown@nist.gov

Abstract

This report documents a series of full-scale fire experiments conducted at the National Institute of Standards and Technology (NIST) to characterize the performance of select wildland-urban interface (WUI) eave vents exposed to fire from noncombustible steel sheds of different sizes and fuel loads (wood cribs). The experiments were conducted indoors under the 20 MW exhaust hood in the National Fire Research Laboratory (NFRL) with the noncombustible steel sheds at varying fuel loads and structure separation distances (SSDs) from the target structure. The target structure included an assembly of an exterior residential wall, a roof, and an eave vent. Experiments recorded a range of measurements including heat release rate (HRR), heat flux, temperature, gas flow velocity, and gas species concentration using open-path absorption spectroscopy. Video and infrared cameras recorded the experiments.

Experimental results show that thermal exposures from different types of sheds with different fuel loadings were very repeatable when quantified in terms of HRR, heat fluxes and temperatures measured at the eaves. In the case of thermal exposures from the noncombustible steel sheds, ignition of the eaves was a function of flame jetting from the door opening and sustained incident peak heat flux at the eaves. Higher fuel packing density in the shed resulted in focused flame jetting and increased the likelihood of an eave ignition. The same fuel loading in different types of sheds resulted in different thermal exposures on the target structure. Thermal exposures to the target structure increased linearly with the fuel mass, however, the eave ignition was a function of flame jetting. Eave ignition started with glowing ignition in thermally vulnerable locations including sharp edges, corners, and joints of the rafters.

The experimental series assessed the performance of three commercially available fire-resistant eave vents subjected to much larger fire exposures (1.5 MW to 2.5 MW) compared to the fire exposure (300 kW) specified in the existing ASTM test methods. The vent performance relates primarily to flame penetration and temperature rise on the unexposed side of the vent. Amongst the commercially available vents tested in this experimental series, the performance of the intumescent-coated baffle vents was superior to the intumescent-coated honeycomb core vents during very high thermal exposures. Intumescent-coated honeycomb core vents that comply with ASTM E2886 are listed as WUI-compliant products but failed to prevent flame penetration when exposed to large thermal exposures, particularly when eave ignition occurs.

The current standardized eave vent test method (ASTM E2886) may not adequately expose the eave vents to real WUI fire exposures. The knowledge generated from this experimental series will inform voluntary standards committees as they consider revisions to existing test methods for evaluating vents suitable for use in WUI construction. Additionally, the exposure quantification data generated from this experimental series will be useful for hazard mitigation and reducing structure ignitions from large thermal exposures and in managing thermal exposures from auxiliary fuels and other exposures, particularly in WUI communities.

Keywords

absorption spectroscopy; auxiliary structures; community fire spread; convective heat exposure; eaves; eave vents; fire; gas flow velocity; gas species concentration; heat flux measurements; heat release rate; modeling; open-path absorption spectroscopy; radiant heat exposure; sheds; temperature measurements; vents; wildfire; wildland fire; wildland-urban interface; WUI

Table of Contents

List of Tables

List of Figures

1. Introduction

1.1. Prior Experimental Series

The experiments outlined in this report are part of a series of experiments related to structure-to-structure fire spread wildland-urban interface (WUI) communities.

A series of indoor experiments without wind was conducted as part of the National Institute of Standards and Technology (NIST) Indoor Structure Separation Experiments (NISSE) series [1,2]. Full-scale shed burn experiments were conducted at the National Fire Research Laboratory (NFRL) at the NIST and at the Insurance Institute for Business & Home Safety (IBHS) with various types of source structures used to generate typical radiative and convective heat exposures to target structures that simulated a residential exterior wall. The spacing between the source and target structures was varied to identify structure separation distances (SSD). Heat release rate, mass loss rate, and heat fluxes were also measured.

The results of these experiments suggested that the radiant heat and flames from both combustible wooden sheds and noncombustible steel sheds could ignite the target structure. While the noncombustible steel shed did not burn, the flames jetting from the burning contents of the steel shed could ignite the target structure. Fire spread on the roof and within the attic space due to ignition of the eaves was evident even with low fuel loadings and in the absence of wind.

Following the NISSE experiments, Phase 1 experiments continued with the NIST Outdoor Structure Separation Experiments (NOSSE) [3,4]. The primary objective of these full-scale outdoor experiments was to study the effects of wind on fire spread and to identify safe SSDs needed to prevent fire spread in WUI communities. These experiments were conducted in an artificially generated wind field. Varying sizes of source structures (sheds) with varying fuel loadings (wood cribs) were used to generate typical radiative and convective heat exposures to the target structure: an assembly of a single-story residential building exterior wall with a window and roof.

This series resulted in the quantification of the minimum SSD between a shed and a primary residence under the experimental conditions. The minimum SSD was identified as 3 m (10 ft) for both combustible and noncombustible sheds with floor area less than 2.4 m^2 (26 ft^2) in scenarios with a fire-hardened target structure. For sheds with floor area between 2.4 m^2 (26 ft^2) and 5.9 m^2 (64 ft^2), the minimum SSD was found to be 4.6 m (15 ft). Since the direction and speed of local winds during a WUI fire are unpredictable, SSD should be the same in all directions.

The focus of this current series is on assessing the failure of eave vents observed during the previous indoor and outdoor experiments. This experimental series is referred to as “EAVEs Phase A.” Following the completion of EAVEs Phase A, additional experiments (EAVEs Phase B) will assess the performance of other commercially available eave vents with different operating mechanisms. The final series will be EAVEs Phase C experiments that will aim to develop

recommendations to revise the ASTM E2886 test method [5] for eave vents or to propose a new test method.

1.2. Vents for WUI Fire Resistant Construction

A number of building codes for application in WUI locations include provisions for ember and flame-resistant vents, including the International Wildland-Urban Interface Code (IWUIC) Sec 504.10.1 and 505.10.1 [6], California Building Code (CBC) Chapter 7A Section 706A.2 [7], NFPA 1140 Section 25.3.3 Standard for Wildland Fire Protection [8], and AS 3959 Construction of buildings in bushfire-prone areas [9]. A vent must resist intrusion of flame or embers through the opening when tested in accordance with ASTM E2886, resulting in no flaming during the ember or flame intrusion tests, and the unexposed side must remain below 350 °C. Certain local and state jurisdictions in the U.S. have adopted these provisions in locations where their WUI building code applies. The Australian standard only requires steel or bronze mesh no greater than 2 mm.

The first edition of the International Wildland-Urban Interface Code (IWUIC) was published in 2003 and was based on the data collected from tests and fire incidents, technical reports, and mitigation strategies from around the world. Sections 504.10 and 505.10 of the IWUIC limit the total area of exterior ventilation openings and stipulate that vents shall be covered with noncombustible mesh with openings less than 6.4 mm (1/4 in) or shall be designed and approved to prevent flame and ember penetration. In 2024, these sections expanded to include performance criteria based on the maximum temperature (shall not exceed 350 °C) on the unexposed side of the vent. Section 706A of the CBC stipulates that ventilation openings shall "resist building ignition from the intrusion of burning embers and flame through the ventilation openings." The California code states that vents must be approved and listed by the State Fire Marshal, or tested to ASTM E2886 and listed if they pass both ember and flame intrusion tests, and the maximum temperature on the unexposed side of the test does not exceed 350 °C.

1.3. Existing Test Methods for Assessing Performance of Vents to Resist Ember and Flame Exposures

The IWUIC [6] and California Building Code, Chapter 7A [7] refer to ASTM E2886 (Standard Test Method for Evaluating the Ability of Exterior Vents to Resist the Entry of Embers and Direct Flame Impingement) [5], which describes the test methods to assess structural integrity and performance of vents when exposed to ember and direct flame contact. The test method is applicable to gable end, crawl space (foundation) and other vents that mount on a vertical wall or in the under-eave area. The test methods described in ASTM E2886 evaluate the response of vents when subjected to ember showers and burner flames under controlled conditions. The vents are exposed to a simulated ember shower for approximately 3 min and to a direct flaming ignition source (with a heat release rate of 300 kW ± 10 kW) for 10 min. The test method also allows for longer exposure periods for more stringent testing.

Embers are generated by burning ten Class C brands (ASTM E108 [10]/UL 790 [11]; approximately 90 g) and agitating burning embers against steel nuts and steel rods placed along

the perimeter of the tumbler. The embers fall vertically on the horizontally mounted vent specimen. Air is pulled through the vents to generate negative air pressure to suck the embers or the flames through the vent. Vents are exposed to embers for 3 min or until all the embers in the tumbler are extracted by the exhaust fan. Smoldering and/or flaming ignition of cotton batting that is used as a combustible target under the vent is reported for the ember intrusion test. Failure of a test specimen is reported when sustained smoldering and/or flaming ignition of cotton batting is observed due to ember intrusion.

The ASTM E2886 [5] refers to the ASTM E2912 (Standard Test Method for Fire Test of Non-Mechanical Fire Dampers Used in Vented Construction) [12] for the test apparatus and test procedure for assessing flame intrusion performance of the vents. The square gas burner used for the direct flame impingement test is similar to the one described in the ASTM E2257 (Standard Test Method for Room Fire Test of Wall and Ceiling Materials and Assemblies) [13] and is designed to simulate exterior fire sources including burning wood piles or ornamental vegetation, or both. The distance between the test specimen (vent) and the fire source (gas burner) was set to address likely exposure of exterior vents to flaming combustion of nearby combustibles. Two likely scenarios considered were: (1) Exterior vents located near storage areas where combustibles are stacked, such as wood piles, and (2) Exterior vents in contact with landscaping (vegetation or forestation, or both). In many cases, these combustible items are just inches from the vent, which is open to allow airflow, and are subject to sudden direct flame impingement.

The ASTM E2912 [12] standard describes test methods for both vertically and horizontally mounted vents. A test box is used to house a vent specimen in a vertical orientation. The pressure within the test box is slightly positive based on the convective heat flow, as in most real-life fire scenarios. Positive pressure is a more severe condition than negative pressure when assessing insulation and integrity of the test specimens. The test specimen is assessed for flame penetration and insulation performance. No flame penetration or flaming ignition of cotton batting (placed on the unexposed side of the vent) shall occur for the test specimen to pass the test. To pass the criteria of insulation, the maximum temperature rise on the unexposed side of the vent shall not exceed 350 °C. The rationale for this particular temperature is based on the fact that it represents the lowest hot-surface ignition temperature of any goods which may be permissibly stored in residential buildings. Section 706A of California Building Code, Chapter 7A [7] and the IWUIC [6] are similar to ASTM E2912 requiring the maximum temperature on the unexposed side of the vent to remain below 350°C.

The State Fire Marshal (SFM) testing standards described in the California Reference Standard Code Part 2 [7] have requirements that were developed based on the knowledge gained from several post-WUI fire studies. It is noted that standard test methods, e.g., ASTM E119 [14], using controlled gas-fired furnaces to assess the fire resistance of building components, do not ensure their performance when exposed to sudden direct flame impingement or ember exposure under radiant heating conditions. Most SFM standards are modified and designed to capture direct flame exposures.

The existing test methods for assessing the performance of vents use thermal exposures that are significantly lower than the exposures from burning auxiliary structures. Previous

experiments indicated that the thermal exposures from residential storage sheds can exceed 1 MW, depending on the type, size, and fuel loading of the shed. The experimental series documented in this report addressed the thermal exposure from residential storage sheds.

1.4. Objective

Previous experiments conducted to evaluate a safe SSD between an auxiliary structure (i.e., small storage shed) and a residential structure highlighted the vulnerability of eave vents when exposed to such flame and ember sources [2,4]. The objective of these current experiments is to characterize the performance of flame and ember resistant vents that are listed as building materials approved to be used in WUI residential constructions (e.g., California Building Code Chapter 7A, hereafter referred to simply as Chapter 7A) when exposed to flames from a burning auxiliary structure. The auxiliary structures considered in this experimental series are storage sheds used in residential settings.

While the experimental set up for this series is similar to prior experiments, i.e., burning from sheds as the source fire and an exterior wall assembly as the target structure, the primary focus of these experiments is to study the failure of the eave vent rather than ignition of the target structure and identification of SSD.

2. Experiment Specifications

A target wall, representing the exterior façade of a residential structure in a WUI setting, was exposed to flames and embers. The source fire comprised commercially available noncombustible steel sheds of varying sizes commonly used on residential parcels for storage of various goods. The sheds were loaded with wood cribs and burned under the 20 MW calorimeter hood in the NFRL in quiescent conditions. The following sections describe the physical configuration, the specifications of the target wall and source structure, and the various measurements and instrumentation used to quantify the experiments.

2.1. Configuration

The experimental layout is shown in Fig. 1 below. Primary components include the target wall, representing the exterior of a residential structure, and a storage shed loaded with wood cribs, representing a commonly occurring fire spread scenario and exposure source in WUI fires.

The peak of the roof of the target structure was centered under the hood. The sheds were centered to the target wall as shown in Fig. 1, or placed against the target wall depending on the shed style. Doors were kept open in all the experiments, representing a worst-case exposure scenario and to avoid changes in burning behavior due to varying ventilation conditions.

Measurement and data acquisition equipment was installed on the target wall. Additional optical measurements using laser spectroscopy were configured in the eaves and in the attic space behind the target wall. Laser measurements are further described in Sec. 2.4.7.

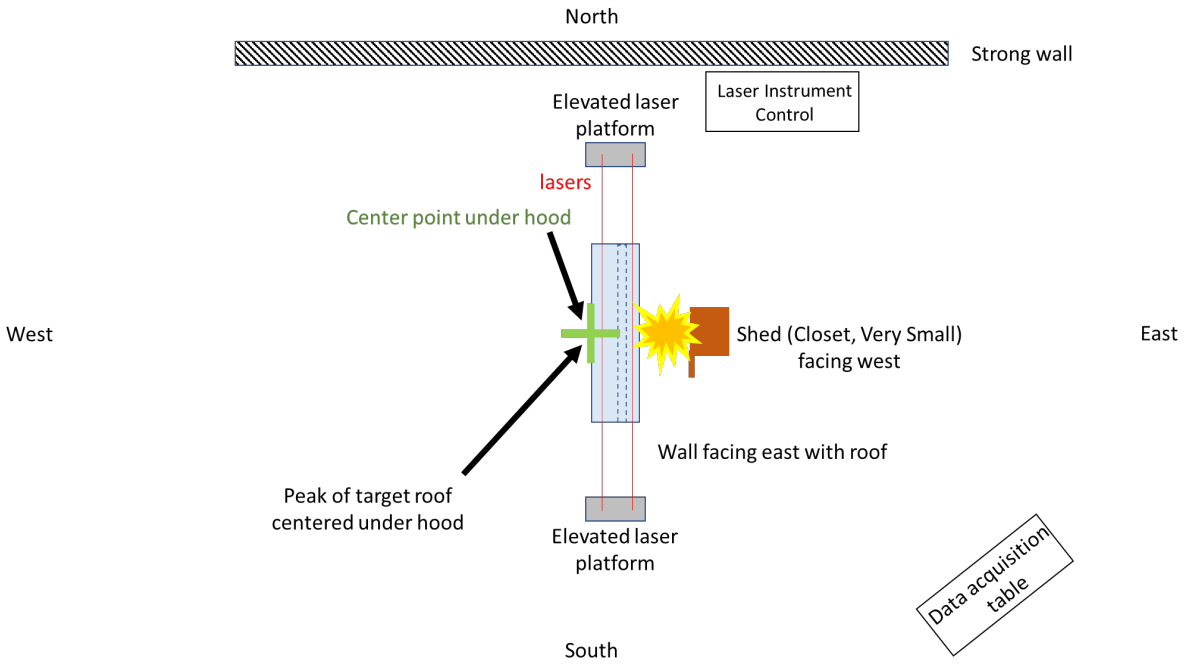

Fig. 1. Plan view of the experiment layout under the 20 MW exhaust hood in the NFRL (figure not to scale).

2.2. Target Structure

The target structure used in this experimental series was similar to those constructed previously [2] to represent the façade of a single-story residence. The target structure included a roof-wall assembly with open eaves and a vented attic space. The window was not included in the target structure for this experimental series to avoid complexities arising from window failures prior to eave ignition.

An eave vent approved for use in WUI locations was installed in the eaves. The target structure was oriented north/south under the exhaust hood with the exterior side of the structure facing east. The door opening of the shed faced west (as shown in Fig. 1) or south depending on the shed style.

2.2.1. Wall

The target wall was constructed as designed in the pre-experiment test plan [15] and similar to previous experiments [2, 4], except without a window. The materials used in the construction of wall and roof are shown in Fig. 2. The wall was over-hardened per Chapter 7A requirements to prevent ignition of the wall before the eaves, and to minimize the need to rebuild the target structure between experiments. The wall was approximately 4 m (13 ft) tall and 4.9 m (16 ft) wide and was framed with nominal 2-in by 4-in wood studs, approximately 41 cm (16 in) on center. Each stud bay was therefore 36.8 cm (14.5 in) wide between the studs. The exterior layer of the wall (cladding) was fiber cement siding with a nominal thickness of 8 mm (5/16 in), the middle layer was noncombustible drywall with a nominal thickness of 16 mm (5/8 in), and an interior layer of oriented strand board (OSB) with a nominal thickness of 11 mm (7/16 in) was attached to the wood studs. Fiberglass insulation approximately 9 cm (3.5 in) thick was inserted between the studs. Drywall was also used on the “interior” unexposed side of the studs to cover the insulation.

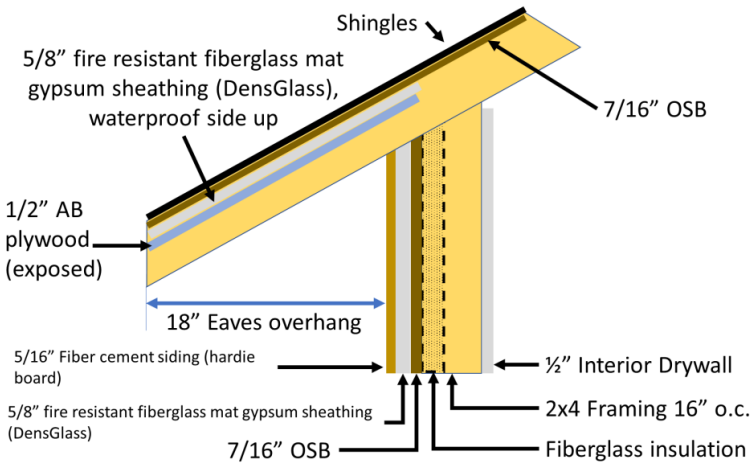

Fig. 2. Target wall construction details with roof overhang (figure not to scale) [15].

The height of the eaves was approximately 4 m (13 ft) from the ground. The overall height of the target structure was approximately 4.6 m (15 ft) from the ground to the peak of the roof (Fig. 3). A window was not used in the target structure assembly to focus on assessing the performance of the eaves and vent.

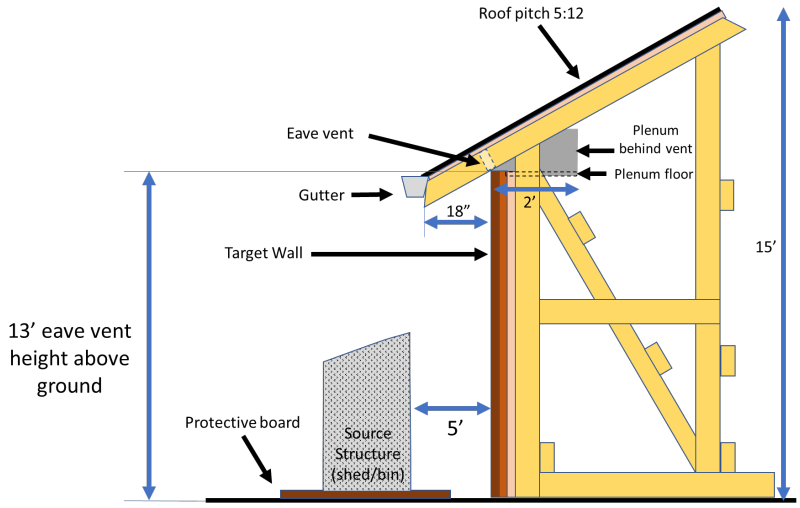

Fig. 3. The target structure with roof, wall, and eave plenum, and source structure (figure not to scale) [15].

2.2.2. Roof

The roof was built in compliance with Chapter 7A requirements [7]. The roof measured approximately 1.8 m (6 ft) from the attached aluminum gutter to the peak and had an approximate pitch of 5:12. It was covered in asphalt shingles and had an open eave configuration. The wood rafters measured approximately 61 cm (24 in) on center so that each rafter bay was approximately 57.2 cm (22.5 in) wide. The roof overhang from the wall was 46 cm (18 in). Aluminum flashing was installed along the drip edge of the roof under the attached gutter.

2.2.3. Eave Vents

Three commercially available eave vents were tested in this series. Each vent conformed to Chapter 7A [7] requirements and met the ASTM E2886 [5] standard for use in WUI construction. Vents were installed in the center rafter bay with nominal dimensions reported in Table 1.

Vent A was an intumescent-coated metal honeycomb matrix (nominal 5 mm (0.2 in) matrix spacing) between metal mesh screens (nominal 1.6 mm (1/16 in) interior mesh screen and nominal 6.4 mm (1/4 in) exterior mesh screen). This vent was observed to perform poorly when exposed to larger thermal exposures during previous experiments [2, 4] and was specifically selected to explore its performance in more detail. Vent B was similar to Vent A, but the

exterior metal mesh screen was different (Vent B had a nominal 3.2 mm (1/8 in) exterior mesh screen). Vent C used intumescent-coated baffles with a metal mesh screen on the interior side of the vent to prevent ember intrusion (nominal 1.6 mm (1/16 in) screen size). Table 1 lists descriptions of each vent type. Fire-resistant caulking was applied around each vent from the exterior side, as per standard installation practice.

Table 1. Eave vent descriptions.

Vent ID	Activation Mechanism	Exterior Mesh	Interior Mesh	Dimensions, cm (in)
A	Intumescent honeycomb	Yes	Yes	19 × 56 (7.5 × 22)
B	Intumescent honeycomb	Yes	Yes	19 × 56 (7.5 × 22)
C	Intumescent slots with baffles	No	Yes	14 x 56 (5.5 x 22)

A plenum was constructed behind the vent on the attic side of the central rafter bay of the target structure, similar to the one used during the NISSE series [2]. The plenum was made of drywall along the sides and the floor that extended approximately 60 cm (24 in) back from the vent on the attic side (Fig. 4).

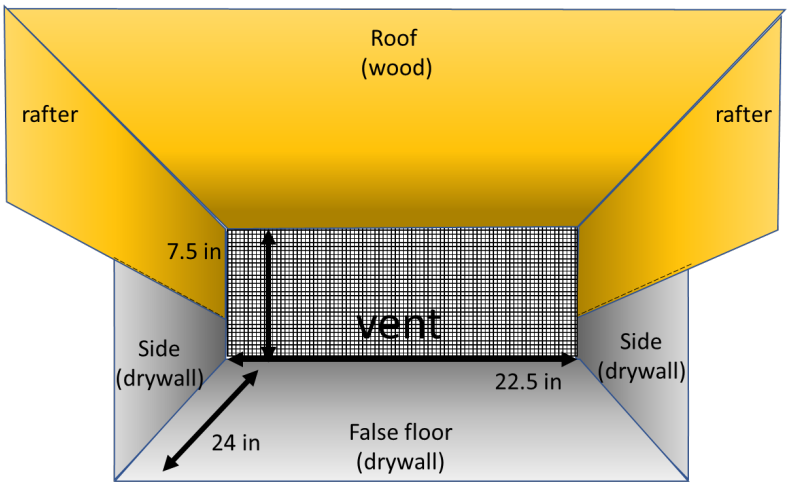

Fig. 4. The eave vent plenum view from the attic side of the vent (figure not to scale) [15].

2.3. Exposure Source

2.3.1. Source Structure

Commercially available noncombustible steel sheds were used as source structures for all experiments. Steel sheds were chosen for this series because previous experiments showed that the structural integrity of the noncombustible steel sheds remained intact, producing a

flame jet that could be aimed towards the eave vent throughout the burn. Additionally, the results from the outdoor experimental series that assessed the effect of wind on the burning behavior of sheds suggested that the flame jetting from the noncombustible steel sheds was not impacted by wind [4].

Three styles of shed were used, including:

Closet (C) — the smallest size used, intended for storing trash cans,

Very Small (VS) — a traditional shed design with a single door and peaked roof, noted as Very Small (VS) in previous experiments [1-4] (named for its relative size compared to other commercially available sheds), and

Narrow (N) — a shed with a longer side and a single sloped roof designed to fit against an exterior wall of a residence.

Doors were propped fully open during the experiments, representing realistic worst-case scenarios if doors were left open or blown open during a WUI fire. Moreover, a fully open-door configuration would minimize complexities arising from reduced ventilation. The ventilation conditions significantly affect the fire hazard, such as HRR, fire growth rate, smoke, and CO production. Closed doors would significantly alter HRR and present a less critical scenario. Shed dimensions are listed in Table 2 and illustrated in Fig. 5.

The Closet and Very Small sheds were positioned so that their doorway was centered relative to the target structure and facing the target structure with a 1.5 m (5 ft) SSD such that the flame from the shed impinged on the vent. The Narrow sheds were positioned against the target structure with a 0 m SSD, with the shed door facing 90° to the target structure (open door facing south). Preliminary experiments to characterize the burning behavior of the Narrow sheds determined that the front face of the Narrow sheds should be offset 1.2 m (4 ft) towards the north so that the flame jet was aligned with the eave vent.

Table 2. Steel shed specifications (1 ft = 0.305 m, 1 lb = 0.45 kg).

		Dimensions		Door			
Shed Style	**Image**	**D × W × H (ft)**	**V (ft^3)**	**w × h (ft)**	**a (ft^2)**	**Weight (lb)**	**Notes**
Closet (C)		3 × 6 × 4	66	4.8 × 4	19	77	Double door and lid Vents: No
Very Small (VS)		5 × 6 × 6	141	2.6 × 5	13.5	107	Single door Vents: 4 gable vents
Narrow (N)		6.5 × 4 × 5	154	3 × 5	16	125	Double door Vents: No

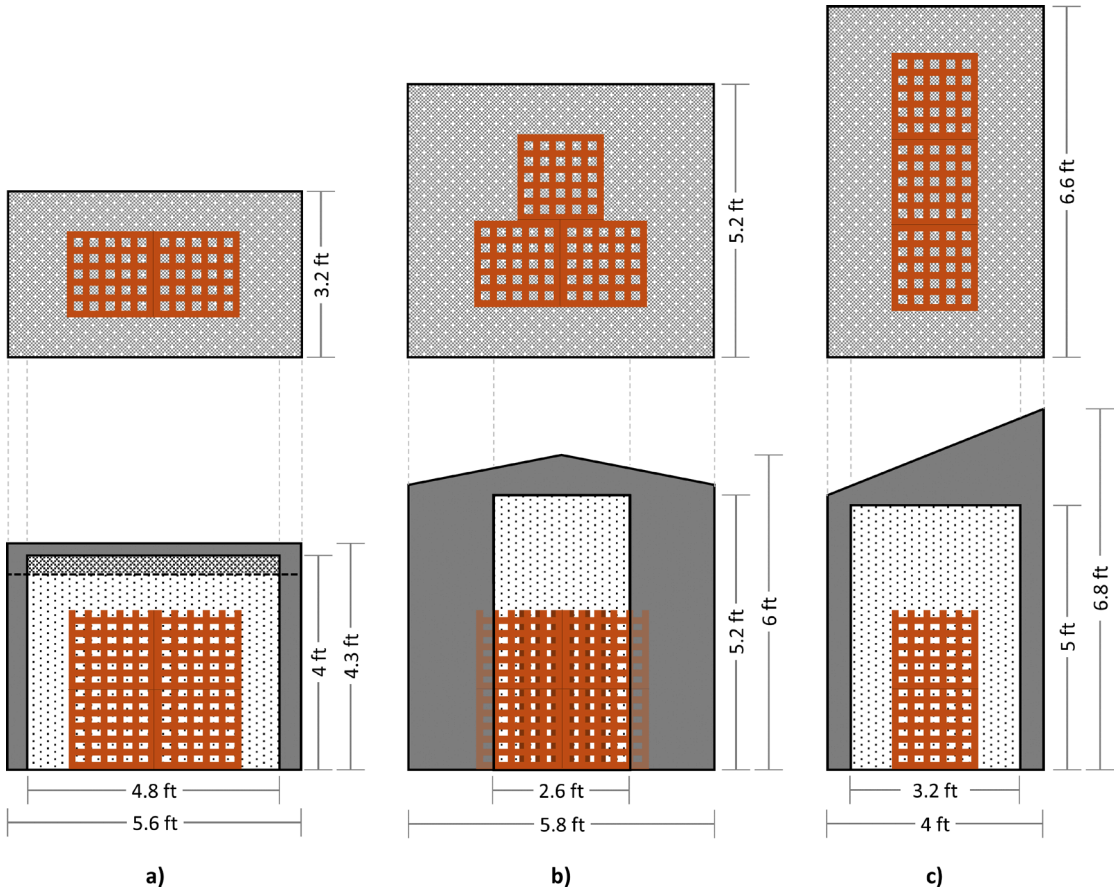

Fig. 5. The Closet (a), Very Small (b), and Narrow (c) shed designs showing dimensions, door configurations, and maximum fuel loadings. Plan view (top) and elevation view (bottom).

2.3.2. Fuel Loading

Pine wood cribs based on the UL 711 design [16] were used as fuel for these experiments. Size 1-A cribs were used, consisting of 12 layers of six members each with approximate dimensions of 38 mm × 38 mm × 500 mm (1.5 in × 1.5 in × 20 in) and 54 mm (2.1 in) between two members. The overall dimensions of the cribs were approximately 500 mm × 500 mm × 456 mm (19.7 in × 19.7 in × 18 in). The average mass of a 1-A crib was 21.6 kg ± 2.7 kg (see Appendix A for a description of measurement uncertainties). The moisture content of the cribs varied between 4 % and 12 %.

The amount of fire exposure to the target structure was varied by changing the number of cribs used in each shed. Figure 5 illustrates the maximum fuel loading and typical configuration in each shed type. Closet sheds had a fuel loading of either two cribs (low fuel loading; both cribs on the floor), three cribs (medium fuel loading; one crib centered on top of the two cribs on the floor), or four cribs (high fuel loading; two stacks of two cribs). Very Small sheds used either

four cribs (low) or six cribs (high). Narrow sheds had either two cribs (low; one crib stacked on the other), three cribs (intermediate; one crib behind two stacked cribs), four cribs (medium; two stacks of two), or six cribs (high fuel; three stacks of two).

2.3.3. Fuel Ignition

The wood cribs inside the source sheds were ignited using 300 mL of heptane in an aluminum pan of nominal dimensions 90 mm × 130 mm × 30 mm (7.5 in × 5 in × 1.25 in). This method of wood crib ignition is known to be reproducible [17]. The heptane in the aluminum pan was ignited using a hand-held propane tank and wand.

2.4. Data Acquisition

Measurements included heat flux, temperature, fire-induced gas flow velocity, heat release rate, and gas species concentrations. Additionally, burning behavior was recorded with standard and infrared cameras.

2.4.1. Heat Flux Gauges

Six water-cooled Schmidt-Boelter heat flux transducers were installed in the eaves, as illustrated in Fig. 6, to measure the combined radiative and convective heat flux (HF) at the target wall. Three gauges faced the source structure from the eave boxing in the bay between rafters (Gauges 1, 3, and 5). These gauge faces were mounted flush with the vertical surface of the wood. Three gauges faced down from within the underside of the roof overhang (Gauges 2, 4, and 6). These gauge faces were flush with the slope of the roof, not perpendicular to the ground. No heat flux gauges were in the center bay of the eaves where the vent was located.

Table **3** lists the specific locations and orientations of each gauge.

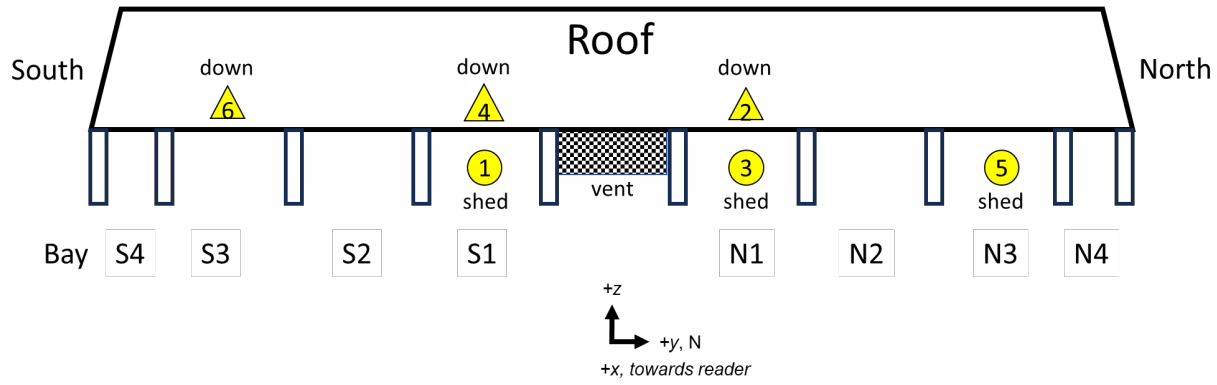

Fig. 6. Locations of the six heat flux gauges in the eaves. Gauges 1, 3 and 5 faced the source structure from the eave bays while Gauges 2, 4 and 6 faced down towards the source structure from the underside of the roof overhang (figure not to scale).

Table 3. Heat flux gauge locations relative to the bottom center of the target wall.

Device	ID	X, cm (East +)	Y, cm (North +)	Z, cm (Up +)	Orientation
Heat Flux Gauge 1	HF1	0	-61	406	Facing shed horizontally
Heat Flux Gauge 2	HF2	30	61	406	Facing shed down
Heat Flux Gauge 3	HF3	0	61	406	Facing shed horizontally
Heat Flux Gauge 4	HF4	30	-61	406	Facing shed down
Heat Flux Gauge 5	HF5	0	183	406	Facing shed horizontally
Heat Flux Gauge 6	HF6	30	-183	406	Facing shed down

2.4.2. Thermocouples

Type K, bare bead, 24 American Wire Gauge (AWG) thermocouples (TC) with a temperature range up to 1250 °C with a standard relative uncertainty value of ± 0.75 %, as reported by the manufacturer, were used for these experiments. A total of 16 thermocouples were installed in the test configuration. Table 4 lists the exact location and orientation of each thermocouple.

Three TCs monitored the performance of the eave vent. Two thermocouples measured air temperatures at the vent; one was centered on the exposed side of the vent (ETC) and one was centered on the attic side of the vent (ATC). One thermocouple on the attic side of the vent measured the temperature of the plywood roof above the vent (PTC). Neither the ETC nor ATC touched the vent itself.

Additionally, thermocouples were used to measure local air temperature in concert with bi-directional probes on the target wall and at the vent to support air flow calculations (10 probes). Ambient reference temperatures were measured at the elevated launch and collection laser instruments, positioned north (LTCN) and south (LTCS) of the target wall. One thermocouple placed near the pressure transducer instrumentation (MTC) measured the temperature to avoid exposing the instruments to high temperatures.

Table 4. Thermocouple locations relative to the bottom center of the target wall.

Device	ID	X, cm (East +)	Y, cm (North +)	Z, cm (Up +)	Orientation
Eave TC 0	ETC	2	0	406	Eave side, front of vent, center
Attic TC 1	ATC	-5	0	406	Attic side, back of vent, center
Plywood TC 2	PTC	-11	0	427	Attic side, plywood, center top of plenum
Laser TC N	LTCN	15	350	416	North side at laser
Laser TC S	LTCS	15	-350	416	South side at laser
Pressure TC	MTC	-61	244	122	Pressure transducer instruments
Vent TC 1	VTC1	-30	15.2	416	Accompany bi-dir. probe at vent north
Vent TC 2	VTC2	-30	0	416	Accompany bi-dir. probe at vent center

Vent TC 3	VTC3	-30	-15.2	416	Accompany bi-dir. probe at vent south
Wall TC 1	WTC1	5.7	-213	91	Accompany bi-dir. probe at front of wall
Wall TC 2	WTC2	5.7	213	91	Accompany bi-dir. probe at front of wall
Wall TC 3	WTC3	5.7	-213	208	Accompany bi-dir. probe at front of wall
Wall TC 4	WTC4	5.7	213	208	Accompany bi-dir. probe at front of wall
Wall TC 5	WTC5	5.7	-213	304	Accompany bi-dir. probe at front of wall
Wall TC 6	WTC6	5.7	213	304	Accompany bi-dir. probe at front of wall
Wall TC 7	WTC7	5.7	0	208	Accompany bi-dir. probe at front of wall

2.4.3. Bi-Directional Probes

Bi-directional probes were used to measure the fire-induced gas flow velocity along the target wall and through the eave vent, positioned as listed in Table 5. Seven bi-directional probes were located on the wall as shown in Fig. 7; three probes each on the north (WBD2, WBD4, WBD6) and south (WBD1, WBD3, WBD5) edges of the target wall, and one probe in the middle of the wall (WBD7). Additionally, three probes were placed on the attic side of the wall behind the vent (VBD1, VBD2, VBD3) to measure the flow through the vent. A thermocouple accompanied each bi-directional probe to determine local air density.

Three S-type pitot probes (S-probes) were paired with the bi-directional probes across the middle of the target wall (SPB1, SPB2, SPB3). The nominal uncertainty for the bi-directional and S-probes is 4 % and 2 %, respectively [18].

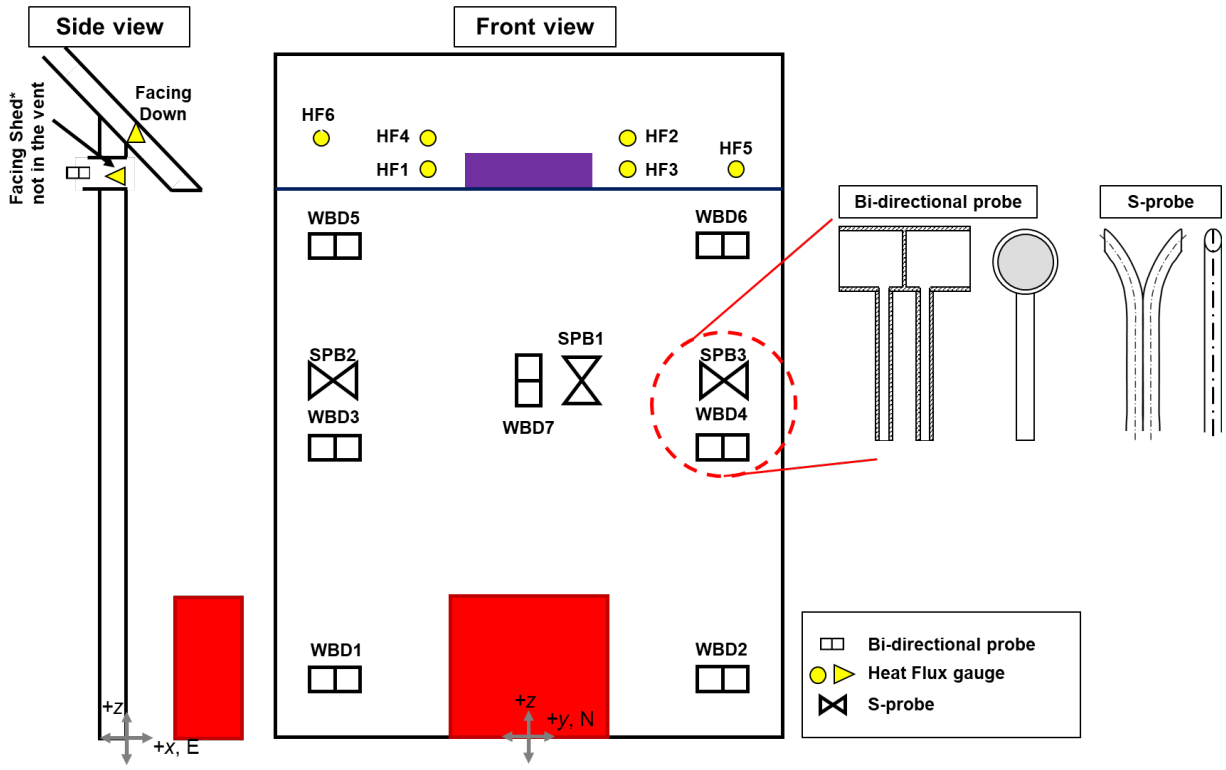

Fig. 7. The heat flux gauge, bi-directional probe, and thermocouple locations on the front face (exposed side) of the target structure (figure not to scale).

Table 5. Bi-directional probe locations relative to the bottom center of the target wall.

Device	ID	X, cm (East +)	Y, cm (North +)	Z, cm (Up +)	Orientation
Vent Bi-Dir 1	VBD1	-30	15.2	416	Horizontal (east-west)
Vent Bi-Dir 2	VBD2	-30	0	416	Horizontal (east-west)
Vent Bi-Dir 3	VBD3	-30	-15.2	416	Horizontal (east-west)
Wall Bi-Dir 1	WBD1	5.7	-213	91	Horizontal (north-south)
Wall Bi-Dir 2	WBD2	5.7	213	91	Horizontal (north-south)
Wall Bi-Dir 3	WBD3	5.7	-213	208	Horizontal (north-south)
Wall Bi-Dir 4	WBD4	5.7	213	208	Horizontal (north-south)
Wall Bi-Dir 5	WBD5	5.7	-213	304	Horizontal (north-south)
Wall Bi-Dir 6	WBD6	5.7	213	304	Horizontal (north-south)
Wall Bi-Dir 7	WBD7	5.7	0	208	Vertical (up-down)
S-Probe 1	SPB1	12	0	208	Same orientation as WBD7
S-Probe 2	SPB2	12	-213	208	Same orientation as WBD3
S-Probe 3	SPB3	12	213	208	Same orientation as WBD4

2.4.4. Heat Release Rate

The 13.7 m × 15.2 m (45 ft × 50 ft) calorimeter with maximum fire capacity of 20 MW in the NFRL was used to measure heat release rate using oxygen consumption calorimetry. The average expanded uncertainty in the normal operating range for the calorimeter for generic combustible fuel and near-steady-state fires is 9.8 %. Transient events (less than 30 s) may have larger uncertainty because of system response time. Detailed information on the NFRL calorimetry measurement system is provided by Bryant and Bundy [19]. Verification (confirmation) of the oxygen consumption calorimetry, using fuel consumption calorimetry as a reference, was conducted immediately prior to these experiments using a calibrated gas burner (Appendix B). The heat release rate data and videos from the current experiments are published in the NIST Fire Calorimetry Database (FCD) [20].

2.4.5. Video Cameras

Seven video cameras recorded the experiments, positioned as shown in the schematic in Fig. 8. One video camera faced the experiment directly from the front (camera 1 facing west), one from the front diagonal position (camera 2 facing northwest), and one from the side of the target wall mounted to a support beam (camera 3 facing north). Camera 4 was mounted to an elevated platform behind the target structure (facing east). Cameras 5, 6 and 7 were mounted to the walls in the NFRL.

2.4.6. Infrared Cameras

A high-speed mid-wavelength infrared camera (model number FLIR SC8300HD) was mounted on an elevated platform behind the target structure (facing east) to record thermal images for qualitative monitoring. It was focused to capture the thermal image of the attic side of the vent. Its position is also indicated in Fig. 8.

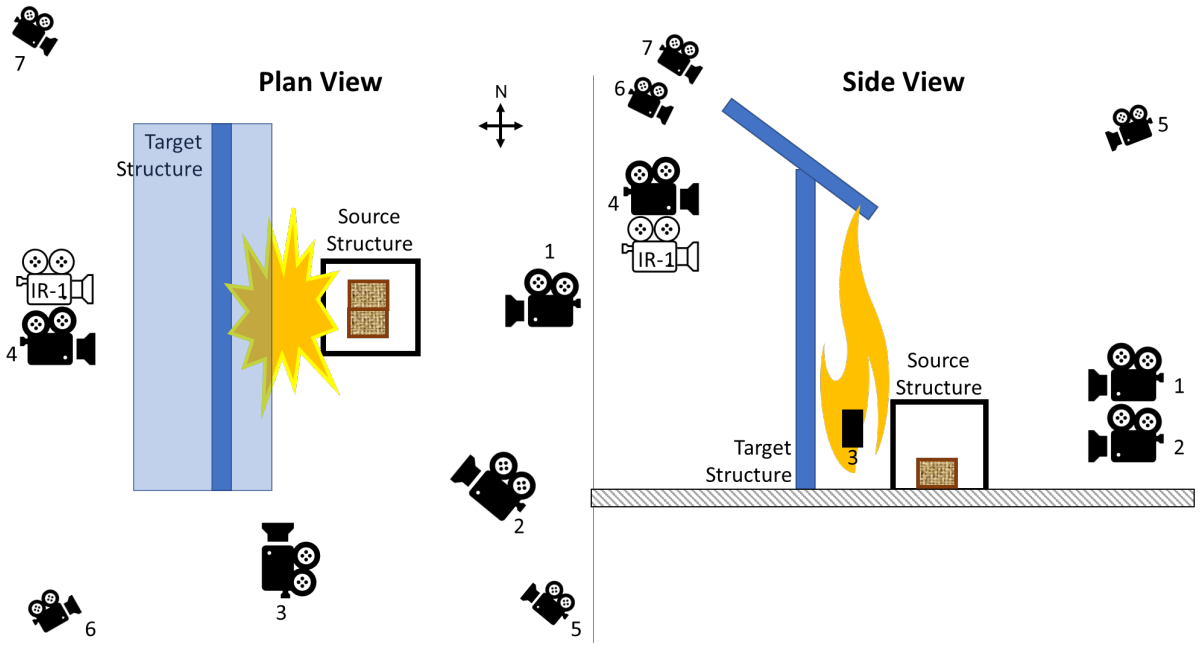

Fig. 8. The positions of the 7 video cameras (black) and one IR camera (white) (figure not to scale).

2.4.7. Open-Path Laser Spectroscopy

An open-path laser spectrometer was deployed to make gas-phase water vapor concentration and temperature measurements in both the eave and the attic space of the target wall structure. These exploratory measurements were conducted to develop measurement science to better quantify the ignition phenomena at the eaves and in the attic. The use of the open-path laser system is to take advantage of a non-intrusive measurement technique that avoids disturbing the flow within the eaves and attic, as compared to a more traditional extractive gas sampling technique.

The spectrometer was custom-built and equipped with a near-infrared laser diode used for molecular absorption measurements and a visible laser for alignment purposes. The instrument design closely followed previous field demonstrations [21]. Platforms elevated the instrument to the required height. In this configuration, shown in Fig. 9, the laser performed a single pass of the target structure (i.e., optics to send laser light were on the North platform and the optics to receive laser light were on the South platform). The distance between the sending/receiving subsystems was approximately 9 m (29.5 ft). The elevated optical components were partially enclosed to protect from splashing water, embers, and ash during experiments and fire suppression.

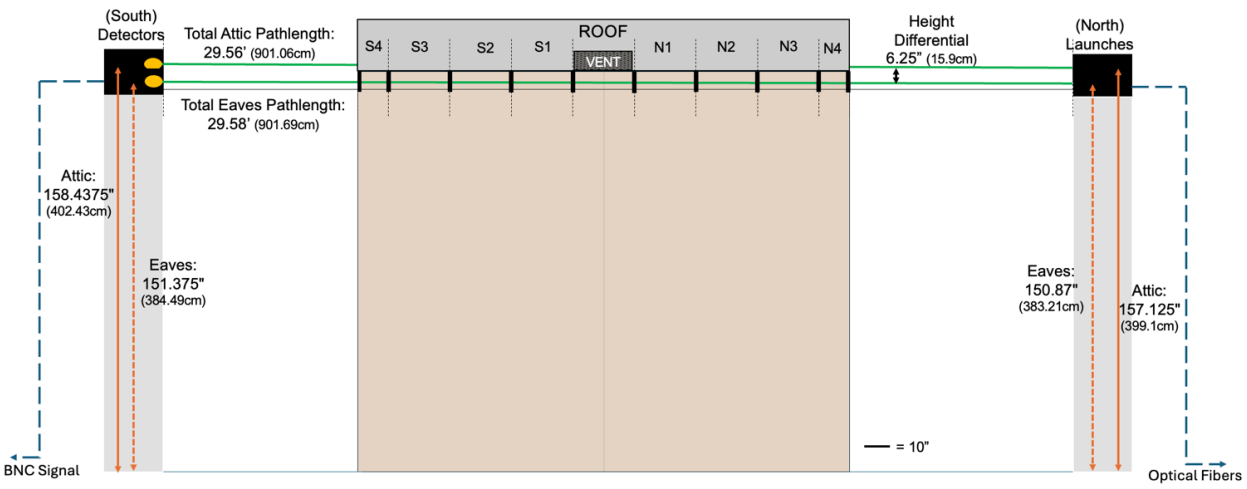

Fig. 9. Scaled schematic of laser instrument incorporated into the target structure setup. The target structure is shown in the center with laser launch and collection platforms (north and south, respectively) on either side. The total path length from launch to detector was approximately 901 cm (29.5 ft).

Fig. 10a shows the location of the laser beams passing under the exterior eave bays (eaves path) and behind the eave vent, on the attic side (attic path). The distance between the two laser beam paths was approximately 0.81 m (32 in). To pass behind the vent plenum box, as shown in Fig. 10b, the laser in the attic path was elevated an additional 15.875 cm (6.25 in) compared to the eaves path. Detailed descriptions for the spectral acquisition and analysis are described in Appendix C.

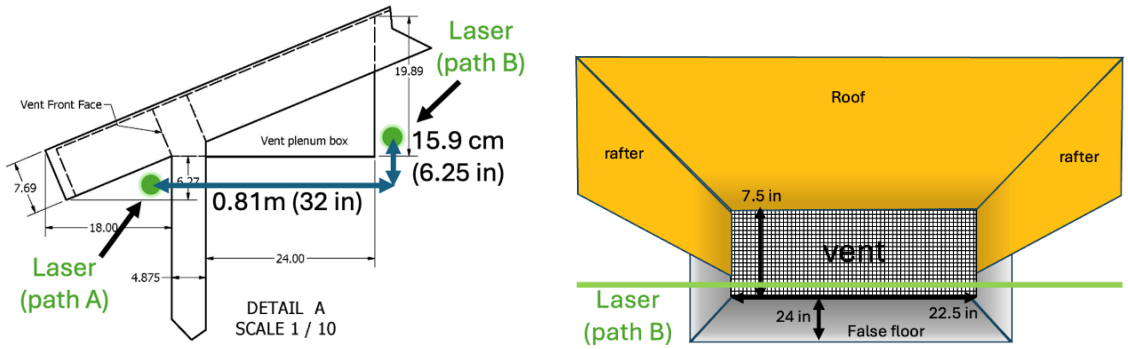

Fig. 10. Diagrams of the laser path locations: a) side view showing path A through the eaves and path B behind the eave vent, b) view from the attic showing path B passing behind the vent plenum box (not to scale; 1 in = 2.54 cm).

2.4.8. Data Acquisition System (DAQ)

A National Instruments (NI) cDAQ-9184 data acquisition (DAQ) chassis with NI-9213 modules for thermocouples and NI-9215 modules for sensors with voltage outputs sampled the output from heat flux gauges and thermocouples at a frequency of 1 Hz. The heat release rate (HRR)

measurements from the calorimeter were made on an independent data collection system called the Modular In-Situ Data Acquisition System (MIDAS). Uncertainties related to the DAQ are orders of magnitude lower than those from the other measurements [2].

3. Results

The following section includes a test matrix specifying the closet type, fuel load, SSD and vent for the target wall experiments and results for eave ignition and vent performance (vent closure, attic temperature and flame penetration). Common terms used throughout the results are defined, and spectroscopy and gas flow results are summarized.

3.1. Test Matrix Summary

The test sequence for the 16 experiments is provided in the following table with shed type, number of wood cribs, SSD, and type of vent (see Table 6). The experiment naming convention is similar to the convention used previously [2, 4]:

> *Experiment Designator and Number* [experiment (e), preliminary (p)], *Material* [Steel (S)], *Size* [Closet (C), Very Small (VS), Narrow (N)], *Fuel Load* [low (l), intermediate (i), medium (m), high (h)] - *Wind Speed* [#, in mi/h] - *SSD* [#, in ft] - *Replicate* [R#].

The letter “R” followed by a number at the end of the experiment name indicates a test replicate. Therefore, experiment 10 in the current series—a steel closet shed with high fuel load, no wind, 5 ft SSD, which is a repeat of a prior experiment—has a test ID e10_SCh0-5-R1.

Table 6. List of test configurations and summary of eave and vent performance results.

Test ID	Shed Type	Fuel Load (1-A cribs)	SSD (ft)	Eave Vent	Objective	Result Summary			
						Eave Ignition	Vent Closure	Max./Vent Act. Attic Temp. (°C)	Flame Penetration
e7_SCh0-5	Closet	4	5	A	Begin with high fuel load in smallest shed.	Yes	Partial	376	Yes
e8_SCl0-5	Closet	2	5	A	Lowest fuel load to determine ignition.	No	No	240	n/a
e9_SCm0-5	Closet	3	5	A	Increase to medium fuel load to determine if it is a sufficient exposure for ignition.	No	Partial	336	n/a
e10_SCh0-5-R1	Closet	4	5	A	Establish repeatability of e7 with eave ignition and vent activation.	Yes	Partial	339	Yes
e11_SCh0-5-R2	Closet	4	5	A	Second repeat of e7 and e10. Fireproof caulking was applied throughout the underside of the overhang and rafter and fascia board edges were routed.	Yes	Partial	358	Yes
e12_SNl0-0	Narrow	2	0	A	Study thermal exposure from a Narrow shed with low fuel load to a WUI eave vent.	No	No	214	n/a
e13_SNi0-0	Narrow	3	0	A	Study thermal exposure from a Narrow shed with intermediate fuel load to a WUI eave vent.	No	No	295	n/a
e14_SNm0-0	Narrow	4	0	A	Study thermal exposure from a Narrow shed with medium fuel load to a WUI eave vent.	No	No	342	n/a
e15_SNh0-0	Narrow	6	0	A	Study thermal exposure from a Narrow shed with high fuel load to a WUI eave vent.	Yes	Partial	369	Yes
e16_SNh0-0-R1	Narrow	6	0	A	Establish repeatability of e15, a Narrow shed with high fuel load to a WUI eave vent.	Yes	Partial	366	Yes
e17_SVSl0-5	Very Small	4	5	A	Study thermal exposure from a Very Small shed with low fuel load to a WUI eave vent.	No	Partial	374	n/a

Test ID	Shed Type	Fuel Load (1-A cribs)	SSD (ft)	Eave Vent	Objective	Result Summary			
						Eave Ignition	Vent Closure	Max./Vent Act. Attic Temp. (°C)	Flame Penetration
e18_SVSh0-5	Very Small	6	5	A	Study thermal exposure from a Very Small shed with high fuel load to a WUI eave vent.	Yes	Partial	390	Yes
e19_SVSh0-5-R1	Very Small	6	5	B	Establish repeatability of e18, a Very Small shed with high fuel load to a similar WUI eave vent.	Yes	Partial	344	Yes
e20_SCh0-5	Closet	4	5	C	Study thermal exposure from a Closet shed with high fuel load to a different WUI eave vent.	Yes	Yes	231	No
e21_SCh0-5-R1	Closet	4	5	C	Establish repeatability of e20, a Closet shed with high fuel load to a WUI eave vent.	Yes	Yes	87	No
e22_SVSh0-5	Very Small	6	5	B	Study thermal exposure from a Very Small shed with high fuel load to the target structure without a centrally located WUI eave vent, but with two vents at either end of the wall.	Yes	Partial	334 (N) 180 (S)	Yes

3.2. Target Results

The EaVE experiments were noted as experiment e7 through e22. Experiment p1 through p6 were preliminary experiments without the target structure and are described in Appendix D. Experiment summaries including data plots and images are located in Appendix E. The results from the Open-Path Laser Spectroscopy are discussed in Appendix C. The results from the flow measurements are provided in Appendix F.

The following terms are commonly used in the description of results:

Vent activation: defined as the process when the intumescent coating on vent begins to develop char, thereby closing the openings in the vent.

Start of vent activation: defined as the maximum negative rate of change in vent flow velocity measurement (after a 15 s smoothing filter was applied) and verified by visual review of IR video focused on the attic side of the vent.

Peak shed HRR (peak HRR_{shed}): defined as the maximum value of HRR measured before the eave ignition time. If the eaves did not ignite during an experiment, then the HRR_{shed} was the maximum value of HRR throughout the experiment.

Eave ignition: defined as sustained flaming at any point on the eave assembly, determined by visual review of video recordings from the front and side of the wall assembly.

Flames through vent: defined as sustained flaming on the interior side of the vent, determined by visual review of video recordings from the back side of the wall focused on the vent.

Suppression: defined as the first application of water to terminate the experiment, determined by visual review of video recordings.

3.3. Spectroscopy

Table 7 shows the data throughput and results from the open-path laser absorption spectrometer. The data throughput for the eaves and attic paths is determined by the percentage of total spectra that met analysis benchmarks (described in Appendix C.2. *Spectral Analysis*). Figure 11A shows an example of this throughput in relation to experimental events. The total number of spectra collected is related to total length of the experiment time. The loss of throughput in both paths, unless noted, is likely due to smoke, flame particulate, and thermal gradients which reduced the laser signal at the detector. Observable changes indicating a clear increase or decrease in temperature and water vapor concentration or in the noise level of the data can indicate a change in the experimental environment after a fire event. These changes are noted in Table 7 within the ignition window of the experiment – defined here as 1 minute prior to fuel ignition and three minutes after – and within the vent activation window – 2 minutes before and after the determined vent activation time. An example is shown in Fig. 11B-C.

Table 7. Open-path laser absorption spectroscopy throughput and results.

Test ID	Total # of Collected Spectra	Attic Data Throughput	Eaves Data Throughput	Result Summary: Observed Change in Data within Ignition Window – Eaves Path	Result Summary: Observed Change in Data within Ignition Window – Attic Path	Result Summary: Observed Change in Attic Data within Vent Activation Window	Notes
e9_SCm0-5	12600	90%	25%	Yes	No	No	
e10_SCh0-5-R1	10200	90%	30%	Yes	Yes	Yes	
e11_SCh0-5-R2	8100	95%	42%	Yes	Yes	No	
e12_SNl0-0	12700	90%	21%	Yes	Yes	N/A	
e13_SNi0-0	12600	90%	17%	Yes	Yes	N/A	
e14_SNm0-0	12000	50%	17%	Yes	Yes	N/A	
e15_SNh0-0	9300	90%	25%	Yes	Yes	No	Excessive steam during fire suppression engaged the laser safety shutdown procedure due to prolonged loss of signal at the detector
e17_SVSl0-5	8000	69%	31%	Yes	N/A	No	Realignment of receiving optics in the attic path prior to this experiment resulted in saturation of the detector and a lower throughput for the ignition window
e18_SVSh0-5	10100	98%	36%	Yes	No	Yes	
e19_SVSh0-5-R1	8400	84%	31%	Yes	No	Yes	
e20_SCh0-5	18800	70%	40%	Yes	No	No	
e21_SCh0-5-R1	20300	23%	29%	Yes	Yes	No	

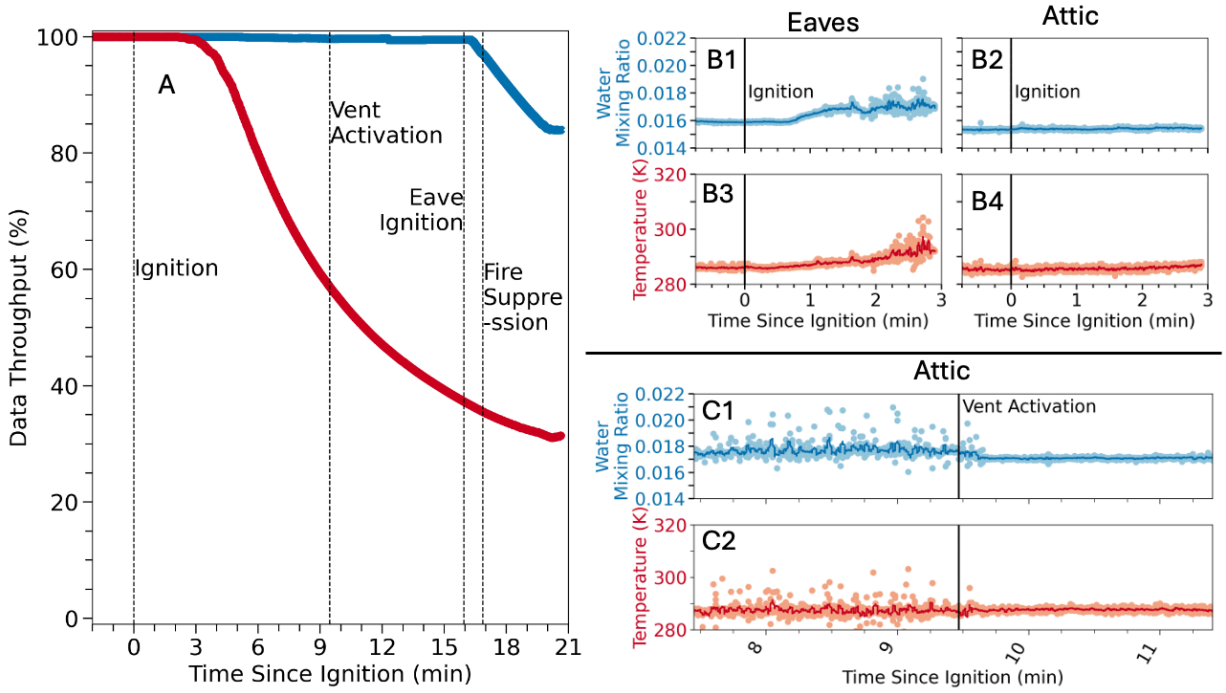

Fig. 11. Experimental data for e19. A) Data throughput for the eaves (red) and attic (blue) laser paths. B) Spectroscopy results during the ignition window for the water mixing ratio and temperature observed in the eaves (B1 and B3, respectively) and attic (B2 and B4, respectively). C) Spectroscopy results from the attic during the vent activation window. Results for vapor mixing ratio and temperature are shown in C1 and C2, respectively. Solid traces in B & C show the time series results when data are treated with a Savitsky-Golay filter over a 15-point window with a 2nd order polynomial.

3.4. Gas Flow Velocity

The various flow velocity probes described in Fig. 7 provided measurements of lateral flows (North-South flows), vertical flows along the center of the wall, and measurements of flow through the vent. Wall and vent flow results are discussed in detail in Appendix F. The vent flow measurements were subsequently used to identify vent activation quantitatively and programmatically (as described in Section 3.2, above). The extracted activation times were confirmed to be accurate through the videos and temperature readings behind the vent. Additionally, the lateral flow velocity probes found that lateral flows along the wall (East-West flows) were minimal and that the hood makeup air supply did not introduce any significant ambient drafts, confirming quiescent laboratory conditions. Finally, the Bi-directional and S-probe measurements were found to be in good agreement with each other, even in the presence of flaming combustion.

4. Analysis and Discussion

The thermal exposure to the eaves and vents from different sizes of sheds with different fuel loading levels was quantified with three measurements, the peak HRR_{shed} from the source fire (sheds), the peak heat fluxes measured at the target structure (in the eaves), and the peak temperatures recorded at the vent. The measured quantities for different variables are discussed in detail below.

4.1. Repeatability of Shed Burn Experiments

For large-scale experiments, assessing the degree of repeatability of data is important to draw strong conclusions from the experimental data. The repeatability of the shed burn experiments was assessed by comparing temporal plots of HRR_{shed}, heat flux, and temperature measurements at the target structure. The repeatability of each of these measurements for different types of sheds and fuel loadings is discussed below.

4.1.1. Repeatability of HRR_{shed} Data

The HRR data for Closet, Narrow, and Very Small shed burns are plotted in Fig. 12, Fig. 13, and Fig. 14, respectively. The three HRR curves in Fig. 12 show that the growth phase of fuel (four cribs with average fuel mass of 93.2 kg ± 3.7 kg) burning in the noncombustible Closet was very similar and the difference in HRR data is within the 9.8 % error of the HRR measurements [19]. For the entire growth period prior to eave ignition, the mean absolute error between each experiment and the mean is 15.5 kW, or less than 5 % error, indicating a very repeatable exposure scenario. A more detailed discussion about the repeatability analysis is provided in Appendix G.

For these experiments, the noncombustible steel Closet was placed at an SSD of 5 ft with the doors fully open and facing the target structure. The peak HRR_{shed} was registered just prior to eave ignition. The fire was suppressed upon ignition of the eaves. The wood cribs in the noncombustible Closet burned with an average peak HRR_{shed} of 1.39 MW ± 0.04 MW, with an average time to peak of 13.7 min ± 1.5 min.

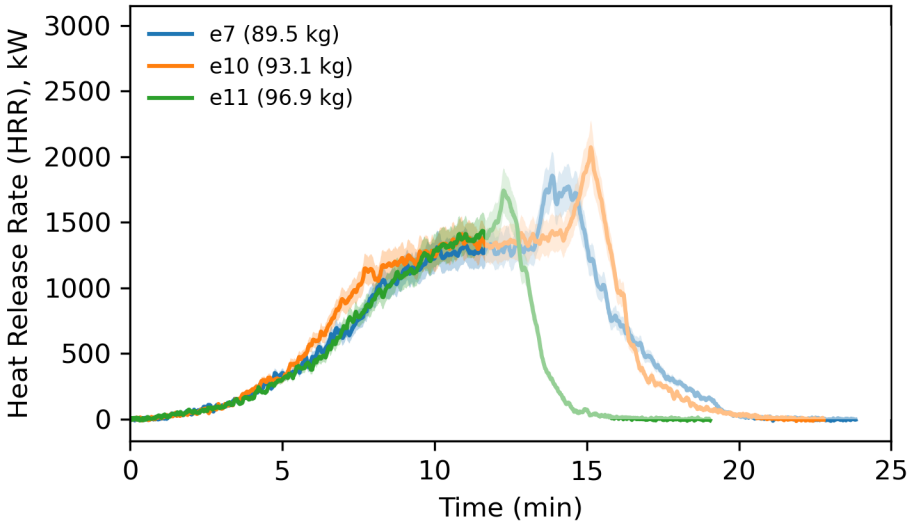

Fig. 12. Repeatability of HRR data for the Closet burns with four cribs. (e7_SCh0-5, e10_SCh0-5-R1, e11_SCh0-5-R2)

One repeat was performed for each of the burns with Narrow and Very Small sheds (two total burns for each shed type). The HRR plots for Narrow sheds and the Very Small sheds, both with fuel loading of 6 wood cribs, are shown in Fig. 13 and Fig. 14, respectively. The Narrow shed was placed next to the target structure with an SSD of 0 ft while the Very Small shed was placed at an SSD of 5 ft. For the two experiments with Narrow sheds that resulted in eave ignition (e15 and e16), the time to eave ignition was within approximately 20 s of each other, and the peak heat flux at the eaves was approximately 10.5 kW/m^2 ± 2.4 kW/m^2. The peak HRR_{shed} for the Narrow shed burns was approximately 1.72 MW ± 0.07 MW. The HRR for e15 was slightly higher when compared to HRR during the e16 burn due to the higher mass of the wood cribs used in e15. For the Narrow and the Very Small shed burns, the HRR profiles for the two repeat burns follow the same contours suggesting good repeatability of the experimental shed burns and HRR data. The HRR profiles for both types of sheds show good repeatability, particularly in terms of time to peak HRR_{shed} as compared to time to peak values for Closet burns. Generally, the overall shapes of the HRR curves are similar for a given type of shed and fuel loading.

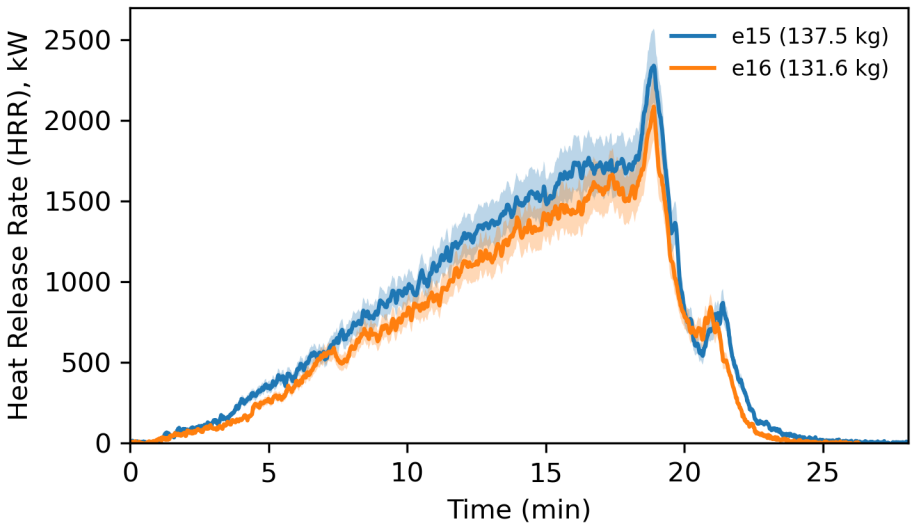

Fig. 13. Repeatability of HRR data for the Narrow shed burns with six wood cribs. (e15 and e16)

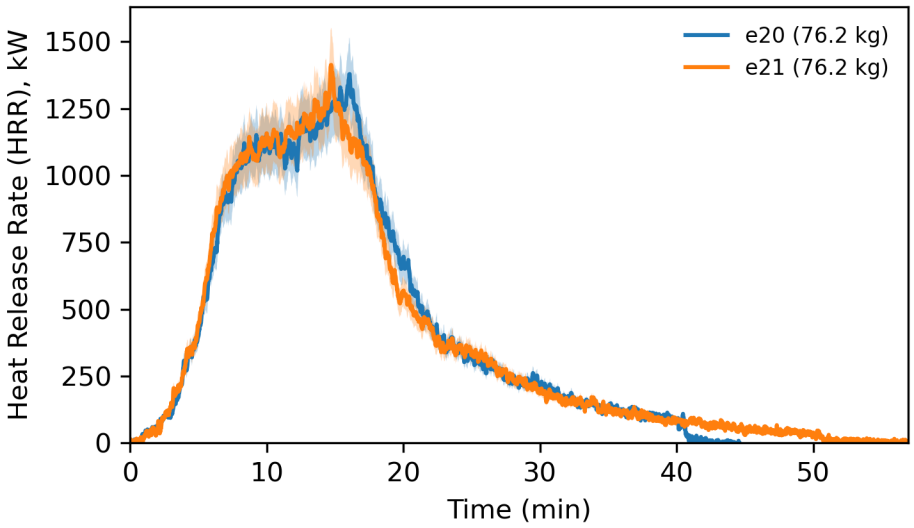

Fig. 14. Repeatability of HRR data for the Very Small shed burns with six wood cribs. (e20 and e21)

4.1.2. Repeatability of Heat Flux Data

Six heat flux gauges were mounted in the eaves to measure incident heat flux from the source (shed) fire as described in Sec. 2.4.1. Temporal plots of HF data measured by six heat flux gauges located in the eaves, for e7 (Closet burn with 4 wood cribs), are shown as an example in Fig. 15. The magnitude of HF measurements changes with the location of heat flux gauges from the centerline of the target structure. The heat flux gauges located close to the centerline of

the target structure recorded a higher magnitude of heat flux as compared to those located further away from the centerline.

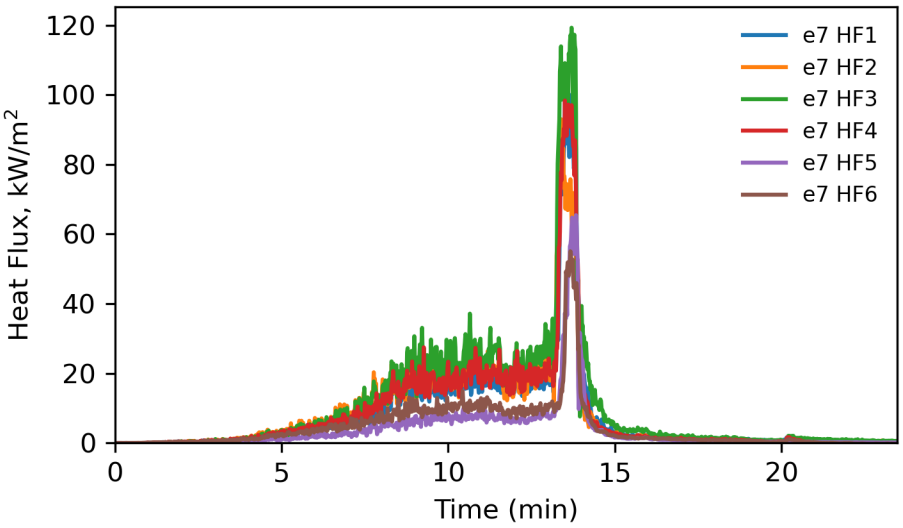

Fig. 15. Temporal plots of heat flux data measured by heat flux gauges located in the eaves (e7, Closet burn with 4 wood cribs).

The heat flux data measured by HF2, located at north bay 1 facing down, is plotted in Fig. 16 for experiments e7 (fuel mass 89.5 kg), e10 (fuel mass 93.1 kg), and e11 (fuel mass 96.9 kg). For similar thermal exposures from a Closet with 4 wood cribs, the measured heat flux data follows the same trend as the HRR plots in Fig. 12, and the peak HF is registered at the time of eave ignition. It is important to note here that the time to eave ignition was a function of fuel mass.

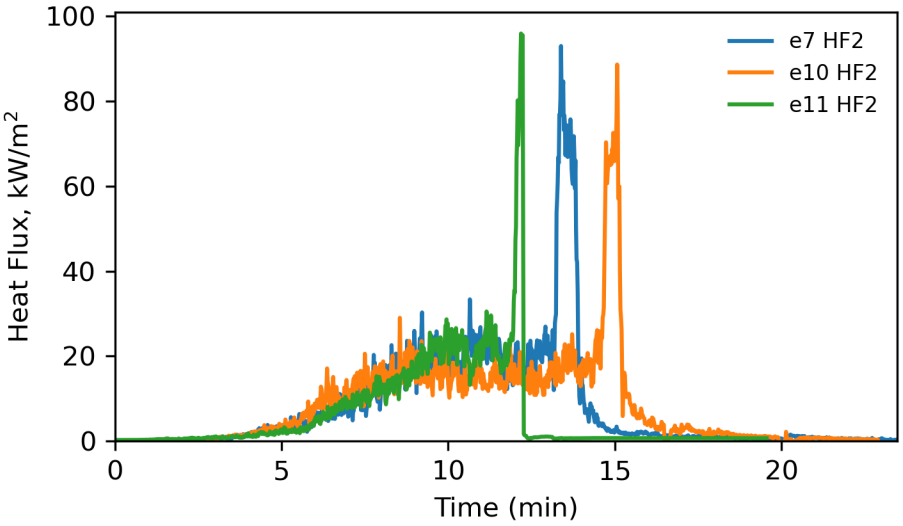

Fig. 16. Temporal plots of heat flux data measured by HF2* for experiments e7 (fuel mass 89.5 kg), e10 (fuel mass 93.1 kg), and e11 (fuel mass 96.9 kg), Closet burn with 4 wood cribs. *Note: HF2 was located in the eaves at north bay 1 facing down.

The HF data measured by HF1 (south bay 1, facing shed) and time to peak HF was remarkably repeatable for Closet shed experiments (e20 and e21) where the mass of four wood cribs was the same (76.2 kg). The temporal profiles for HF1 data for e20 and e21 are shown in Fig. 17 below.

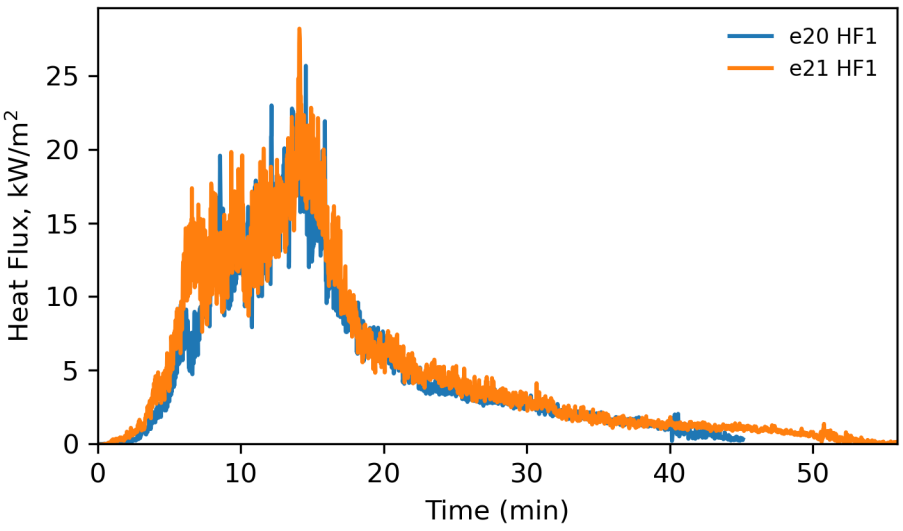

Fig. 17. Temporal plots of heat flux data measured by HF1* for experiments e20 and e21 (fuel mass 76.2 kg), closets with 4 cribs. *Note: HF1 was located in the eaves at south bay 1 facing the shed.

The repeatability of heat flux data for thermal exposures from the Narrow sheds with six cribs is shown in Fig. 18. For both experiments (e15 and e16) the HF data from HF3 (north bay 1, facing

away from the target structure) follows the same shape and magnitude, showing fairly good repeatability.

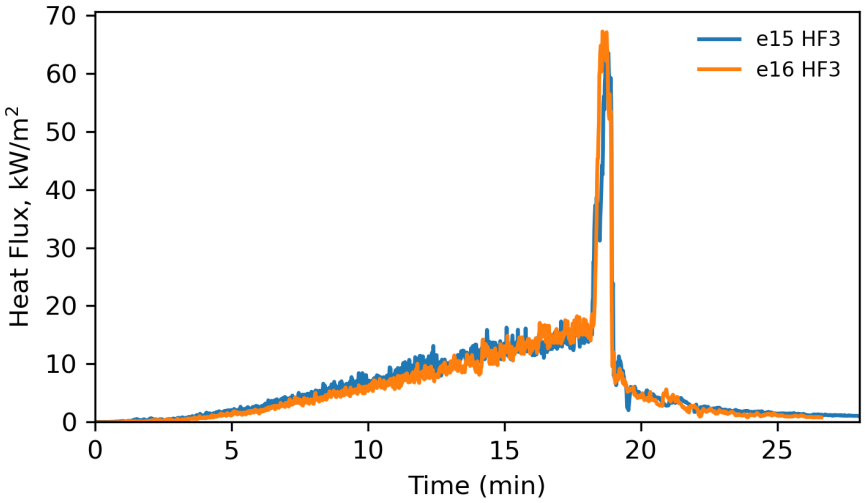

Fig. 18. Temporal plots of heat flux data measured by HF3* for experiments e15 (fuel mass 137.5 kg) and e16 (fuel mass 131.6 kg), Narrow sheds with 6 cribs. *Note: HF3 was located in the eaves at north bay 1 facing the shed.

4.1.3. Repeatability of Temperature Data

The temperature-time data provide useful insights into vent performance. However, it is important to note that the recorded TC temperatures measurement may not accurately represent the medium temperature due to radiative and convective heat transfer effects.

In this study, TCs were used to measure temperature at the exposed (eave) side and unexposed (attic) side of the vent. A TC was used to measure the temperature of the plywood on the attic side (attic plywood) of the vent. The repeatability of the temperature data recorded by the eave vent TC, attic vent TC, and attic plywood TC for three repeat experiments (e7, e10, and e11) is shown in Fig. 19. The thermal exposure for these experiments was from the Closet with fuel loading of 4 wood cribs; and Vent A was used in the target structure. The temperature-time profiles recorded by the eave vent TCs follow the same shape as that of the HRR and HF curves suggesting a rise in temperature at the exposed side of the vent corresponding to the HRR from the source (shed) fire and the measured heat flux at the target structure.

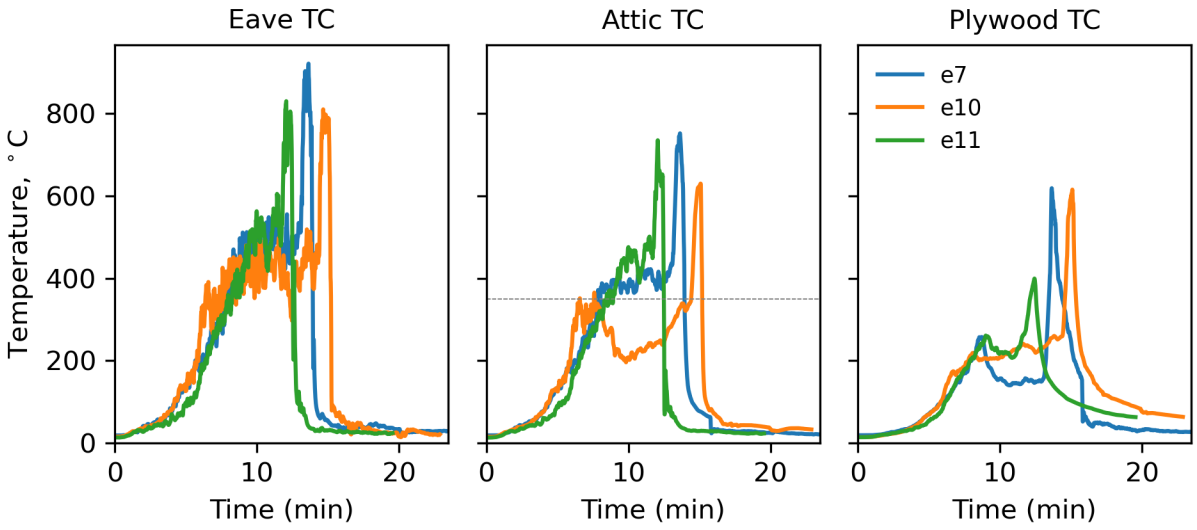

Fig. 19. Repeatability of the temperature-time data from the eave vent TC, attic vent TC, and attic plywood TC for experiments e7 (fuel mass 89.5 kg), e10 (fuel mass 93.1 kg), and e11 (fuel mass 96.9 kg), Closet sheds with four cribs and Vent A. Note: The dotted line shows the threshold temperature (350 °C) on the unexposed side of the vent as specified in the ASTM E2886 test method.

Similar comparisons for time-temperature data for experiments e20 and e21 are shown in Fig. 20. While the thermal exposures for these experiments were the same as experiments e7, e10, and e11, the vent (Vent C) used in the target structure was different from the vent (Vent A) used in the target structure of experiments e7, e10, and e11. The repeatability of the temperature data collected at the eave side of the vent is consistent however, the repeatability of the temperature data on the unexposed side of the vent is not consistent. This inconsistency in temperature measurements on the unexposed side of the vent for the repeat experiment may be attributed to the vent performance.

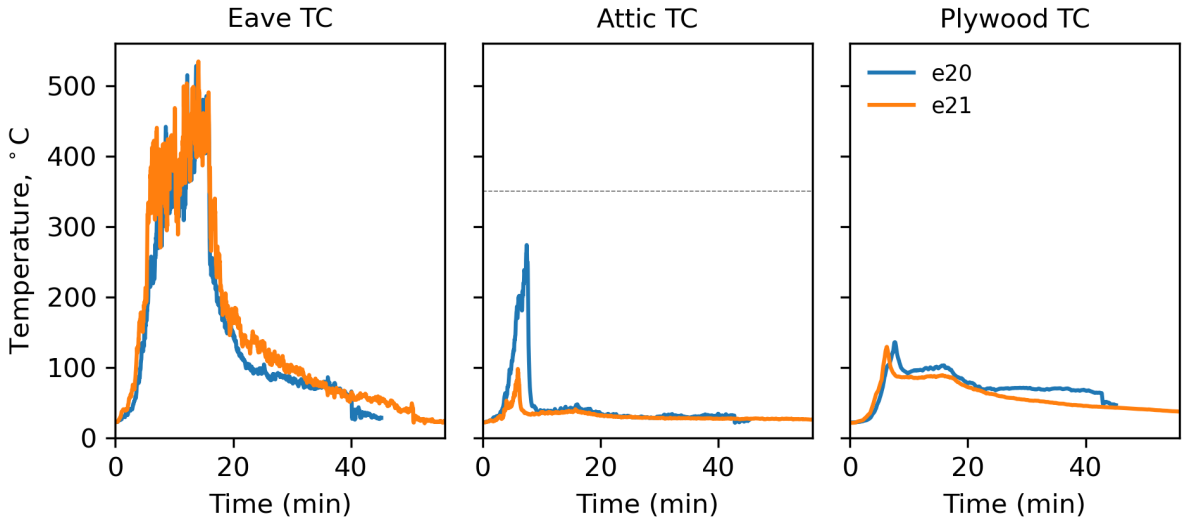

Fig. 20. Repeatability of the temperature-time data from each of the TCs at the eave vent from experiments e20 and e21 (fuel mass 76.2 kg), Closets with 4 cribs and Vent C. Note: The dotted line shows the threshold temperature (350 °C) on the unexposed side of the vent as specified in the ASTM E2886 test method.

Generally, the temperature-time profiles recorded by the attic vent TC and the attic plywood TC were not as repeatable as those recorded by the eave vent TCs. This can be attributed to variability in vent performance which is discussed in more detail in the following sections.

The repeatability of temperature measurements for experiments e15 and e16 are shown in Fig. **21** below. For these experiments, the exposure to the target structure was from a Narrow shed with a fuel loading of six wood cribs, placed next to the target structure (SSD = 0 ft). The vents (Vent A) used in the construction of the target structure for these experiments were similar to the ones used in experiments e7, e10, and e11. The temperature-time data in Fig. 21 follow the same profile as the HRR and HF curves in Fig. 13 and Fig. 18, respectively.

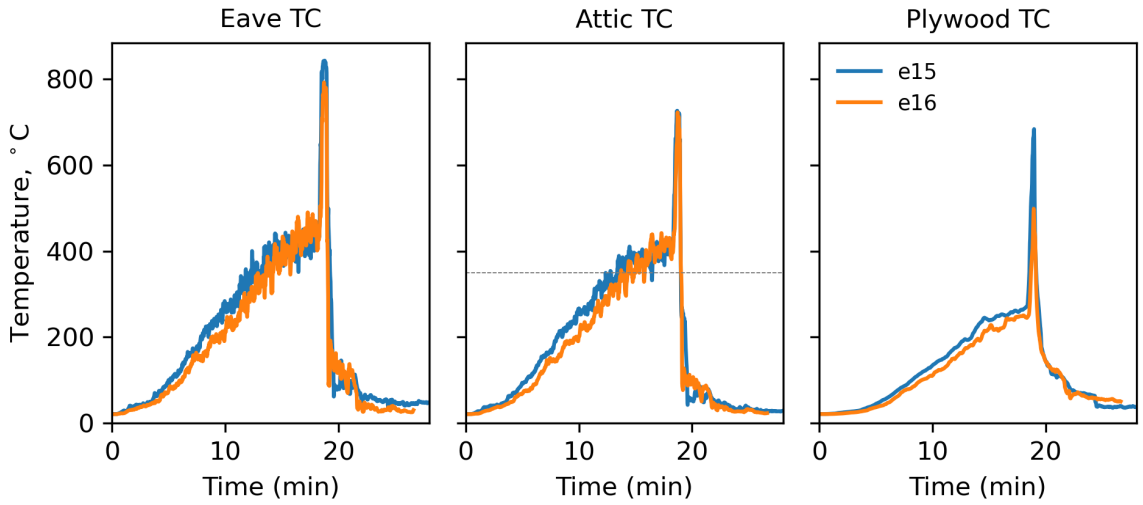

Fig. 21. Repeatability of the temperature-time data from each of the TCs at the eave vent from experiments e15 (fuel mass 137.5 kg) and e16 (fuel mass 131.6 kg), Narrow sheds with 6 cribs and Vent A. Note: The dotted line shows the threshold temperature (350 °C) on the unexposed side of the vent as specified in the ASTM E2886 test method.

4.2. Thermal Exposure, Eave Ignition, and Vent Performance

In this study, the fire hazard (thermal exposure) of a source (shed) has been quantified in terms of peak HRR_{shed} and peak heat flux measured at the target structure. The performance of the vents has been evaluated using temporal profiles of temperature data, qualitative IR videography, and visual inspection of vents following the experiments. The effects of different variables on measured quantities are discussed below.

4.2.1. Effect of Shed Types on HRR

The temporal profiles of HRR for the Closet, Narrow, and Very Small sheds with 4 wood cribs are shown in Fig. 22. The sharp peak in the HRR curve for e10 represents eave ignition. The HRR for e10 dropped sharply after fire suppression following the eave ignition. The HRR profiles for e14 and e17 were very similar. Despite the same fuel loading, the ignition of the eaves was not noted for exposures from the Narrow (e14) and Very Small (e17) sheds. All three types of sheds have a fuel loading of 4 wood cribs. However, the storage capacity of the Closet, Narrow, and Very Small sheds were 66 ft^3, 154 ft^3, and 141 ft^3, respectively (see Table 2). The size and the shape of the door opening was also different as shown in Fig. 5. The door opening area of the Closet, Narrow, and Very Small shed were 19 ft^2, 16 ft^2, and 13.5 ft^2, respectively. The Closet has a wider door opening compared to the Narrow and the Very Small sheds. The Closet also has the highest fuel packing density considering the storage capacity of the shed and the volume of wood cribs (see Table 8). Fuel packing density can be defined as energy per unit storage capacity of the shed, having units of MJ/ ft^3. The lower the storage capacity of the shed, the higher fuel packing density for a given number of wood cribs. The Closet had the highest fuel packing density of 27 MJ/ ft^3 ± 1 MJ/ ft^3 compared to the Narrow (10 MJ/ ft^3) and the Very

Small (10.5 MJ/ ft^3 ± 0.5 MJ/ ft^3) sheds with 4 wood cribs. The high fuel packing density forced the flames out from the closet, thereby causing intense flame jetting, and directing the thermal exposure and measured HRR.

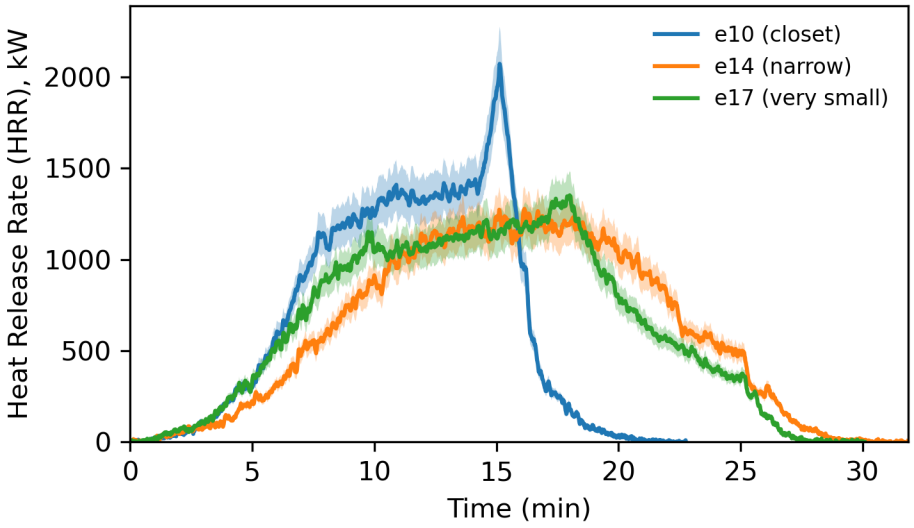

Fig. 22. Temporal profiles of HRR for the Closet, Narrow, and Very Small sheds with 4 wood cribs. Ignition of the eaves is noted in the Closet experiment but not the others.

Table 8. Experiment fuel loading characteristics.

Test ID	Fuel Load (1-A cribs)	Total Comb.[a] Mass (kg)	Fuel Density[b] (MJ/m^2)	Fuel Packing Density[c] (MJ/m^3)
p1_SNm0	4	90.5	719	398
p2_SVSh0	6	143.5	989	695
p3_SNl0	2	46.5	370	205
p4_SCl0	2	47.6	547	489
p5_SNh0	6	137.6	1094	606
p6_SVSl0	4	89.2	614	432
e7_SCh0-5	4	89.5	1028	919
e8_SCl0-5	2	39.4	452	405
e9_SCm0-5	3	62.9	722	646
e10_SCh0-5-R1	4	93.1	1069	956
e11_SCh0-5-R2	4	96.9	1113	995
e12_SNl0-0	2	48.9	389	215
e13_SNi0-0	3	59.7	475	263
e14_SNm0-0	4	84.2	669	371
e15_SNh0-0	6	137.5	1093	605
e16_SNh0-0-R1	6	131.6	1046	579

Test ID	Fuel Load (1-A cribs)	Total Comb.[a] Mass (kg)	Fuel Density[b] (MJ/m^2)	Fuel Packing Density[c] (MJ/m^3)
e17_SVSl0-5	4	80.4	554	389
e18_SVSh0-5	6	124.0	854	601
e19_SVSh0-5-R1	6	112.9	778	547
e20_SCh0-5	4	76.2	875	783
e21_SCh0-5-R1	4	76.2	875	783
e22_SVSh0-5	6	118.1	814	572

It is also important to note that the SSD for the Narrow shed was zero whereas the SSD for the Closet and the Very Small shed was 5 ft. Flames from the Closet were visually observed to be more focused towards the target structure with less turbulence than those for the Narrow and the Very Small sheds. This focused thermal exposure from the Closet shed resulted in the ignition of the eaves whereas eave ignition was not noted for the Narrow and Very Small shed burns for similar experimental conditions.

Thermal exposure to the target wall from three different types of sheds was quantified by measuring incident heat flux in the eaves. Temporal profiles of HF data for e10, e14 and e17 experiments are plotted in Fig. 23. The HF curves represent heat flux data collected by HF1 gauge (south bay 1, facing shed). The peak in the HF profile for e10 indicates ignition of the eaves. The HF profile for e17 has a similar magnitude to e10 before ignition except that the eave ignition did not occur. The HF measured for the e14 experiment was the lowest despite the proximity of the Narrow shed to the target wall. The lower thermal exposure from the Narrow shed can be attributed to the direction of flame jetting, shape of the door opening, and orientation of the door opening/shed with respect to the target wall. The higher heat flux values for the Closet and the Very Small shed are likely due to heat entrapment in the eaves as a result of the direction of flame jetting. As shown in Fig. 24, the flame jetting was upwards and perpendicular to the target structure in the case of a Closet and the Very Small shed placed 5 ft away from the target structure. In the case of the Narrow shed burn, the flame jetting was upwards and parallel to the target structure. The heat entrapment in the eaves in the case of the Narrow shed burn was significantly lower as shown in Fig. 23.

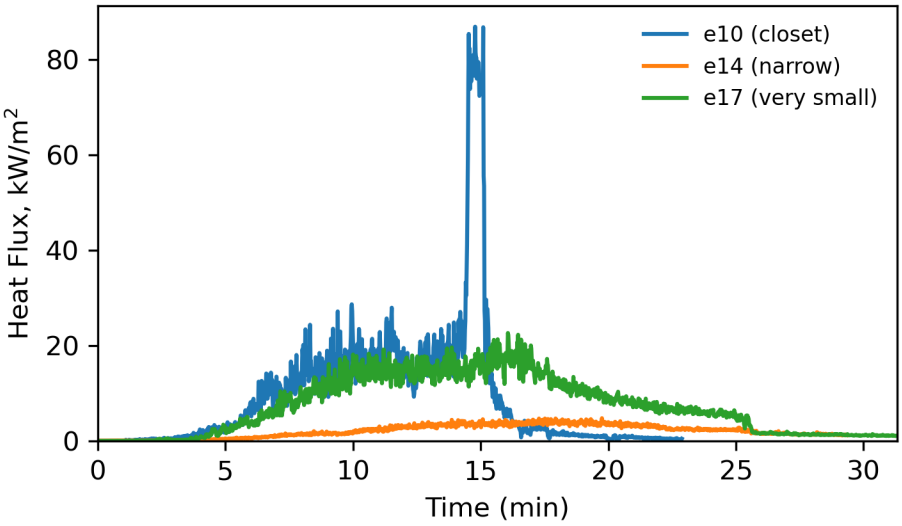

Fig. 23. Temporal profiles of HF for the Closet, Narrow, and Very Small sheds with 4 wood cribs. Although there are similar HF magnitudes between the Closet and Very Small burns, ignition of the eaves occurred only in the Closet experiment.

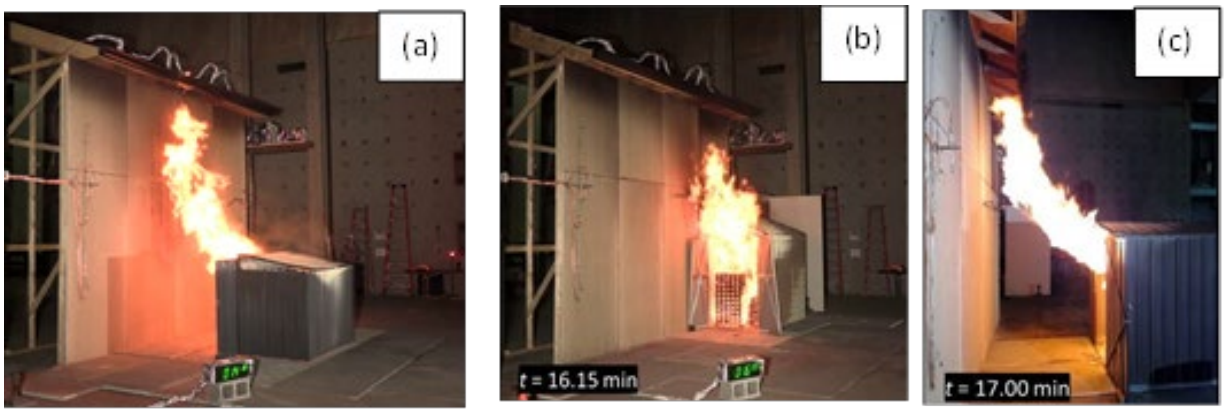

Fig. 24. Images of shed burn experiments showing the effect of shed types (Closet e10, Narrow e14, and Very Small e17) on flame jetting. Note: Images are captured from the video camera located from the front diagonal location (camera 2) for the Closet (a) and Narrow (b) sheds, and from the side (camera 3) for the Very Small shed (c).

The vent performance during exposures from three different sheds can be seen from the temperature-time profiles plotted in Fig. 25. As discussed earlier, the time-temperature profiles from the eave-vent TC follow the same shape as the HRR curves, however, temporal plots of temperature data measured at the attic vent TC show differences in shapes. Generally, the attic vent TCs and the attic plywood TCs measured lower temperatures than the eave vent TCs. The temporal profile of the temperature data from the attic TC shows a dip in the curve after an initial rise in temperature for the Closet burn in e10. This decrease in temperature on the attic side of the vent can be attributed to activation of the intumescent coating on the honeycomb

cells thereby closing the vent openings. A subsequent rise in the temperature could be due to vent failure, i.e., the vent cells reopened due to collapse of the intumescent coating. The flame jetting through the vent can be seen in Fig. 26 below.

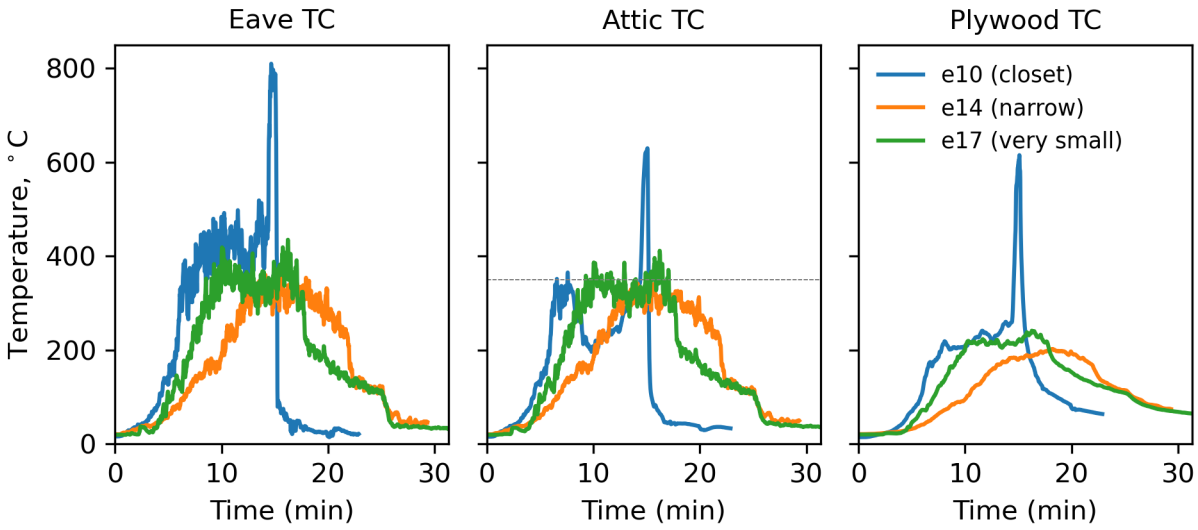

Fig. 25. Temporal profiles of the temperature measured from the eave, attic, and attic plywood TCs for Closet (e10), Narrow (e14), and Very Small (e17) shed experiments with 4 cribs. Note: The dotted line shows the threshold temperature (350 °C) on the unexposed side of the vent as specified in the ASTM E2886 test method.

Fig. 26. Interior vent image showing flame penetration through the vent into the attic side following eave ignition during e10.

Temporal profiles of temperatures measured on the unexposed side of the vent, for experiments where eave ignition did not occur, were similar to those measured on the exposed side of the vent except the temperatures measured on the unexposed side were lower. The

dotted line in Fig. 25 (b) shows the threshold temperature (350 °C) on the unexposed side of the vent as specified in the ASTM E2886 test method.

4.2.2. Effect of Fuel Loading on Peak HRR

The peak HRR_{shed} from noncombustible steel sheds of different sizes and different fuel loadings follow an increasing linear relationship with fuel mass as shown in Fig. 27. Plotted in Fig. 27 are the peak HRR_{shed} for noncombustible shed burns with and without a target structure. The peak HRR_{shed} for shed-only burns (preliminary, without the target structure) are represented by unfilled shapes and those with the target structure are represented by filled shapes. Full opacity fill indicates the eaves ignited, while 50 % opacity fill indicates no eave ignition. For the experiments where ignition of the eaves occurred, the peak HRR_{shed} was defined as the maximum HRR prior to eave ignition. For experiments where the eave ignition did not occur, the peak HRR_{shed} was defined as the maximum HRR measured during the experiment. Given the uncertainties of measuring HRR and the repeatability of the experiments, the peak HRR_{shed} versus fuel loading relationship follows a similar linear trend as in the previous shed burn series [2].

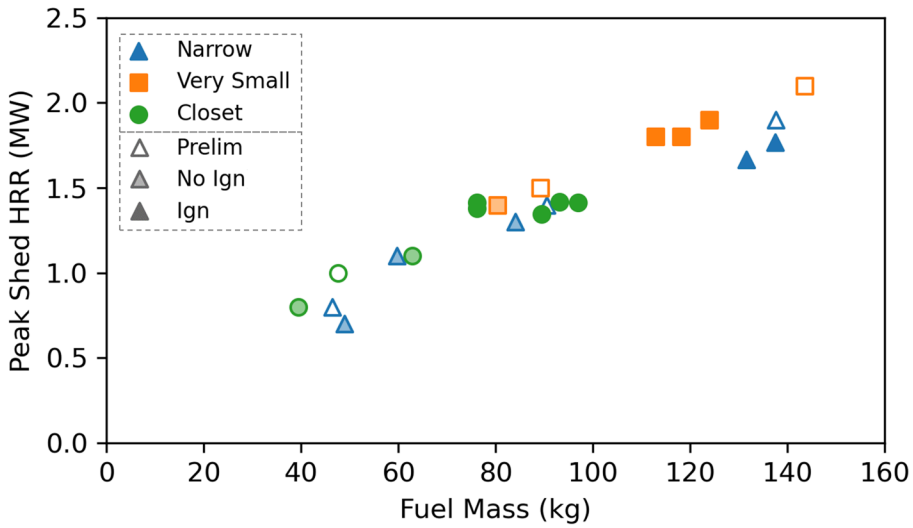

Fig. 27. Peak HRR_{shed} versus fuel loading for noncombustible shed burns. Shape and color correspond to shed type. Shading corresponds to experiment result (Ign=ignition). A star in the symbol indicates the result was observed during comparable prior NISSE series.

4.2.2.1. Closet Shed

The effect of fuel loading on HRR from a Closet shed can be noted in Fig. 28. The initial gradual increase in HRR for e8, e9, and e7 experiments is similar for Closets with two, three, and four wood cribs, respectively. The HRR for the Closet with four wood cribs (e7) continued to rise until approximately 10 mins from ignition of the cribs and then plateaued until the eaves ignited. The ignition of the eaves resulted in a sudden rise in the HRR thereby resulting in a peak in the HRR data. HRR gradually decreased following the fire suppression. This peak in the

HRR profile was not noted for Closet burns with two (e8) or three (e9) wood cribs suggesting that the eaves did not ignite due to insufficient thermal exposure. The HRR profiles for e8 and e9 have similar shapes where HRR gradually increased to maximum HRR and plateaued for some duration before the HRR gradually decreased as the wood cribs were consumed by the fire.

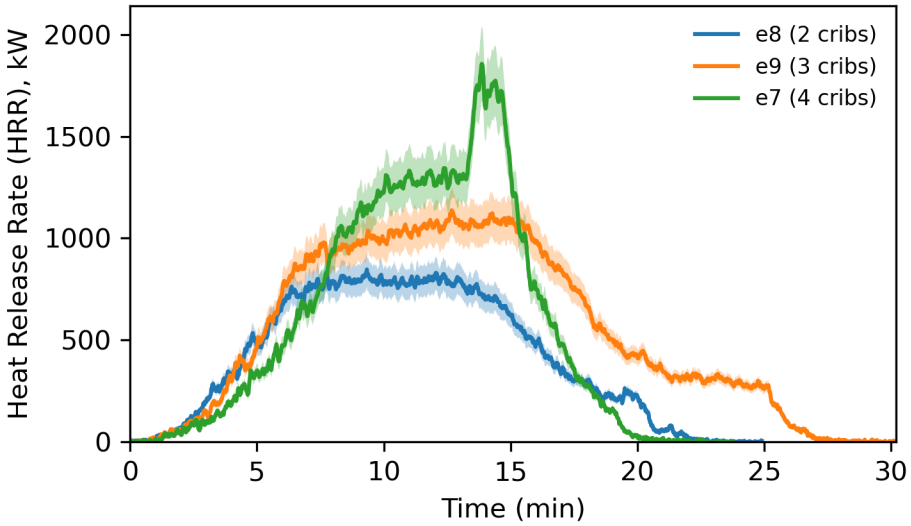

Fig. 28. The effect of fuel loading on HRR for a Closet shed with two (e8), three (e9), and four (e7) wood cribs, respectively.

The heat flux data for the Closet burns with different fuel loading in Fig. 29 show similar profiles as the HRR data. The thermal exposure from Closet sheds with two wood cribs (e8) resulted in the lowest measured HF in the eaves while measured HF for the Closet with 3 (e9) and 4 (e7) wood cribs increased with the total mass of wood cribs.

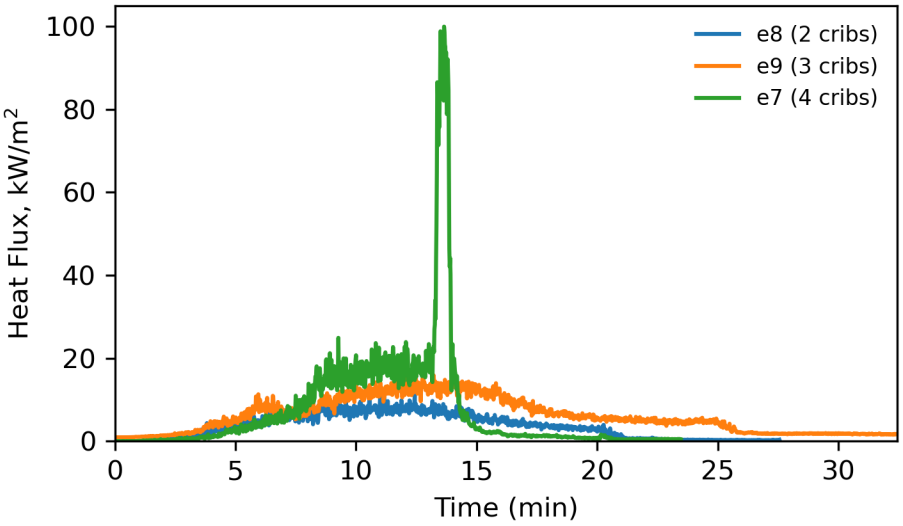

Fig. 29. The effect of fuel loading on HF for a Closet shed with two (e8), three (e9), and four (e7) wood cribs, respectively.

The effect of fuel loading on measured heat fluxes at the eaves (central section of the target structure) can be further explained by examining the flame jetting with respect to the eaves. Flame jetting from three experiments with fuel loading of two (e8), three (e9), and four (e10) wood cribs can be noted in Fig 30(a), (b), and (c), respectively, at times corresponding to the peak HRR_{shed}. Increased flame lengths for higher fuel loading can be clearly noted from Fig 30. The flame jetting differences in Fig 30. can also be explained based on fuel packing density. The fuel packing density increased from 11 MJ/ft^3 to 18 MJ/ft^3 and 27 MJ/ft^3 with the addition of one and two wood cribs, respectively.

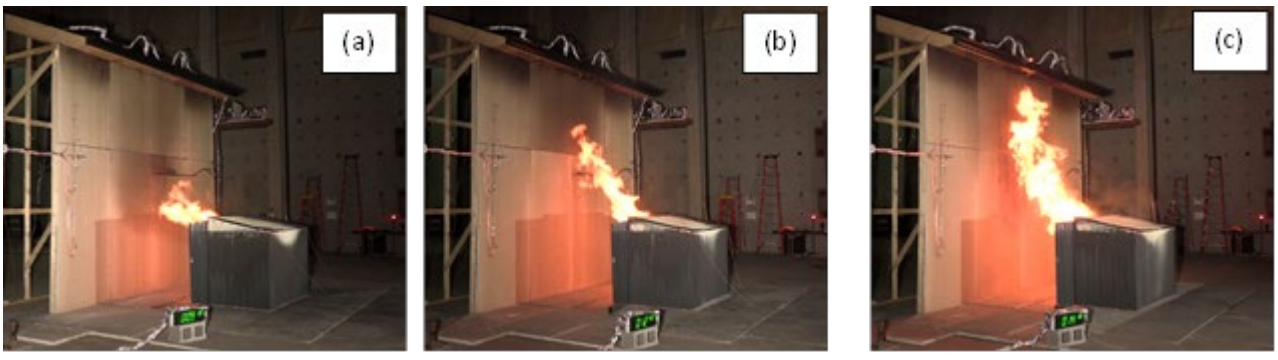

Fig 30. Images of Closet burn experiments showing the effect of fuel loading on flame jetting, where (a) is 2 cribs (e8), (b) is 3 cribs (e9), and (c) is 4 cribs (e10), at times corresponding to the peak HRR_{shed}. Note: Images are captured from the front diagonal camera location (camera 2).

The time-temperature profiles of the attic vent TC shown in Fig. 31 for three different levels of thermal exposures from a Closet placed at SSD of 5 ft, shows differences in the performance of

Vent A. Activation of the intumescent coating for Vent A does not occur for a lower thermal exposure from burning of two wood cribs in a Closet (e8). The temperature at the attic side of the vent remains below 250 °C, however, with increased thermal exposure from burning of three wood cribs, the intumescent coating was activated and approximately 50 % of the honeycomb cells were observed to be closed. No flames were observed to penetrate through the vent. However, temperatures on the attic side of the vent were recorded above the allowable temperature limit of 350 °C [7]. The thermal exposure from the burning of four cribs resulted in increased temperature on the attic side of the vent until the intumescent coating was activated. The temperature on the attic side of the vent first plateaued due to a partial closure of the vent and then suddenly increased. The vent cells reopened as the intumescent char that had closed the honeycomb cells collapsed due to local air flow. Flames were observed to penetrate the attic side of the vent. A peak temperature above 750 °C was recorded as the eaves ignited just before fire suppression was performed.

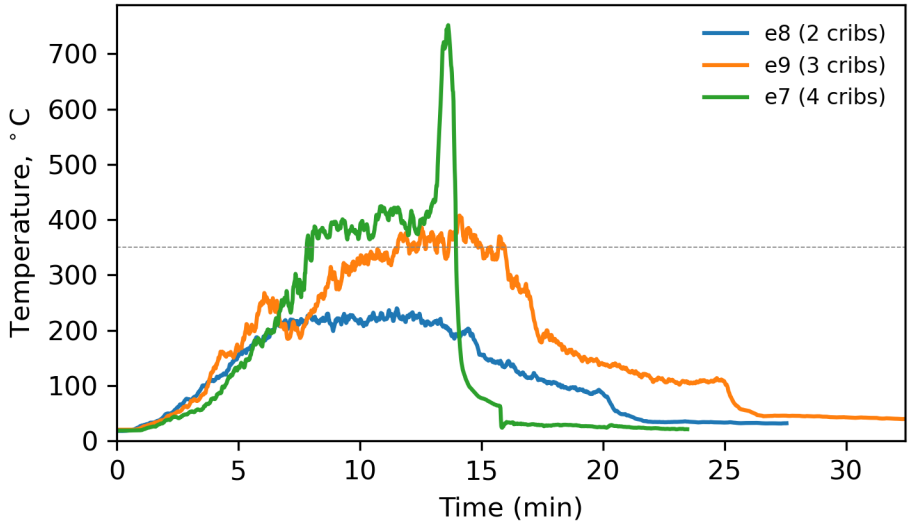

Fig. 31. Time-temperature profiles for temperature data measured by the attic vent TC for three different levels of thermal exposures from the Closet shed for Vent A (4 cribs (e7), 3 cribs (e9), and 2 cribs (e8)). Note: The dotted line shows the threshold temperature (350 °C) on the unexposed side of the vent as specified in the ASTM E2886 test method.

4.2.2.2. Narrow Shed

The effect of increased fuel loading for the Narrow shed on HRR data is shown in Fig. 32. The temporal profiles of HRR data for the Narrow shed with two, three, and four wood cribs show a plateau after an initial rise in HRR. The HRR for the Narrow shed with six wood cribs does not show a clear plateau in the temporal profile. The HRR continued to rise until the ignition of the eaves at approximately 18 min. The HRR decreased sharply upon the suppression of the fire. In cases where the ignition of the eaves did not occur, the HRR gradually decreased as the wood cribs were consumed in the fire. The total heat released (area under the HRR curves) is representative of fuel loading and increased linearly with increase in fuel loading.

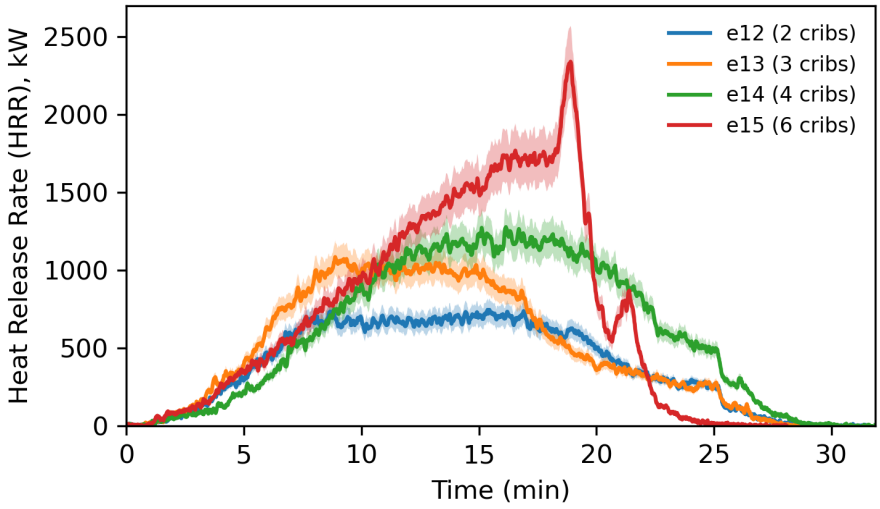

Fig. 32. The effect of increased fuel loading from 2 wood cribs (e12), 3 cribs (e13), 4 cribs (e14), and 6 cribs (e15) on the HRR data for the Narrow shed.

The HF profiles for HF1 (south bay 1, facing shed) measured in the eaves and the temperature data at the vent (both on the eave side and on the attic side) for the Narrow sheds in Fig. 33 and Fig. 34 respectively, show similar shapes as the HRR profiles.

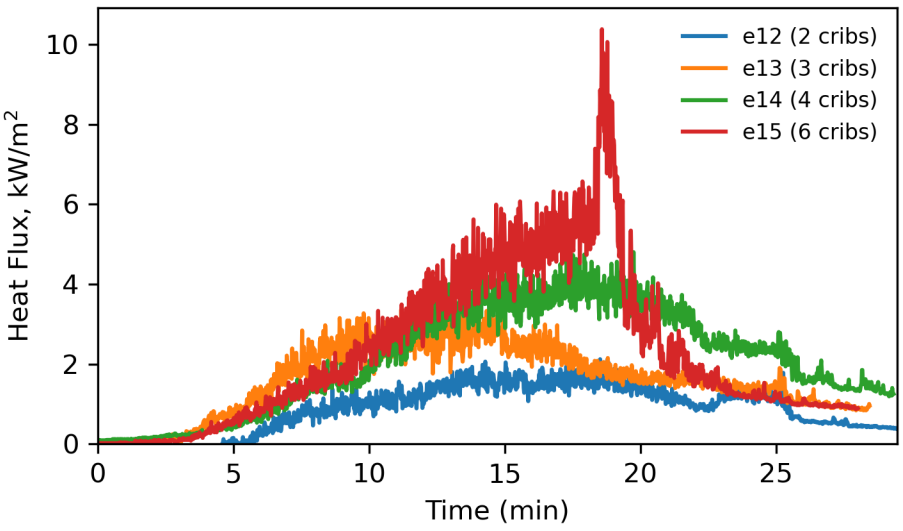

Fig. 33. The effect of increased fuel loading from 2 wood cribs (e12), 3 cribs (e13), 4 cribs (e14), and 6 cribs (e15) on the HF data for the Narrow shed from HF1 (south bay 1, facing shed).

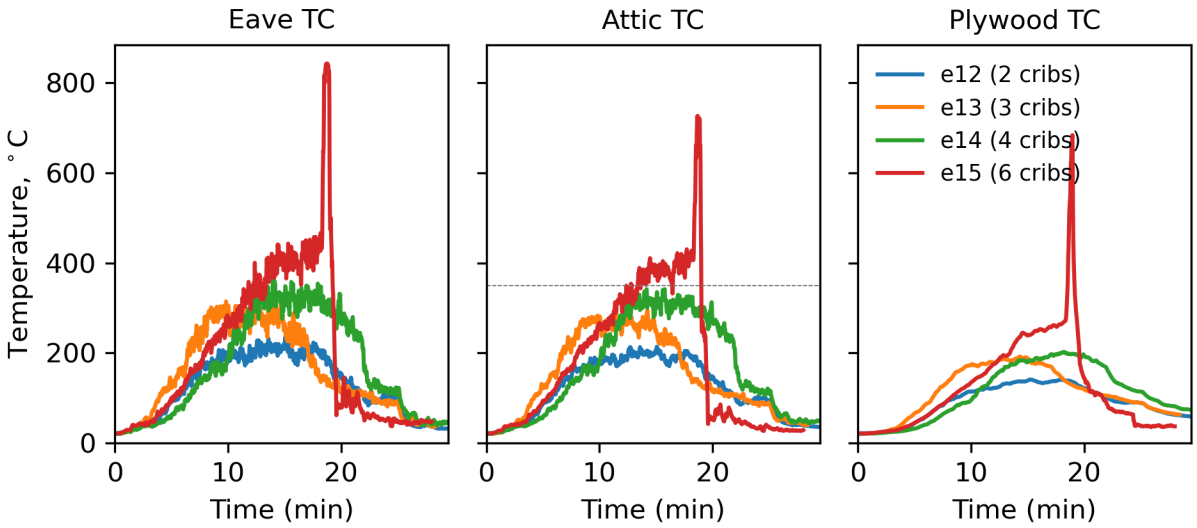

Fig. 34. The effect of increased fuel loading from 2 wood cribs (e12), 3 cribs (e13), 4 cribs (e14), and 6 cribs (e15) on the attic temperature measured by the eave vent, attic vent, and attic plywood TCs for the Narrow shed. Note: The dotted line shows the threshold temperature (350 °C) on the unexposed side of the vent as specified in the ASTM E2886 test method.

Figure 35 shows the images from four Narrow shed burn experiments showing the effect of fuel loading on flame jetting, at times corresponding to the peak HRR_{shed}.

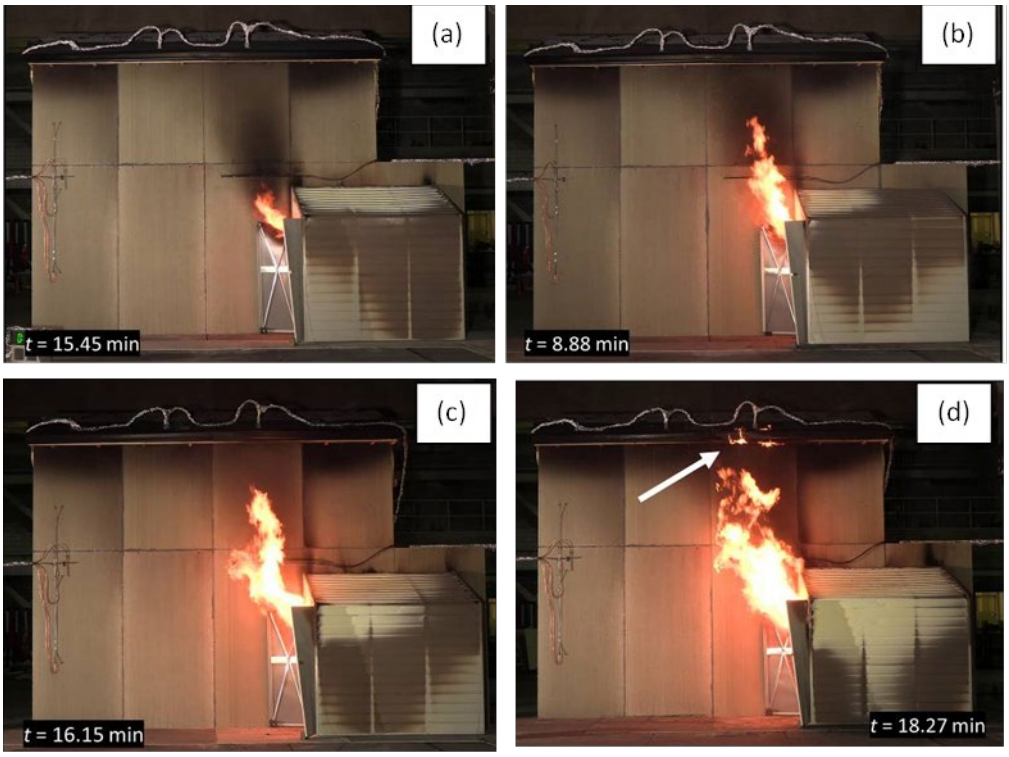

Fig. 35. Images of the Narrow shed burn experiments with (a) 2 wood cribs (e12), (b) 3 cribs (e13), (c) 4 cribs (e14), and (d) 6 cribs (e15) showing the effect of fuel loading on flame jetting, at times corresponding to the peak HRR_{shed}. Note: Images are captured from the front camera location (camera 1).

4.2.2.3. Very Small Shed

Only two levels of fuel loadings (4 and 6 wood cribs) were studied for the exposure from the Very Small shed. Temporal profiles of HRR for the Very Small sheds with 4 and 6 wood cribs are shown in Fig. 36. The initial gradual growth of the HRR for the two shed burns (e17 and e18) are very similar and within the experimental uncertainty of 9.8 %. The HRR profile for the Very Small shed with 4 wood cribs plateaus after 10 min from ignition of the cribs and the HRR peaks at 1.4 MW. However, ignition of the eaves is not seen for this thermal exposure. The HRR profile for the Very Small shed with 6 wood cribs shows a steady rise in heat release rate until the ignition of the eaves. A sudden drop in HRR following ignition of the eaves is due to the suppression of the fire.

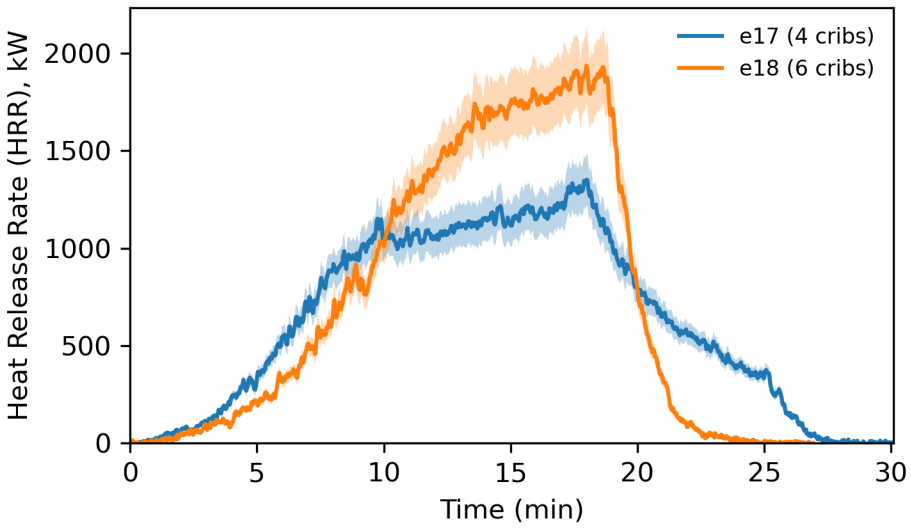

Fig. 36. Temporal profiles of HRR for the Very Small sheds with 4 (e17) and 6 (e18) wood cribs.

The HF profiles for HF1 (south bay 1, facing shed) measured in the eaves and the temperature data measured at the eave vent TC for the Very Small sheds in Fig. 37 and Fig. 38 respectively, show similar shapes as the HRR profiles. The temperature profiles for the attic vent side TCs are different for the two burns with different fuel loadings. This is due to differences in vent performance for a given thermal exposure.

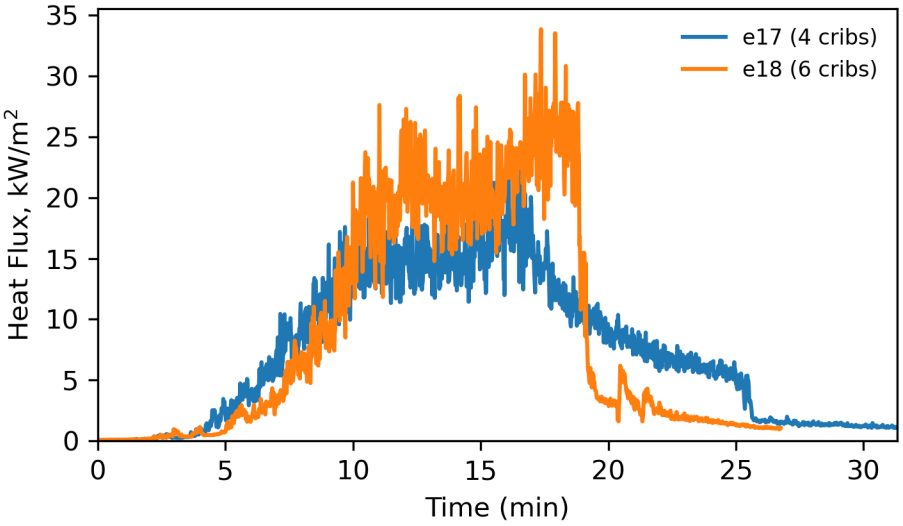

Fig. 37. The effect of increased fuel loading from 4 (e17) and 6 (e18) wood cribs on the HF data for the Very Small shed from HF1 (south bay 1, facing shed).

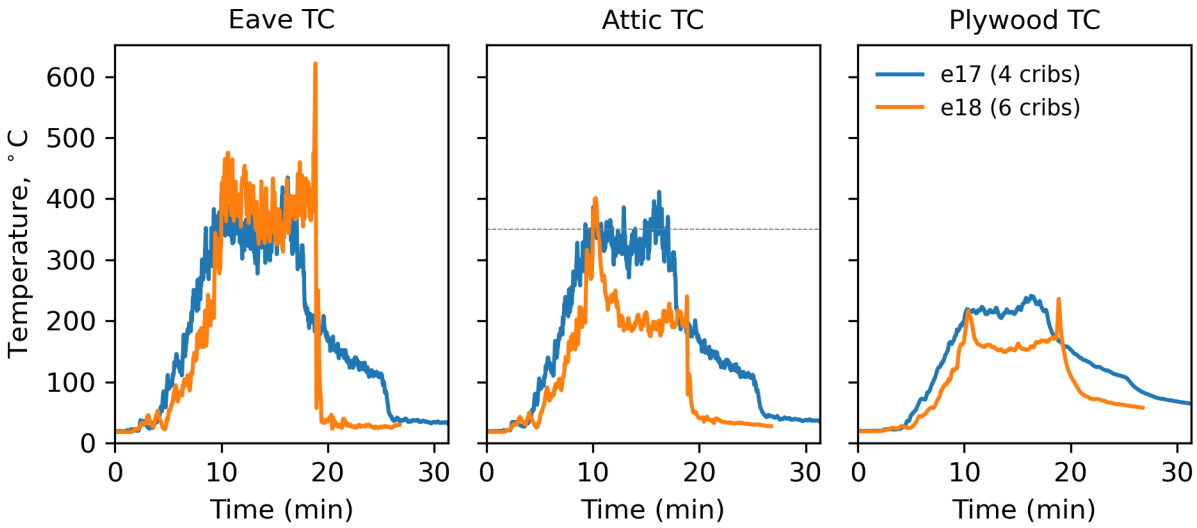

Fig. 38. The effect of increased fuel loading from 4 (e17) to 6 (e18) wood cribs on the attic temperature measured by the eave vent, attic vent, and attic plywood TCs for the Very Small shed. Note: The dotted line shows the threshold temperature (350 °C) on the unexposed side of the vent as specified in the ASTM E2886 test method.

Fig. 39 shows the images from two Very Small shed burn experiments showing the effect of fuel loading on flame jetting, at times corresponding to the peak HRR_{shed}.

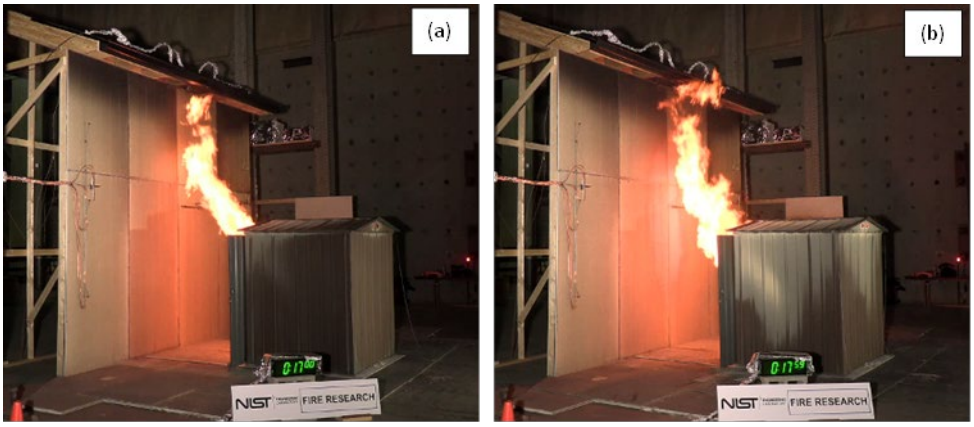

Fig. 39. Images of Very Small shed burn experiments showing the effect of fuel loading on flame jetting, where (a) is 4 cribs (e17) and (b) is 6 cribs (e18), at times corresponding to the peak HRR_{shed}. Note: Images are captured from the front diagonal camera location (camera 2).

4.2.3. Eave Performance

Eave performance was assessed in terms of ignitability for a given exposure. The thermal exposure from the burning shed was quantified in terms of peak heat fluxes measured in the eaves.

Experimental findings from the NISSE and NOSSE experiments suggested that heat fluxes of 15 kW/m^2 and above, sustained for at least 5 min, resulted in glowing ignition of the eaves. Flame contact for prolonged duration also played a major role in igniting the eaves. The data from the current experimental series support this threshold heat flux regardless of the shed type, door opening size, and the SSD. In experiments where the central heat flux gauges measured above 15 kW/m^2, steadily for several minutes, eave ignition occurred. However, when the heat flux remained consistently lower than 15 kW/m^2 or peaked at or above 15 kW/m^2 momentarily, an eave ignition did not occur.

In experiments where eave ignition occurred, a typical ignition pattern was observed. Glowing ignition was observed at three eave locations prior to flaming ignition. These thermally vulnerable locations where glowing ignition was noticed are highlighted in Fig. 40 and listed below:

1. the joint between the plywood along the underside of the roof and the fascia board
2. along the lower edge of the fascia board
3. along the lower edge of the rafters

It is also likely that the metal gutter obscured other locations of the fascia board thereby preventing visible glowing ignition in those locations.

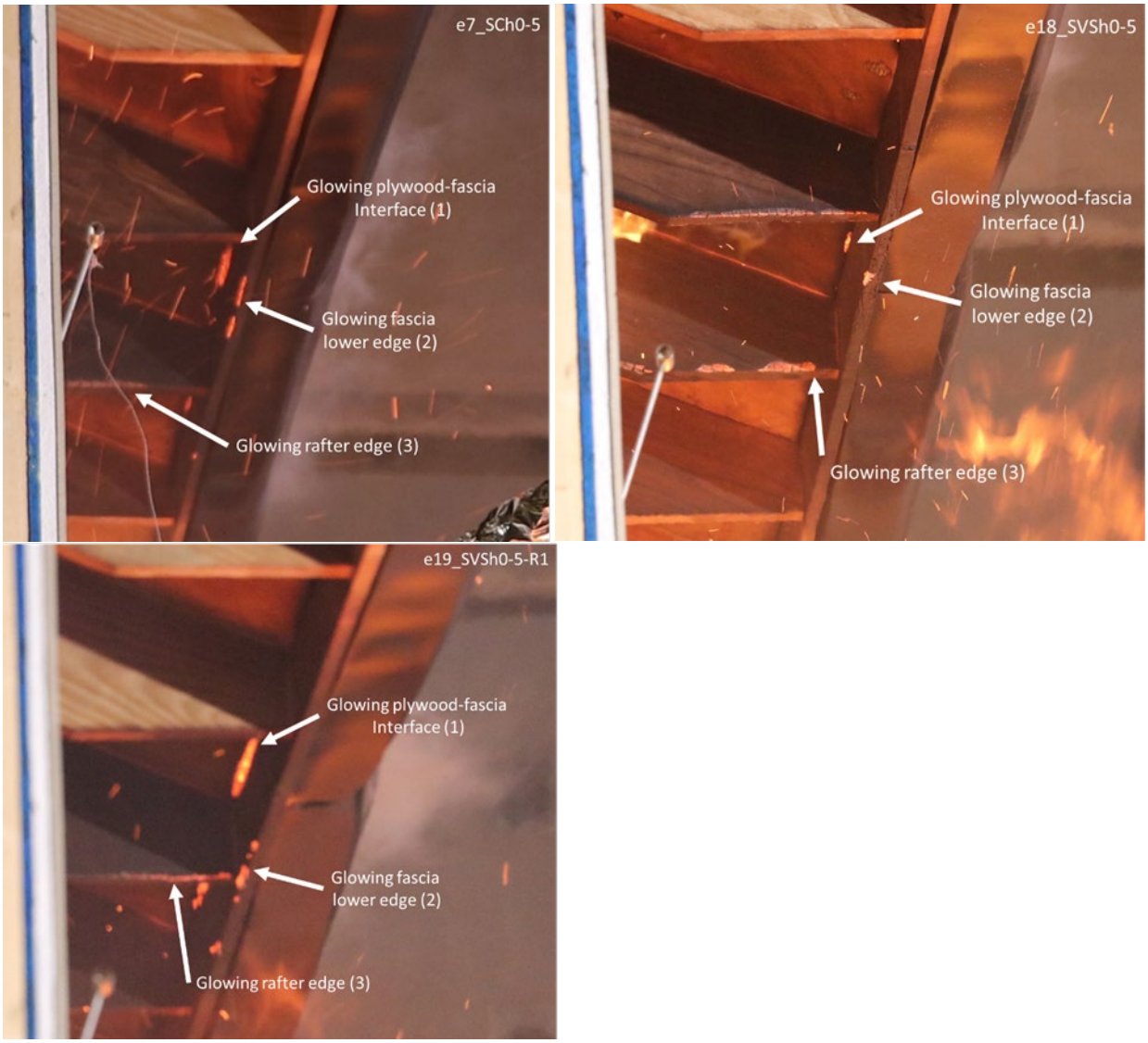

Fig. 40. Typical ignition sites observed in the eaves for three experiments (e7_SCh0-5, e18_SVSh0-5, e19_SVSh0-5-R1). Eave locations are numbered per the above list.

These repeated observations suggested that eave ignition is likely to occur at the sharp corners and/or edges of the wooden rafters and eaves. Experiment e10_SCh0-5-R1 was repeated as an exploratory experiment e11_SCh0-5-R2 with changes to the eave construction (Fig. 41). The rafter edges and the lower edges of the fascia board were rounded with a router to smooth the edges and corners, and high temperature caulk was applied throughout the eaves in addition to caulking around the vent. Rounding of the edges and corners rendered a minimally higher surface area when compared to sharp edges and corners. These changes may have contributed to the quicker ignition time for e11_SCh0-5-R2 when compared to e10_SCh0-5-R1 (see repeatability Fig. 12). The caulking of all wood joints throughout the eaves may have served to trap heat under the eaves and accelerate the eave ignition. The ignition origin was observed to

be different as a result of the changes, where ignition appeared to occur higher into the eaves at the plywood-vent interface instead of along the rafter and fascia edges.

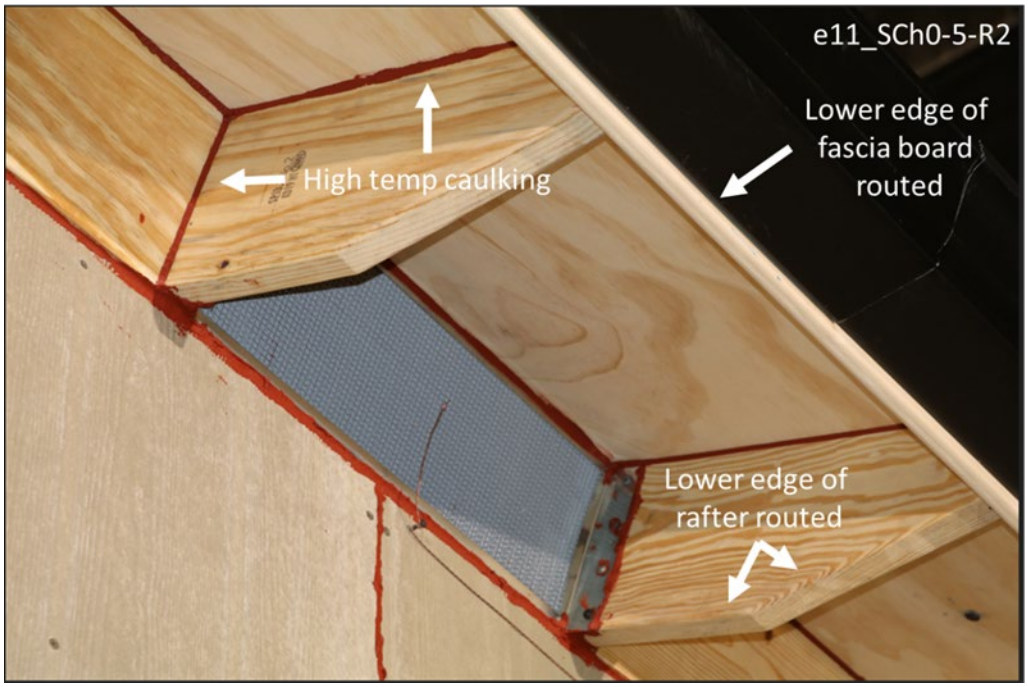

Fig. 41. Eave conditions for e11_SCh0-5-R2 with rounded rafter edges, rounded fascia board edges, and high temperature caulk applied throughout the eaves.

4.2.4. Vent Performance

Existing test methods to assess the performance of vents when exposed to embers and flames are described in Sec. 1.3. A vent must be able to resist ember and flame penetration on the unexposed side to comply with the requirements of IWUIC [6] as well as with Chapter 7A of the California Building Code [7]. Additionally, Section 706A of California Building Code (Chapter 7A) has a requirement that the maximum temperature on the unexposed side of the vent shall not exceed 350 °C.

This experimental series assessed the performance of three commercially available fire-resistant eave vents with much larger fire exposures (1.5 MW to 2.5 MW) compared to the fire exposure (300 kW) specified in the existing test methods (ASTM E2886). The vent performance was assessed primarily for flame penetration and temperature rise on the unexposed side of the vent.

Vent A and Vent B are listed as conforming to Chapter 7A of the California Building Code for residential construction in WUI areas (see Section 2.2.3 for vent details). The cores of Vent A and B were made of an aluminum honeycomb structure, coated with a proprietary intumescent material, encased within a galvanized metal casing, and covered with a fine metal mesh. The metal mesh prevents ember and pest penetration while the intumescence material forms a

char structure on the walls of the honeycomb which closes the cells and prevents hot gases and flame penetration. The operating mechanisms, materials, and the design of Vent A and Vent B are similar. However, Vent A and Vent B were from the same manufacturer but purchased years apart. Vent C uses intumescent coated baffles that are activated to close the openings in the vent.

In the case of the intumescent coated eave vents, vent performance is achieved primarily through the activation of the intumescent coating to close the vent openings. Closing the vent openings also assists in keeping the temperature on the unexposed, or attic side, of the vent below 350 °C. To quantify vent performance, the attic vent TC was used to measure temperature on the unexposed side of the vent. The flame penetration was monitored using visual and IR cameras on the unexposed side of the vent.

4.2.4.1. Vent Performance – Comparing Vent A and Vent B

As mentioned earlier, the operating mechanisms of Vent A and Vent B were similar. However, since the vents were purchased from two different manufacturing batches, the differences in vent activation and performance of intumescent char were noted.

Figure 42 compares the performance of Vent A and Vent B exposed to similar thermal exposure from burning six wood cribs placed in a noncombustible Very Small shed (5 ft SSD) with visible and IR images of the vents. A comparison of experimental parameters is provided in Table 9. The top images in Fig. 42 show the vents before the activation occurred. Small size embers enter the attic area in both cases. The insets show IR snap shots captured at the same time using a forward looking infrared (FLIR) camera. Preliminary qualitative analysis of IR images suggest that vent activation was not uniform. The bottom images in Fig. 42 show closure of vents, however, the IR images in the inset show spots where vent closure is not seen. While quantitative analysis of the IR images was not done for this study, the qualitative data where the red and the yellow color suggests higher temperatures and the blue and green represents colder areas indicate that vent activation was not uniform. Some cell openings were either not closed or they reopened due to structural collapse of the intumescent char. Flame penetration through the cell openings is shown in Fig. 43 for Vent A and Vent B.

Table 9. Comparison of e18_ SVSh0-5 and e19_ SVSh0-5-R1 with similar experiment conditions (VS shed, 6 cribs) but different vents.

Exp #	Vent	Fuel (kg)	Peak HRR_{shed} (MW)	Time to Vent Act (min)	Eave Temp at Vent Act (°C)	Attic Temp at Vent Act (°C)	Closure	Post Eave Ignition
e18	A	124.0	1.9	10.27	430	390	partial	flames
e19	B	112.9	1.8	9.45	402	344	partial	small flames

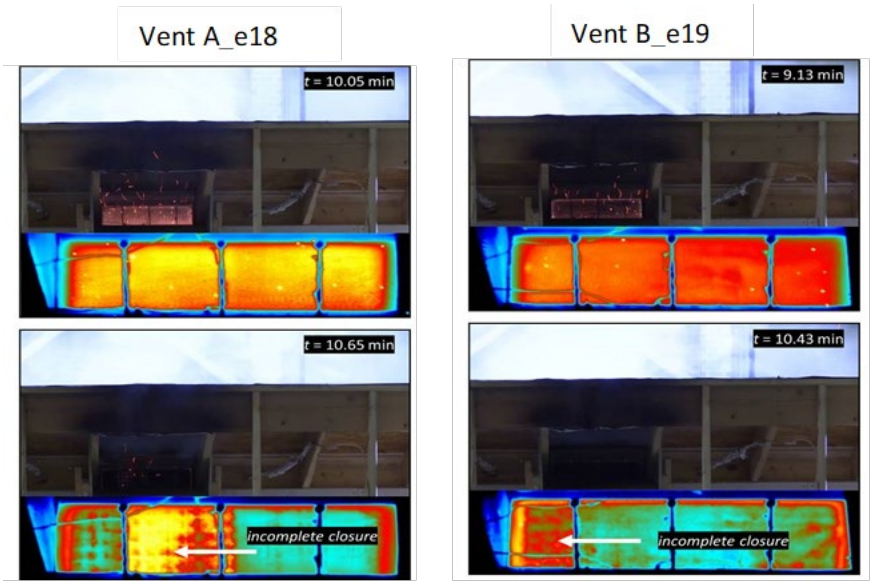

Fig. 42. Images showing Vents A and B before (top) and after (bottom) activation. Insets are IR images captured at the same time.

Fig. 43. Images showing flame penetration through Vent A and Vent B at the same thermal exposures.

Vent performance can also be studied by comparing the temporal plots of temperature measurements on the exposed and unexposed sides of the vent. Figure 44 compares temporal profiles of temperature data measured on the exposed (eave side of the vent) and unexposed (attic side of the vent) for Vent A and Vent B. The shift in the data is likely due to the difference

in fuel mass for the two experiments (e18 and e19). Temperature profiles on the exposed side follow the same pattern as the HRR and heat flux profiles. The temperature data on the unexposed side of the vent indicates differences in vent performance. In both experiments, the vents closed and a sharp decrease in temperature on the unexposed side of the vent is noted. Differences in the temporal profiles of temperatures recorded by attic vent TC for Vent A and Vent B can be attributed to the fact that the vent closure was not uniform, and temperature data is collected from a single point on the unexposed side of the vent. Neither vent closed completely, which allowed flames to penetrate through the vents and enter the attic plenum. A similar observation was made throughout the experimental series, where the intumescent coating did not activate fully for Vents A and B, leaving a non-activated vent section open allowing flames to enter the attic after eave ignition.

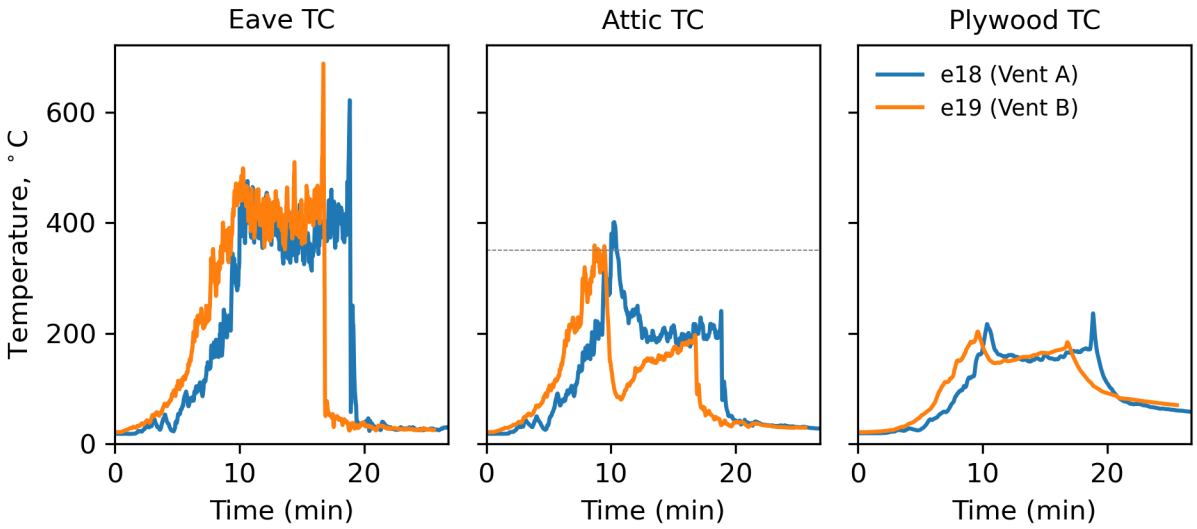

Fig. 44. A comparison of the eave vent, attic vent, and attic plywood TCs for a Very Small shed with 6 wood cribs with Vent A (e18) and Vent B (e19). The shift in the data is likely due to the difference in fuel mass. Vent activation occurred at a lower attic temperature for Vent B as seen in the attic vent TC plot. Note: The dotted line shows the threshold temperature (350 °C) on the unexposed side of the vent as specified in the ASTM E2886 test method.

4.2.4.2. Vent Performance – Comparing Vent A and Vent C

The experimental set up for assessing Vent A (intumescent coated honeycomb) and Vent C (intumescent coated baffles) were similar in terms of the exposure for five experiments listed in Table 10. In all five experiments the Closet was loaded with four wood cribs and the ignition of eaves occurred. Vent A failed to prevent flame penetration while Vent C was effective in keeping the flames from entering the attic side of the vent. Images in Fig. 45 (a) and Fig. 45 (b) show stages of vent closures for Vent A and Vent C, respectively. Figure 45 (a) shows vent closure with small flame penetration. However, the intumescent coating eventually failed and significant flame penetration occurred at t = 13.27 min. On the contrary, complete vent closure is seen in Fig. 45 (b) for Vent C and no flame penetration occurred. This difference in vent performance can be explained by comparing the temporal profiles of the temperature data.

Table 10. Comparison of Vents A and C with similar experimental conditions (Closet shed, 4 cribs).

Exp #	Vent	Fuel (kg)	Peak HRR_{shed} (MW)	Time to Vent Act (min)	Eave Temp at Vent Act (°C)	Attic Temp at Vent Act (°C)	Vent Closure	Post Eave Ignition
e7	A	89.5	1.3	8.22	418	376	Partial	flames
e10	A	93.1	1.4	7.7	376	339	Partial	flames
e11	A	96.9	1.4	8.95	402	358	Partial	flames
e20	C	76.2	1.4	7.2	289	231	Yes	no flame
e21	C	76.2	1.4	5.93	356	87	Yes	no flame

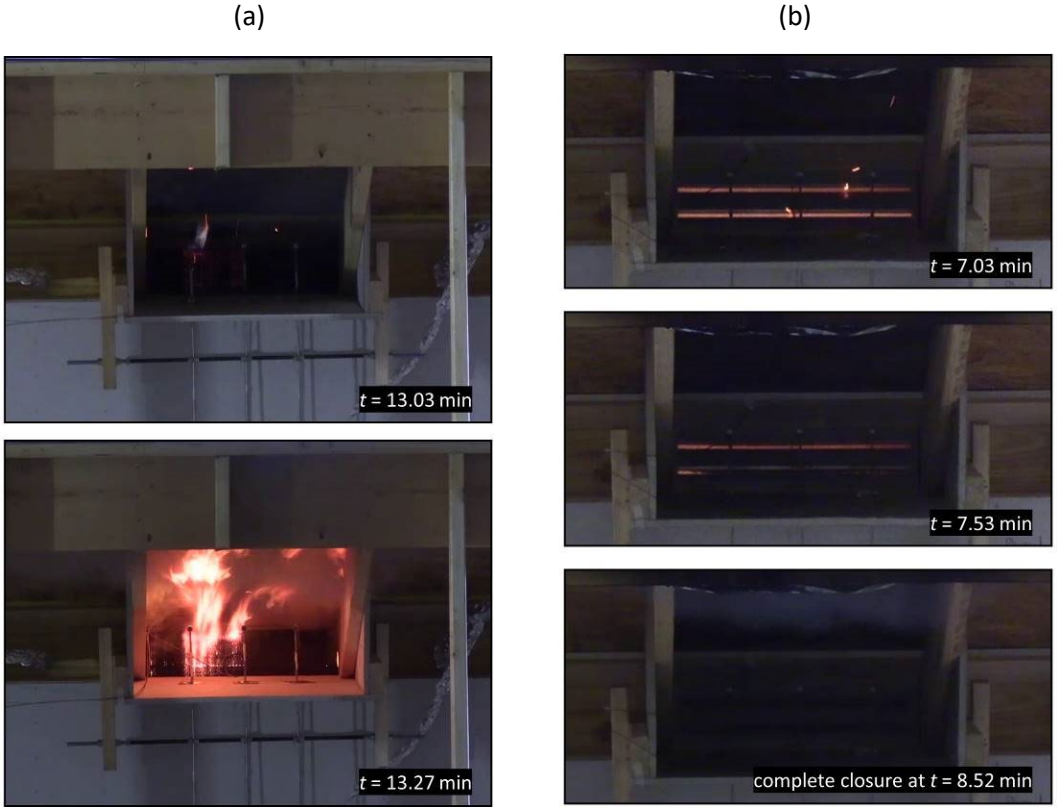

Fig. 45. Images showing vent performance following ignition of eaves: (a) Vent A and (b) Vent C.

Comparisons of the temporal profiles of temperature data measured for e7 and e20 at the exposed side of the vent (eave vent TC), unexposed side of the vent (attic vent TC), and in the plywood over the vent on the unexposed side (attic plywood TC) for Vent A and Vent C are shown in Fig. 46. While eaves ignition occurred in both experiments, the eave vent TC for e7 registered a peak temperature in excess of 900 °C and a peak temperature of 500 °C was measured for e20. The differences in the peak temperature measurement could be due to intermittent contact of flames with the target structure. However, these peak temperatures were sufficient to activate the intumescence and close the vent openings. As mentioned earlier,

the vent performance can be assessed by monitoring the temperature on the unexposed side of the vent (attic vent TC). The time-temperature curves in Fig. 46 (b) clearly show that Vent C performed significantly better than Vent A. Vent C was completely closed thereby preventing hot gases from entering the attic side of the vent. The peak temperature of 274 °C was measured on the unexposed side of the Vent C. The vent mechanism activated at the peak temperature and closed the vent for the remainder of the exposure period. The temperature on the unexposed side of the vent remained below 100 °C even while the eaves ignited.

The vent activation occurred at temperatures in excess of 400 °C for e7 (Vent A), thereby closing the vent. Visual observations from Fig. 45 (a) indicated that Vent A was partially closed. Temporal plots of temperature data measured on the attic side of the vent show that the temperature curve plateaued around 400 °C before it peaked at 750 °C due to eave ignition. This indicates that the intumescent coating in Vent A was activated but the formed char structure collapsed. This resulted in flame penetration and rise in temperature on the unexposed side in excess of 350 °C. Moreover, visual observations and IR videography confirmed flame penetration through Vent A.

Figure 46 (c) compares temperature data measured at the plywood on the attic side of the vent. The temperature for Vent C peaked at 125 °C during vent activation and remained around 100 °C or less thereafter, thus confirming superior vent performance. The temporal profile of the temperature data collected at the plywood on the unexposed side of Vent A has two peaks. The vent activation occurred at the first peak temperature of 217 °C. The temperature in the plywood decreased due to momentary closure of the vent which was followed by a sharp peak in temperature due to flame penetration. A peak temperature in excess of 600 °C was recorded, indicating ignition of the plywood. IR video of Vent A during the experiments indicated that the intumescent in the honeycomb cells did not close completely, allowing flames to penetrate through the vent and enter the attic plenum.

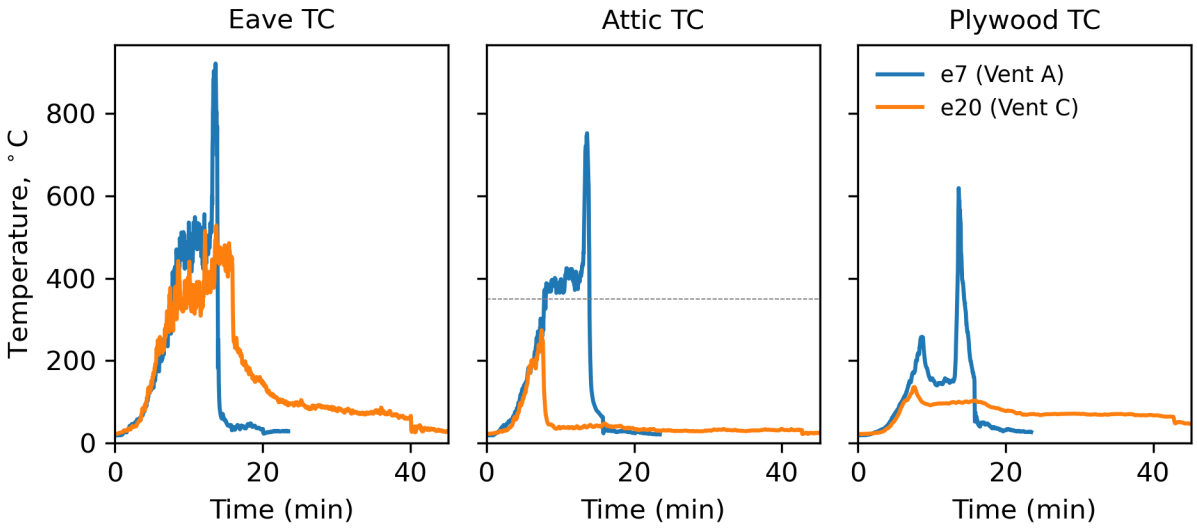

Fig. 46. A comparison of the eave vent, attic vent, and attic plywood TCs for a Closet shed with 4 wood cribs. Vent activation occurred, and was maintained, at a lower attic temperature for Vent C. The lower temperatures measured on the attic side of the vent indicated high vent performance. Note: The dotted line shows the threshold temperature (350 °C) on the unexposed side of the vent as specified in the ASTM E2886 test method.

5. Limitations

The experimental data serves as guidance for exposure quantification, hazard assessment and for hazard mitigation. However, the following limitations may affect the usability of the results.

Source Fire Limitations

1. The experiments only used noncombustible steel sheds with fuel loading of standard 1-A wood cribs as the source fire. The experiments did not use typical fuels stored in residential sheds that could result in an explosion such as gasoline or liquified petroleum gas due to safety concerns and potential damage to the surroundings. An explosion from a shed is likely to cause window breakages at a minimum.
2. The experiments were conducted on flat ground. The experiments did not study the effects of topography on flame spread or thermal exposures to the target structure.
3. The experiments used a limited number of shed sizes, orientations, and door openings with respect to the target structures.
4. The experiments were not conducted in the presence of additional fuels between the source fire and the target structure, such as ladder fuels, vegetation, fences, and vehicles.

Target Structure Limitations

1. The target structure is assumed to be hardened for ember exposures.
2. The experiments only used target structures that complied with the hardened requirements of SFM standard 12-7A-1 [7], SFM standard 12-7A-2 [7], and ASTM E2886 [5] as described in Chapter 7A of the California Building Code requirement [7].
3. The experiments only used single story target structures.
4. The experiments only used limited types of eave vents in the target structures.
5. The experiments simulated the target structures as a simple flat wall with no corners or other complex geometries.
6. The experiments did not evaluate the effect of weathering, cracking, or deterioration of the target structures.

6. Technical Findings

6.1. Eave Ignition and Vent Failure

EAVE TF1 - Thermal exposures from different types of sheds with different fuel loadings were found to be very repeatable when quantified in terms of heat release rate (mean absolute error < 60 kW) and heat fluxes (mean absolute error < 1.5 kW/m^2).

EAVE TF2 - In the case of noncombustible steel sheds, ignition of the eaves was a function of flame jetting and sustained incident peak heat flux at the eaves.

> **EAVE TF2.1** - Since the noncombustible shed itself did not burn while the contents were burning, flame jetting from the door opening was noted. Flame jetting was a function of fuel packing density, size and orientation of door opening of the shed with respect to the target structure. Higher fuel packing density resulted in focused flame jetting and increased the likelihood of an eave ignition.
>
> **EAVE TF2.2** - The same fuel loading in different types of sheds had different thermal exposures on the target structure. Fuel packing density also changed with the type of shed thereby affecting flame jetting and thermal exposure to the target structure.
>
> **EAVE TF2.3** - Thermal exposures to the target structure increased linearly with the fuel mass, however, the eave ignition was a function of flame jetting.

EAVE TF3 - Eave ignition started with glowing ignition in thermally vulnerable locations including sharp edges, corners, and joints.

EAVE TF4 – The current eave vent test methods may not adequately expose the eave vents to realistic WUI fire conditions. In the event of a real WUI fire, it is important to consider the performance of the entire wall and roof assembly and their combined contributions towards the eventual survivability of the target structure, not just a single element within the assembly. In several experiments (e10, e18, and e19), the eave vent activated and lowered the attic temperature as designed, however once the eave ignited, the vent was unable to prevent flames from penetrating into the attic. Therefore, effective hardening of the structure requires sufficient hardening to all elements; the assembly will only be as hardened as its weakest element.

EAVE TF5 - Amongst the vents tested in these experiments, the performance of the intumescent coated baffle vents was superior compared to the intumescent coated honeycomb core vents during very high thermal exposures.

> **EAVE TF5.1** - Intumescent coated honeycomb core vents used in these experiments that complied with ASTM E2886 and are listed as WUI-code-compliant products failed to prevent flame penetration when exposed to large thermal exposures, particularly when eave ignition occurred.
>
> **EAVE TF5.2** - Vent closure is not uniform and re-opening of the honeycomb cells occurred due to the collapse of intumescent char.

EAVE TF5.3 – The performance of vents with the honeycomb core varied from one batch to another.

6.2. Spectroscopy and Measurement Science

Throughout this experimental series, we successfully demonstrated the utility of open-path tunable laser absorption spectroscopy to retrieve path-averaged water mole fraction and gas-phase temperature in areas under the eaves and in the attic of the test structure. This approach offers a non-perturbing sampling scheme of an active fire environment. High data throughput was consistently achieved in the attic with more limited throughput observed in the eaves. This can be attributed to the difference in fire activity in the optical paths (e.g., the flame front, smoke, and particulate matter are more prominent in the eaves). Two key challenges that can reduce data throughput, as a result of signal loss at the photodetector, include 1) laser beam steering across thermal gradients and 2) laser beam scattering due to particulates in the air. Future experiments can pursue an increased acquisition rate or active alignment control to mitigate this signal loss.

A path-averaged approach, as demonstrated here, is advantageous for evaluating gas-phase characteristics over large physical distances. There are inherent limitations, however, in identifying discrete changes along the probed optical path. For example, vent activation during an experiment can limit flow through the vent, thus potentially impacting the observed mole fraction of water and gas temperature in that region. Since the vent region comprises approximately 6 % of the total attic optical path, changes due to an activation event would appear as fractional changes orders of magnitude smaller than the path-integrated signal. To better determine differences along the total path, layered spectral fitting approaches could be pursued [22] or broadband absorption spectroscopy techniques [23] could be implemented. Additionally, the existing open-path spectrometer design could be modified to probe a shorter physical distance across the test structure which would amplify any impact from changing vent conditions. Such modifications would support scenarios requiring more localized, simultaneous probing of two vent regions, like the structure displayed in e22.

Further, numerical simulations with Fire Dynamics Simulator (FDS) have shown that an enclosed attic space experiences a time-dependent trend for volume-averaged gas concentration (see Fig. 29 in [15]). This time-dependent effect, and subsequent changes imparted by vent activation, could be readily measured with the open-path laser system. The simulations also indicated that the gas fraction is nearly constant without an enclosed attic area, which is consistent with the target structure, and spectroscopic observations, in this experimental series.

6.3. Recommendation for Future Work

Future work will complete the assessment of other commercially available eave vents. This information may be used to enhance hazard mitigation and reduce structure ignitions either by revising the existing test methods or managing thermal exposures from auxiliary fuels and other exposures.

References

[1] Maranghides A, Nazare S, Link E, Prasad K, Hoehler M, Bundy M, Hawks S, Bigelow F, Mell W, Bova A, McNamara D, Milac T, Gorham D, Hedayati F, Raymer B, Frievalt F, Walton W (2021) Structure Separation Experiments Phase 1 Preliminary Test Plan. NIST Technical Note 2161. National Institute of Standards and Technology, Gaithersburg, MD. https://doi.org/10.6028/NIST.TN.2161

[2] Maranghides A, Nazare S, Link E, Hoehler M, Bundy M, Hedayati F, Gorham D, Monroy X, Morrison M, Mell W, Bova A, Milac T, McNamara D, Hawks S, Bigelow F, Raymer B, Frievalt F, Walton W (2022) Structure Separation Experiments: Shed Burns without Wind. NIST Technical Note 2235. National Institute of Standards and Technology, Gaithersburg, MD. https://doi.org/10.6028/NIST.TN.2235

[3] Maranghides A, Nazare S, Link E, Bundy M, Chernovsky A, Johnsson E, Butler K, Hawks S, Bigelow F, Mell W, Bova A, McNamara D, Milac T, Gorham D, Hedayati F, Raymer B, Frievalt F, Walton W (2022) NIST Outdoor Structure Separation Experiments (NOSSE): Preliminary Test Plan. NIST Technical Note 2199. National Institute of Standards and Technology, Gaithersburg, MD. https://doi.org/10.6028/NIST.TN.2199

[4] Maranghides A, Nazare S, Butler KM, Johnsson EL, Link E, Bundy M, Chernovsky A, Walton WD, Hawks S, Bigelow F, Mell W, Bova A, McNamara D, Milac T, Raymer R, Frievalt F (2023) NIST Outdoor Structure Separation Experiments (NOSSE) with Wind. NIST Technical Note 2253. National Institute of Standards and Technology, Gaithersburg, MD. https://doi.org/10.6028/NIST.TN.2253

[5] ASTM International (2020) *ASTM E2886 Standard Test Method for Evaluating the Ability of Exterior Vents to Resist the Entry of Embers and Direct Flame Impingement* (ASTM International, West Conshohocken, PA).

[6] International Code Council (2024) *2024 International Wildland-Urban Interface Code (IWUIC).* https://codes.iccsafe.org/content/IWUIC2024V1.0

[7] International Code Council (2022) *2022 California Building Code, Title 24, Part 2 (Volumes 1 & 2) with July 2024 Supplement updated, Chapter 7A Materials and construction methods for exterior wildfire exposure*. https://codes.iccsafe.org/content/CABC2022P4/chapter-7a-sfm-materials-and-construction-methods-for-exterior-wildfire-exposure#CABC2022P4_Ch07A_Sec706A

[8] National Fire Protection Association (2022) *NFPA 1140 Standard for Wildland Fire Protection (2022).* https://www.nfpa.org/codes-and-standards/nfpa-1140-standard-development/1140

[9] Standards Australia (2018) *AS 3959:2018 Construction of buildings in bushfire-prone areas.*

[10] ASTM International (2025) *ASTM E108 Standard Test Methods for Fire Tests of Roof Coverings* (ASTM International, West Conshohocken, PA).

[11] Underwriters Laboratory (2022) *UL 790 Standard Test Method for Fire Tests of Roof Coverings.*

[12] ASTM International (2017) *ASTM 2912 Standard Test Method for Fire Test of Non-Mechanical Fire Dampers Used in Vented Construction* (ASTM International, West Conshohocken, PA).

[13] ASTM International (2022) *ASTM E2257 Standard Test Method for Room Fire Test of Wall and Ceiling Materials and Assemblies* (ASTM International, West Conshohocken, PA).

[14] ASTM International (2022) ASTM E119 Standard Test Method for Fire Testing and Building Construction and Materials (ASTM International, West Conshohocken, PA).

[15] Brown CU, Maranghides A, Nazare S, Di Cristina G, Bailey DM, Fox L, Link E, Ramesh S, Monroy X, Miller JH, McCaughey EE, Flores MM (2024) NIST Eave and Vent Experiments (EaVE) EaVEs Phase A: Test Plan. (National Institute of Standards and Technology, Gaithersburg, MD), NIST Technical Note (TN) NIST TN 2288. https://doi.org/10.6028/NIST.TN.2288

[16] UL 711, 8th Edition, January 5, 2023 - UL Standard for Safety Rating and Fire Testing of Fire Extinguishers.

[17] Walton W. (1988) Suppression of Wood Crib Fires with Sprinkler Sprays: Test Results. NBSIR 88-3696, National Bureau of Standards, U.S. Department of Commerce.

[18] Di Cristina Torres G, Bryant RA (2024) Comparison of flow measurement devices for large fire experiments. NIST Technical Note 2285. National Institute of Standards and Technology, Gaithersburg, MD. https://doi.org/10.6028/NIST.TN.2285

[19] Bryant RA and Bundy MF (2019) The NIST 20 MW Calorimetry Measurement System for Large-Fire Research. NIST Technical Note 2077. National Institute of Standards and Technology, Gaithersburg, MD. https://doi.org/10.6028/NIST.TN.2077

[20] NIST Fire Calorimetry Database (FCD) https://doi.org/10.18434/mds2-2314

[21] Bailey DM, Adkins EM and Miller JH (2017). An open-path tunable diode laser absorption spectrometer for detection of carbon dioxide at the Bonanza Creek Long-Term Ecological Research Site near Fairbanks, Alaska. Appl. Phys. B 123, 245. https://doi.org/10.1007/s00340-017-6814-8.

[22] Bomse DS, Tso JE, Flores MM, J.H. Miller, (2020) Precision heterodyne oxygen-corrected spectrometry: vertical profiling of water and carbon dioxide in the troposphere and lower stratosphere, Appl. Optics, 55(7), B10-B17. https://doi.org/10.1364/AO.379684

[23] Malarich NA, Rieker GB (2021) Resolving nonuniform temperature distributions with single-beam absorption spectroscopy. Part II: Implementation from broadband spectra, *J. Quant. Spectrosc. Radiat. Transfer* 272, 107805. https://doi.org/10.1016/j.jqsrt.2021.107805

[24] Taylor BN, Kuyatt CE (1994) Guidelines for evaluating and expressing the uncertainty of NIST measurement results. NIST Technical Note 1297. National Institute of Standards and Technology, Gaithersburg, MD. https://doi.org/10.6028/NIST.TN.1297

[25] Maranghides A and Johnsson EL (2008) Residential Structure Separation Fire Experiments. NIST Technical Note 1600. National Institute of Standards and Technology, Gaithersburg, MD. https://doi.org/10.6028/NIST.TN.1600

[26] Gordon IE, Rothman LS, Hargreaves RJ, Hashemi R, Karlovets EV, Skinner FM, *et al.*, (2022) The HITRAN2020 molecular spectroscopic database, *J. Quant. Spectrosc. Radiat. Transfer,* 277, 107949. https://doi.org/10.1016/j.jqsrt.2021.107949

Appendix A. Uncertainty of Measurements

The measurements of heat release rate, heat fluxes, temperatures, times, gas and airflow velocities, and distances have associated uncertainties. Measurement uncertainties have several components that are typically grouped into two categories based on the method used to estimate their value. Type A uncertainties are evaluated by statistical methods, and Type B uncertainties are evaluated by other means, often based on scientific judgement using all available relevant information [24]. The component standard uncertainty includes resolution, calibration, installation, and random errors. The resolution is the minimum change in the data measurement the instrument can exhibit. Calibration error includes uncertainties from sensor calibration. The resolution and calibration uncertainties were derived from instrument specifications (Type B). Uncertainty due to the installation method was estimated based on engineering judgment (Type B) considering misalignment, quality of the sensor mounting method, and previous data.

Given the nature of experiments and hence the singular measurements in this study, the evaluation of Type A uncertainties was not feasible for the majority of measurements. Most uncertainties reported herein are Type B uncertainties, either estimated through scientific judgment or obtained from the literature.

Type K thermocouples used in these experiments have an inherent standard uncertainty for the temperature measurements reported by the manufacturer as ± 0.75 %. Additional uncertainties in measured temperature are primarily due to radiative heating and cooling of the thermocouple bead that causes it to respond to phenomena other than the surrounding gas temperature. Due to the nature of fire testing, the thermal environment surrounding a given thermocouple is difficult to characterize. These uncertainties will overwhelm the inherent uncertainties in the thermocouple described earlier.

The FLIR camera has a standard uncertainty of 2 °C (4 °F) or 2 % of the measured temperature. The uncertainties in temperature measurement using the IR camera may result from the emissivity value employed, reflected temperature, distance between the camera lens and the target surface, ambient temperature, transmittance, and calibration accuracy. The FLIR temperature measurements will be used qualitatively, and these additional factors will not be quantified.

The average expanded uncertainty in measuring the heat release rate in the normal operating range of the 20 MW (13.7 m x 15.2 m) hood for generic combustible fuels is 9.8 %. This uncertainty is valid for near steady state fires. Transient events (less than 30 s) may have more significant uncertainty because of system response time. Bryant and Bundy [19] provide detailed information on the NFRL calorimetry measurement system.

The nominal uncertainty for the bi-directional and S-probes are 4 % and 2 %, respectively [18].

The relative expanded uncertainty reported by the manufacturer for the heat flux gauges is ± 3 % of the gauge sensitivity (the slope of the calibration curve) with a coverage factor of 2. This would result in an uncertainty of about 4 kW/m^2 for a nominal reading of 140 kW/m^2. The main sources of uncertainty for the total heat flux measurements are: (1) the uncertainty of the

analog/digital conversion, (2) uncertainty in the calibration, and (3) uncertainty due to soot deposition on the sensing surface of the gauge [25].

The uncertainty in the A/D conversion is inherent to the data acquisition system. It is system-specific and is associated with the digitization of the analog signals from the gauge. This type of uncertainty is negligible. The uncertainty due to soot deposition is more challenging to quantify. The amount of soot deposition depends on many parameters, such as the location of the gauge, the flow field and temperature fields near the gauge, the duration of an experiment, and the soot volume fraction. No attempt will be made to quantify the soot effect on heat flux measurements for these experiments. Additional uncertainty due to flame impingement on the gauges is considered negligible.

The structure separation distances (SSDs) between the target wall and the source structure and the distance between the source structure and instrumentation including the heat flux gauge will be measured using a tape measure. Sources of uncertainty include the placement of the tape measure and the ability to adjust the positions of the source structure and sensors accurately. The construction dimensions are rounded to the nearest tenth. The expanded uncertainty for engineering measurements with a confidence level of 95 % was estimated as 1.2 cm (0.5 in). For longer tape measures, the expanded uncertainty was ± 2.54 cm (± 1 in).

The users of this report are advised to be informed that the experimental results presented in this report are either raw data or the statistics of raw data acquired by the measurement systems. Incorporating the measurement uncertainty reported herein into the validation of predictive models is highly recommended.

Appendix B. Measurement Verification Experiments for the 20 MW hood

Verification (confirmation) of the oxygen consumption calorimetry using fuel consumption calorimetry as a reference was conducted for the 20 MW hood immediately prior to these experiments using a calibrated natural gas burner. Two burns were conducted with increasing step changes in heat release from the burner.

For the first series, the burner was kept at a lower HRR range, up to approximately 5 MW to confirm that the larger hood was sensitive enough to detect the HRR at the lower range where the current experiments were anticipated. Five target values were chosen at the following HRR: 250 kW, 500 kW, 1 MW, 3 MW, and 5 MW. The graph in Fig. 47 shows the comparison of HRR determined by the gas flow rate (orange line) to the HRR calculated via oxygen consumption (black line). For the second series, the burner range was expanded through the full range of the hood, up to 20 MW. Five HRR targets were chosen at approximately the following HRR: 1 MW, 3 MW, 5 MW, 10 MW, and 20 MW. Results of the full scale HRR burns are plotted in Fig. 48. The temporal plots confirm that the two independent measurements of heat release, fuel consumption and oxygen consumption calorimetry, agree within the estimated uncertainty limits.

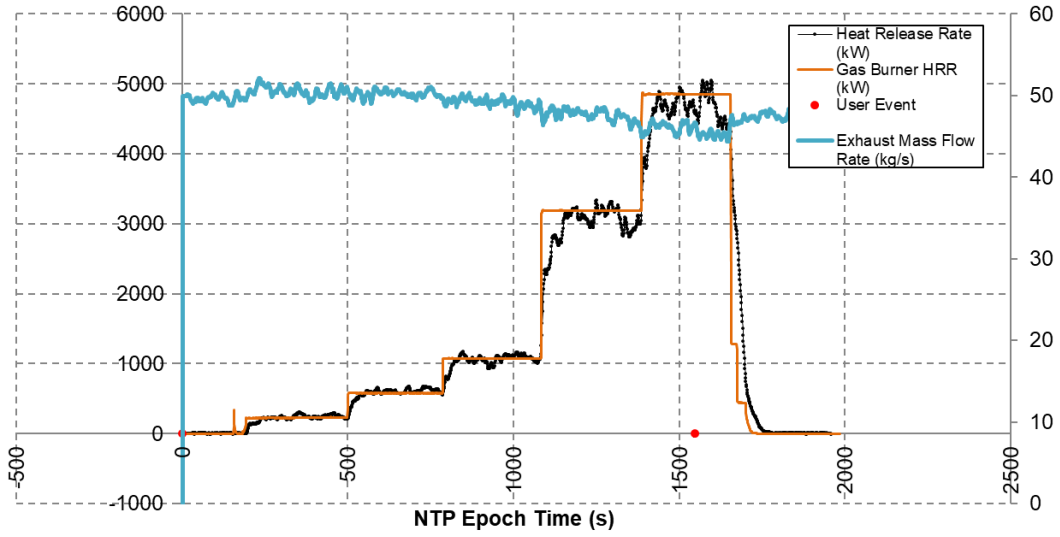

Fig. 47. Temporal plot of HRR by oxygen consumption (black) and fuel consumption (orange) calorimetry in the expected experimental range, up to 5 MW.

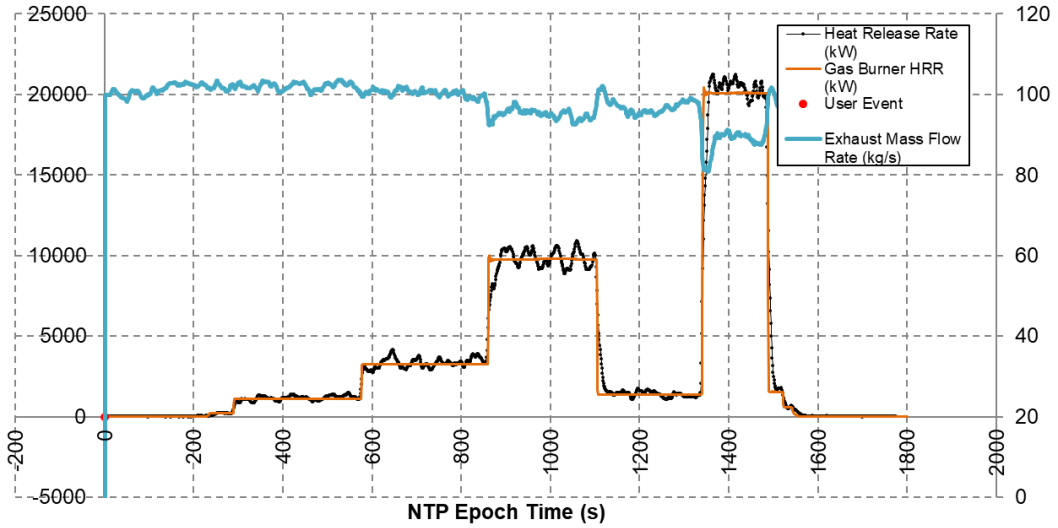

Fig. 48. Temporal plot of HRR by oxygen consumption (black) and fuel consumption (orange) calorimetry for the full range of operation, up to 20 MW.

Appendix C. Open-Path Laser Spectroscopy Results per Experiment

C.1. Spectral Acquisition

A fiber-coupled, near-infrared distributed feedback diode laser centered near 1393 nm was used to retrieve water vapor concentration and temperature in the laser's paths. The output wavelength was tuned via current to span 1393.70 nm to 1393.42 nm (7175.13 cm^{-1} to 7176.58 cm^{-1}) while the diode temperature was stabilized at 26.5 °C. A 50:50 fiber-optic splitter coupled laser light onto two, 10 m single-mode fiber patch cables to simultaneously transmit laser light in the elevated eave and attic paths. The intensity of laser light launched from the north platforms was monitored over time by fixed-gain photodetectors located on the south platforms. BNC cables relayed the photodetector output signal to a high-speed multichannel 12-bit digitizer. Data were collected at a rate of approximately 7 Hz (1 spectrum every 143 ms). Laser tuning and data acquisition were synchronized and automated using a custom python script.

C.2. Spectral Analysis

The spectral analysis procedure described here is illustrated in Fig. 49. To retrieve water vapor concentration and gas-phase temperature, the photodetector output signal must first be converted to absorbance using the following relation:

$$A = -\ln\left(\frac{I}{I_0}\right) \tag{C.1}$$

where A is absorbance, I is the intensity of transmitted laser signal when an absorbing molecule is present, and $I_0$is the intensity of transmitted laser signal when there is no absorber in the optical path. To calculate I0 across the tuning range, we performed a linear baseline fit using 15 points on either side of the photodetector output (I). Resulting experimental absorbance spectra are then fit with a spectral model which is calculated as:

$$A(v) = S(T) \cdot g(v, P, T) \cdot \rho(P,\ T) \cdot x_j \cdot \ell \tag{C.2}$$

where $S(T)$ is the molecular transition strength from the HITRAN database [26], $g(v, P, T)$ is the calculated line shape factor, $\rho(P,\ T)$ is the molecular density, x_j is the concentration of the target species, and ℓ is the optical path length. The path lengths for this experiment were 901.69 cm and 901.06 cm, for the eaves and attic paths, respectively. For the data presented here, a Voigt line shape profile was used.

To optimize the fit residuals, water mole fraction and temperature were allowed to float. Initial values for temperature were selected by using a pathlength-weighted average of data from auxiliary thermocouple sensors placed on the width of the structure (Table 4). Initial values for water mole fraction were calculated using the ambient humidity, temperature, and pressure in the experimental zone on the day of the experimental trial leveraging auxiliary ambient sensors placed in the National Fire Research Laboratory. During pre-processing, data files with a maximum photodetector throughput less than 1.0 V or non-linear baselines were excluded from further analysis.

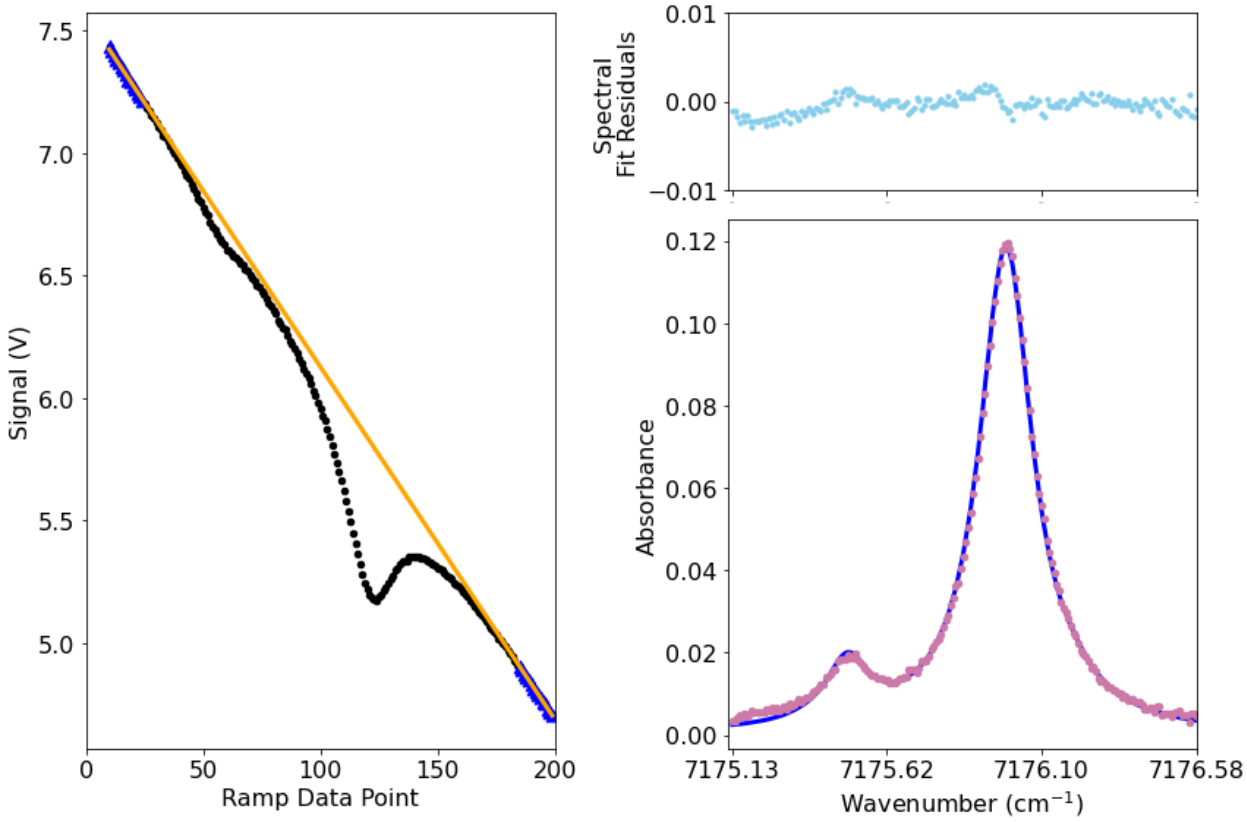

Fig. 49. Example spectral analysis from experiment e10. Left: Photodetector signal (black dots) with selected points for baseline fitting (blue triangles) and the calculated linear baseline (orange line). Right: Calculated absorbance signal (pink dots) and the best fit model (blue line) are shown in the lower panel with corresponding fit residuals in the upper panel. Fit results indicate a temperature of 296.51 K (23.36 °C) and a water mixing ratio of 0.62 %.

Appendix D. Preliminary Experiments (Source Structure Only)

A set of six preliminary experiments were conducted without the target structure to study burning behavior and test instrumentation. The three different steel shed styles were burned with a pre-determined number of 1-A wood cribs as the fuel load under the 20 MW calorimetry hood. These preliminary experiments facilitated determination of the effect of fire and heat on the operation of the open-path absorption spectrometer. This was also the first experimental burn of the Narrow shed. The burning behavior and flame jetting dimensions and characteristics were documented so that the Narrow shed could be positioned to direct the heat and smoke plume under the eave vent during the subsequent target wall experiments. This set of experiments also showed that the 20 MW calorimetry was capable of measuring heat release rates at the low end of its range.

Experimental Configuration

Preliminary burns were conducted in the same location as the subsequent main experiments. The overall configuration, illustrated in Fig. 50, was similar to that described in Sec. 2, with three primary differences.

1. The target wall was not used.
2. Three sets of heat flux gauges were positioned at 2 m, 3 m, and 4 m away from the shed door opening.
3. All shed doors faced west (including the Narrow shed, which was rotated 90° counterclockwise when placed with the target wall), positioned 1.5 m (5 ft) from the future target wall.

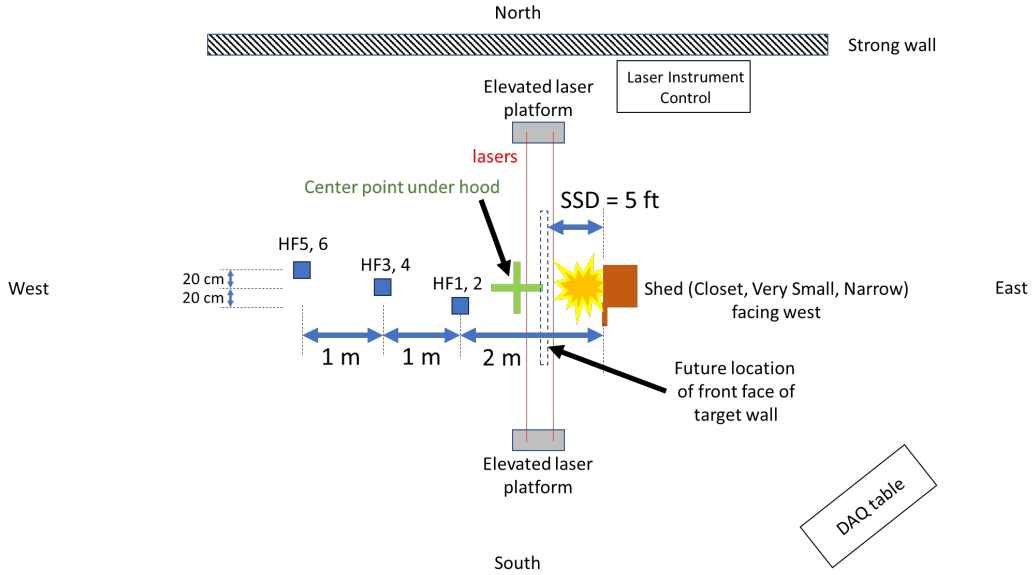

Fig. 50. Plan view of the preliminary experiment layout with the sheds facing the heat flux gauges (figure not to scale).

Data Acquisition and Instrumentation

Since the target structure was not included in the preliminary experiments, a limited number of measurements were made. Heat release rate was measured using the same calorimetry system (Sec. 2.4.4).

Six Schmidt-Boelter heat flux transducers faced the front of the shed door as shown in Fig. 51. Three metal stands held 2 heat flux gauges each, at heights of 1 m and 3 m from the floor. The closest stand with HFG 1 and 2, was approximately 2 m from the front face of shed, HFG 3 and 4 were 3 m from the shed, and HFG 5 and 6 were 4 m from the shed.

Fig. 51. Three heat flux gauge stands in front of the shed.

The data from HFG 2 was typically noisy, likely due to the heat plume causing the gauge to sway at the elevated position 3 m high during the experiments. Stiffening rods were added to the stands to reduce the noise but were minimally successful.

The open-path absorption spectrometer was tested to measure concentrations of H_2O and temperature in the same elevated location as if the target structure was in place. This instrument was used for a subset of the preliminary experiments (p1 and p2) to collect initial data, which allowed for instrument upgrades prior to the experiments.

Results

Table 11 lists the shed type, fuel loading, objective, and peak HRR of the six preliminary experiments. Additional results include observation of flame jetting dimensions from the Narrow shed, comparison of repeat configurations in the Very Small shed to results from previous NISSE burns, and initial findings from the open-path spectroscopy.

Table 11. Test matrix, objective, and peak HRR of preliminary experiments with no target wall.

Test ID	Shed Type	Fuel Load (1-A cribs)	Objective	Fuel Mass (kg)	Peak HRR (kW)	Time to Peak HRR (min)
p1_SNm0	Narrow	4	Observe flame jet location and height from Narrow shed with medium fuel load. Test the open-path spectroscopy system.	91	1351	14.2
p2_SVSh0	Very Small	6	Comparison to NISSE 1B-SVSh0. Test the open-path spectroscopy system.	144	2105	14.1
p3_SNl0	Narrow	2	Observe flame jet location and height from Narrow shed with low fuel load.	46	758	8.52
p4_SCl0	Closet	2	Comparison to NISSE 1B-SCl0.	48	976	8.4
p5_SNh0	Narrow	6	Observe flame jet location and height from a Narrow shed with high fuel load.	138	1897	18.3
p6_SVSl0	Very Small	4	Characterize a 4-crib fuel load in the Very Small shed, which had not been conducted during previous experiment series. Compare to the high fuel load in p2.	89	1518	14.6

Closet Shed

Preliminary experiment p4 was a repeat experiment from the previous experimental series with a Closet shed (Fig. 52). A fuel loading of two cribs was used. A peak HRR of 976 kW was recorded at 8.4 min for p4 compared to a peak HRR of 912 kW at 8 min in the previous experimental series [2].

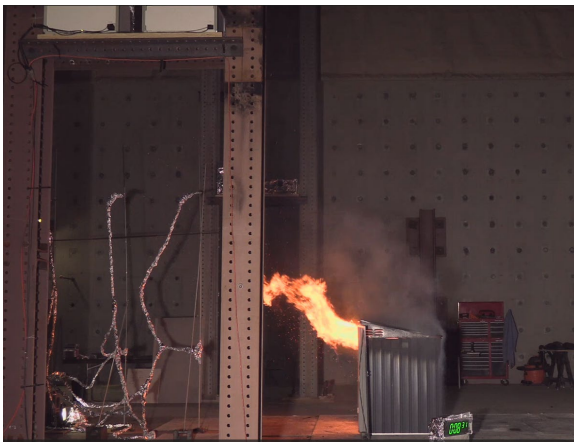

Fig. 52. Side view of experiment p4 at approximately maximum HRR.

Narrow Shed

The Narrow shed was a new type of shed that was not tested in a previous experimental series. Preliminary experiments p1, p3, and p5 provided an opportunity to observe and measure the burning behavior from this shed type with three different fuel loads. Figure 53 shows a comparison of the flame and plume jetting from the door near the time of peak HRR. After observing the smoke and plume position for the three different fuel loads, it was determined that the Narrow shed should be offset 1.2 m (4 ft) north from the target wall centerline so that the plume would be directed under the eave vent when the target wall was in place.

a) b) c)

Fig. 53. Side view of the flame jetting from the Narrow shed near the time of peak HRR with different fuel loadings, a) high (6 cribs), b) medium (4 cribs), c) low (2 cribs).

Very Small Shed

Preliminary burn p2 was a repeat burn of a Very Small shed with a fuel loading of 6 woods cribs tested in a prior series [2]. The peak HRR and the time to peak were consistent with previous results. In the case of p2, the peak HRR was 2105 kW at 14.1 min, compared to a previously recorded peak HRR of 2182 kW at 14 min.

Preliminary burn p6 with a new fuel loading of 4 wood cribs in the Very Small shed was not previously tested. The burn was conducted to measure the full HRR profile and to study the flame jetting. The maximum HRR was measured to be approximately 1518 kW at about 14.6 min after ignition of wood cribs.

In all cases, it was confirmed that a 5 ft SSD between the target wall and the shed would direct the flame to the eaves and vent. Figure 54 shows the view of the flame jetting at the time of peak HRR for burns p2 and p6.

a) b)

Fig. 54. Side view of experiments p2 and p6 at approximately maximum HRR.

Appendix E. Experiment Summary Sheets

This appendix includes two-page summary sheets that describe each experiment. The top of each summary includes the experiment ID; shed, fuel loading, and vent parameters; the objective of the specific experiment; and the status of the vent response. A representative photo is included to visualize the shed type, position, and a snapshot of fire behavior.

Four plots show the complete time history of measured values including heat release rate (HRR), heat flux at the eaves, temperatures at the vent, and air flow velocity through the vent. Vertical lines indicate when the vent began to activate (Actv) and when suppression was initiated (Supp). The data lines were not smoothed and illustrate the variability of the values as measured at a frequency of 1 Hz.

Tables list values of temperature and heat flux measurements at the time of vent activation. For the four experiments in which the vent did not activate (e8, e12, e13, e14), the maximum measured value is listed. Tabulated values were calculated using a 15 s average centered on the activation time. Values were rounded to the nearest whole number.

The time of occurrence of several key events is tabulated, listed in the most frequent order of events:

1. Start of vent activation: defined as the maximum negative rate of change in vent flow velocity measurement (after a 15 s smoothing filter was applied) and verified by visual review of IR video focused on the interior side of the vent.
2. Peak shed HRR (peak HRR_{shed}): defined as the maximum value of HRR measured before the eave ignition time.
3. Eave ignition: defined as sustained flaming at any point on the eave assembly, determined by visual review of video recordings from the front and side of the wall assembly.
4. Flames through vent: defined as sustained flaming on the interior side of the vent, determined by visual review of video recordings from the back side of the wall focused on the vent.
5. Suppression: defined as the first application of water to terminate the experiment, determined by visual review of video recordings.

The second page includes more detailed information about the observed key events. Sets of photos are included for several key events, prioritizing photos of vent activation, eave ignition, and flames through the vent. Photos of the peak HRR_{shed} are included if one of the other three events did not occur for that experiment. No photos at the start of suppression are included. Below each photo set is a plot of relevant measurements spanning one minute before and after the event time.

Vent Response: Partial Closure

EAVE_Phase_A_e7

Test ID: e7_SCh0-5
Date: 4/12/2024

WUI Eave Vent ID: A
Eave Ignition: Yes

Shed Material: Steel
Shed Type: Closet (18 ft^2)

Fuel Loading: High (4 × [1-A wood cribs])
Combustible Mass: 89.5 kg (197.3 lb)

Wind Speed: 0 m/s
SSD: 5 ft

Objective: To assess the performance of WUI Eave Vent A and quantify the heat exposure from 4 wood cribs in the closet style steel shed. This is the first experiment using these conditions. The closet was chosen first because it is the smallest shed. The high fuel load was chosen first because if the vent passed, then the lower fuel loads would not be necessary.

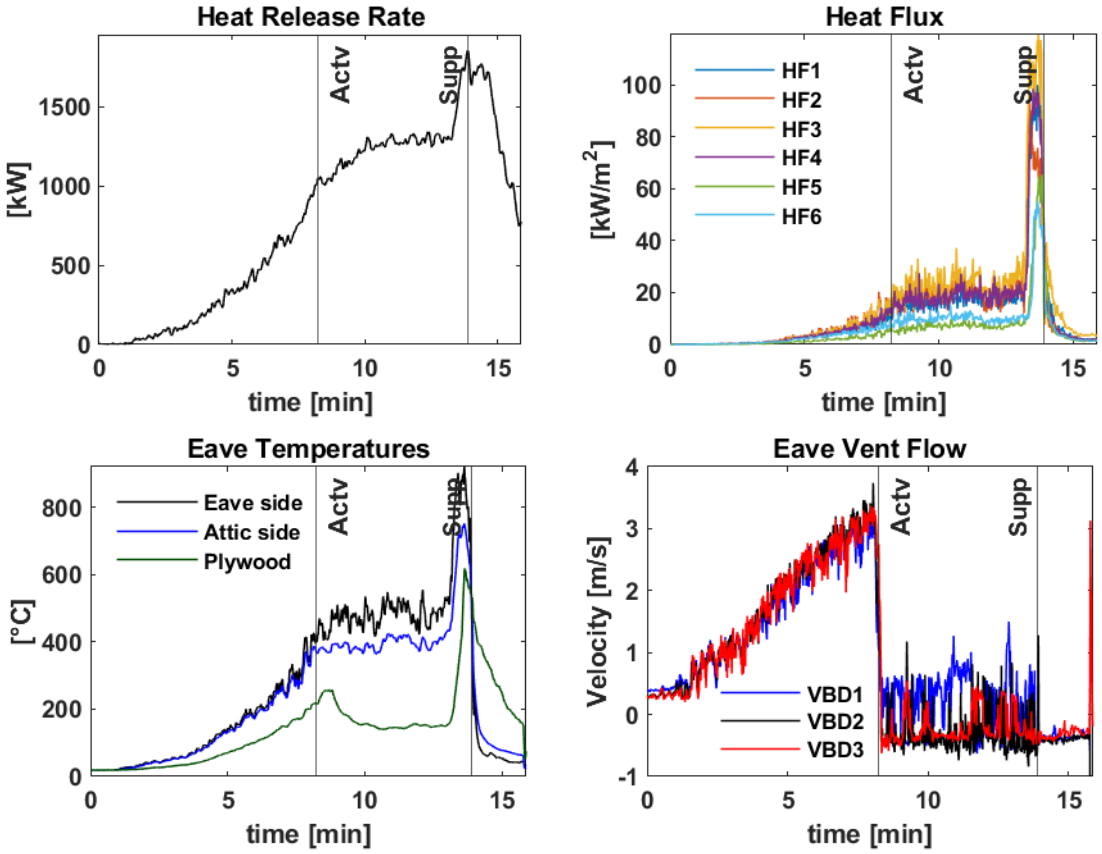

Temperature at Vent Activation

Location	(°C)
Vent – eave side	418
Vent – attic side	376
Attic plywood	217

Heat Flux at Vent Activation

Location	(kW/m^2)
HF 1 (S center, out)	11
HF 2 (N center, down)	16
HF 3 (N center, out)	17
HF 4 (S center, down)	14
HF 5 (N, out)	5
HF 6 (S, down)	7

Key Events (time after ignition)

Event	Time (min)
Vent activation begins	8.22
Peak shed HRR	12.37
Eave ignition	13.03
Flames through vent	13.03
Suppression	13.93

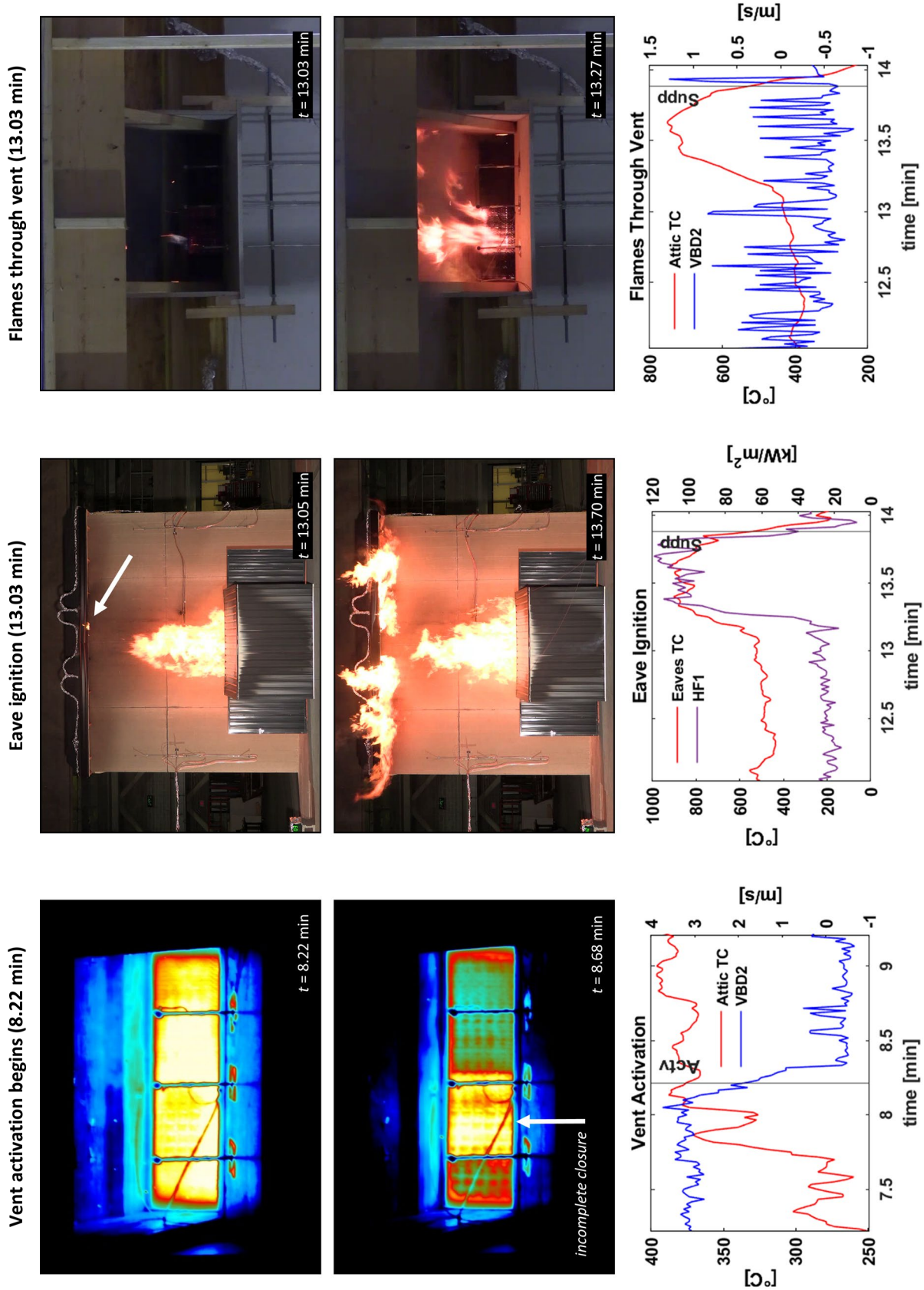
Vent activation begins (8.22 min)
Eave ignition (13.03 min)
Flames through vent (13.03 min)
t = 8.22 min
t = 8.68 min
incomplete closure
t = 13.05 min
t = 13.70 min
t = 13.03 min
t = 13.27 min
Vent Activation
Eave Ignition
Flames Through Vent
Attic TC
VBD2
Eaves TC
HF1
Supp
Activ
[°C]
[m/s]
[kW/m²]
time [min]

Vent Response: No Closure

EAVE_Phase_A_e8

Test ID: e8_SCl0-5
Date: 4/17/2024

WUI Eave Vent ID: A
Eave Ignition: No

Shed Material: Steel
Shed Type: Closet (18 ft^2)

Fuel Loading: Low (2 × [1-A wood cribs])
Combustible Mass: 39.4 kg (86.9 lb)

Wind Speed: 0 m/s
SSD: 5 ft

Objective: To assess the performance of WUI Eave Vent A and quantify the heat exposure from 2 wood cribs in the closet style steel shed. This is the first experiment using these exact conditions. These conditions were chosen because the closet with 4 cribs caused vent failure. Therefore, the 2 crib configuration was chosen to try to target the vent failure threshold.

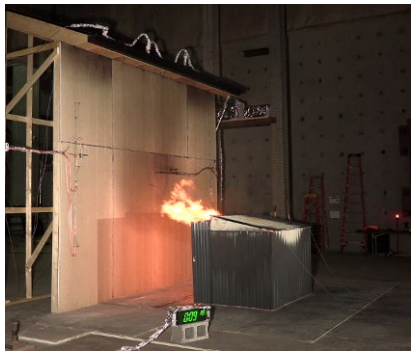

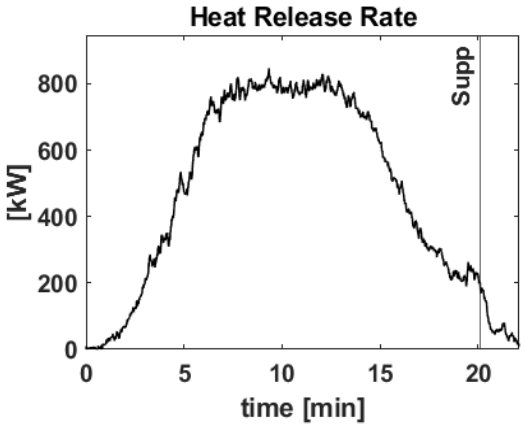

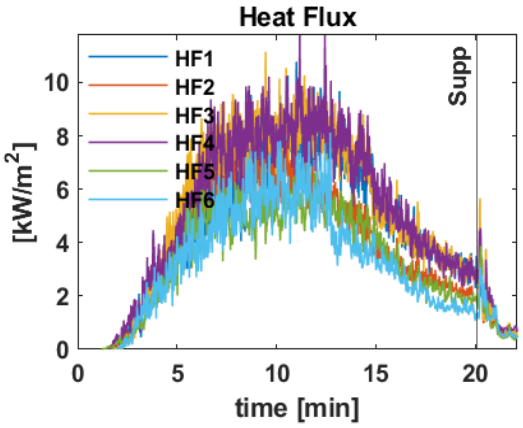

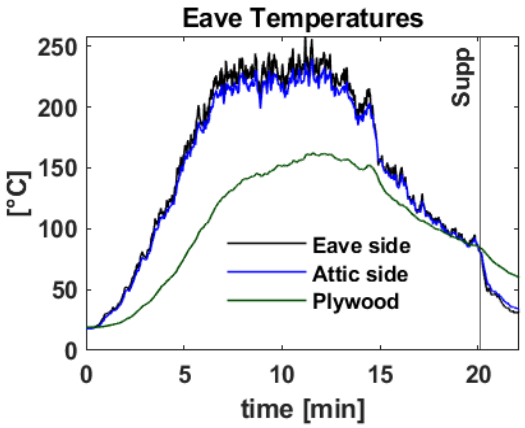

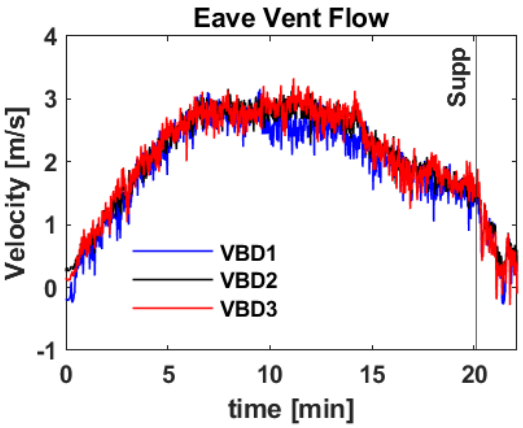

Maximum Temperature

Location	(°C)
Vent – eave side	258
Vent – attic side	240
Attic plywood	162

Maximum Heat Flux

Location	(kW/m^2)
HF 1 (S center, out)	11
HF 2 (N center, down)	9
HF 3 (N center, out)	11
HF 4 (S center, down)	12
HF 5 (N, out)	7
HF 6 (S, down)	8

Key Events (time after ignition)

Event	Time (min)
Vent activation begins	n/a
Peak shed HRR	9.33
Eave ignition	No
Flames through vent	n/a
Suppression	20.13

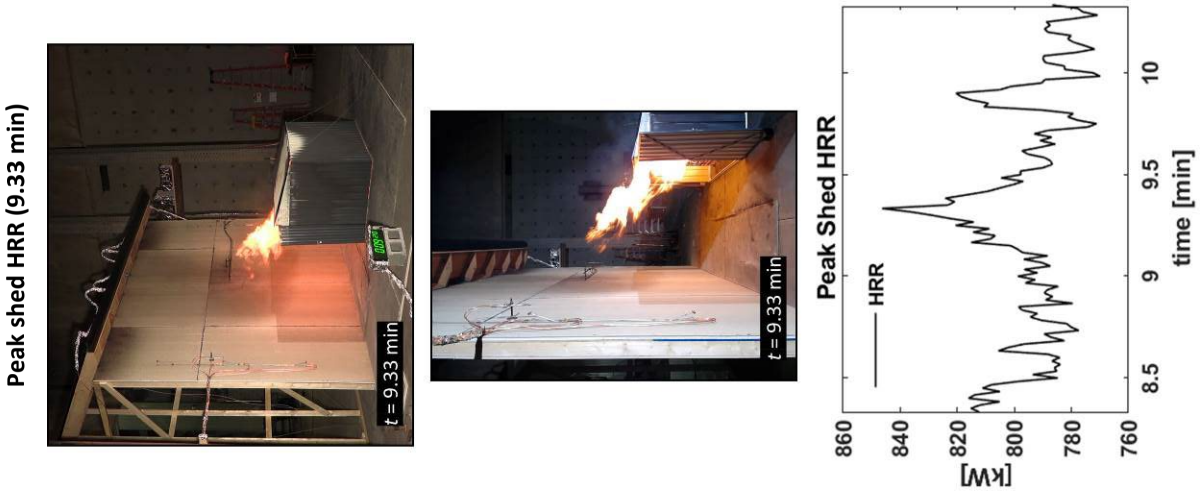
Peak shed HRR (9.33 min)
t = 9.33 min
t = 9.33 min
Peak Shed HRR
HRR
860
840
820
800
780
760
[kW]
8.5
9
9.5
10
time [min]

Vent Response: Partial Closure

EAVE_Phase_A_e9

Test ID: e9_SCm0-5
Date: 4/18/2024

WUI Eave Vent ID: A
Eave Ignition: No

Shed Material: Steel
Shed Type: Closet (18 ft^2)

Fuel Loading: Medium (3 × [1-A wood cribs])
Combustible Mass: 62.9 kg (138.7 lb)

Wind Speed: 0 m/s
SSD: 5 ft

Objective: To assess the performance of WUI Eave Vent A and quantify the heat exposure from 3 wood cribs in the closet style steel shed. These conditions were chosen because the closet with 4 cribs caused vent failure while the closet with 2 cribs did not. Therefore, the 3 crib configuration was chosen to establish the vent failure threshold.

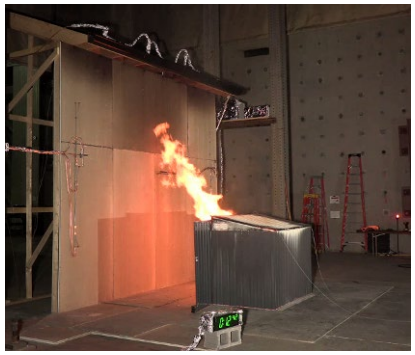

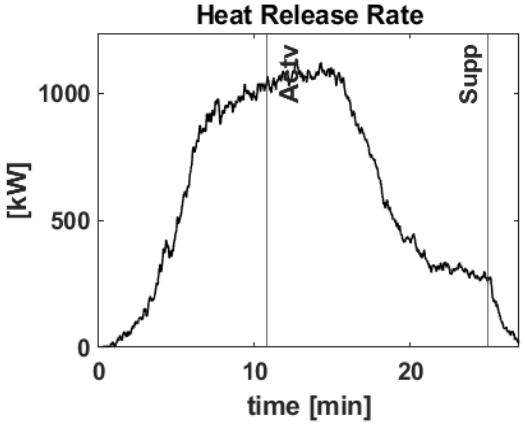

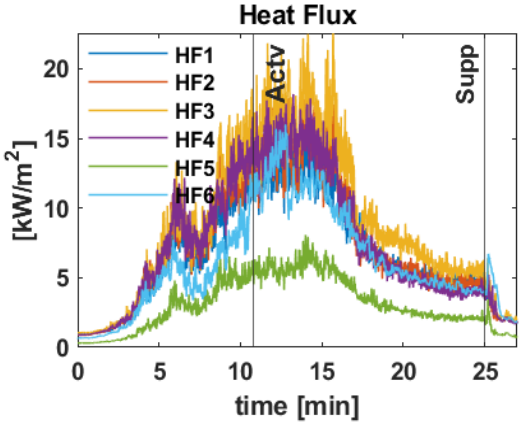

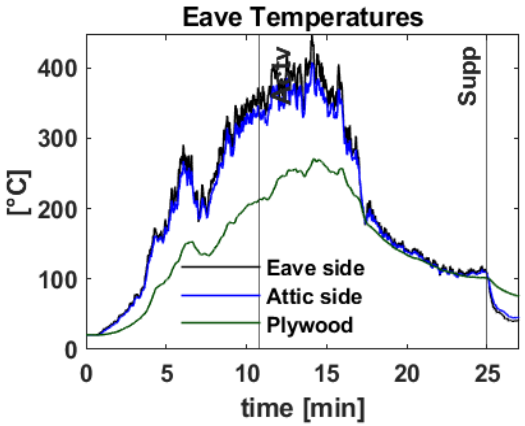

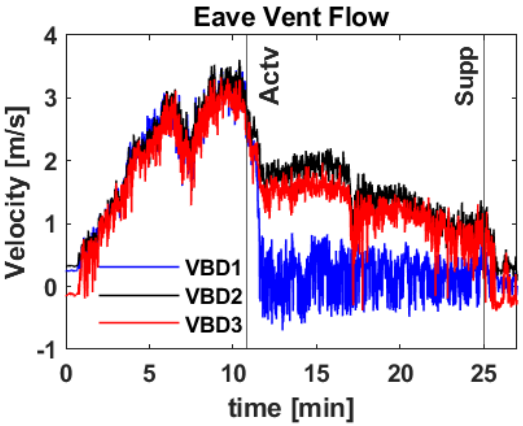

Temperature at Vent Activation

Location	(°C)
Vent – eave side	359
Vent – attic side	336
Attic plywood	212

Heat Flux at Vent Activation

Location	(kW/m^2)
HF 1 (S center, out)	12
HF 2 (N center, down)	13
HF 3 (N center, out)	15
HF 4 (S center, down)	14
HF 5 (N, out)	6
HF 6 (S, down)	11

Key Events (time after ignition)

Event	Time (min)
Vent activation begins	10.80
Peak shed HRR	12.68
Eave ignition	No
Flames through vent	n/a
Suppression	25.02

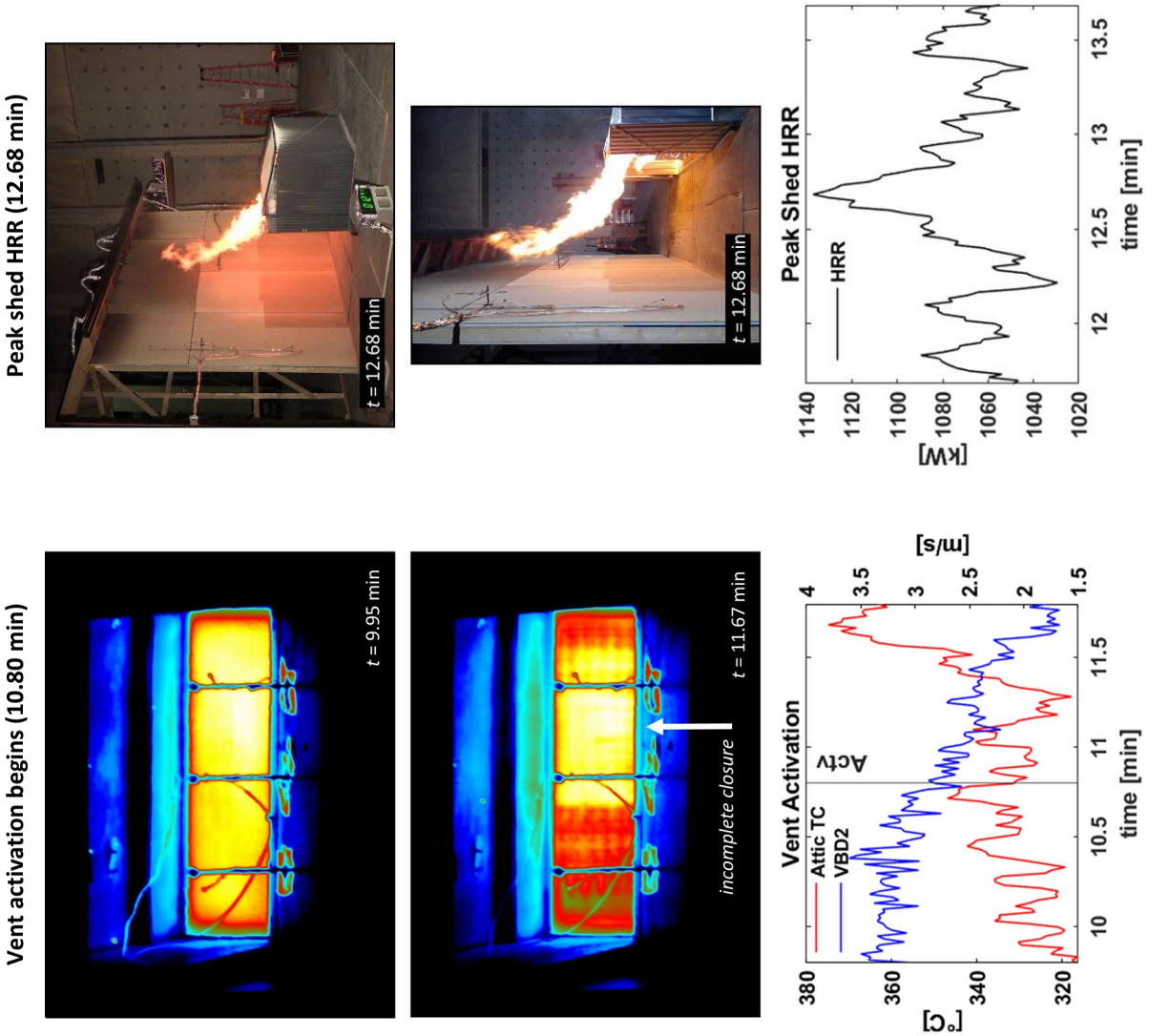
Vent activation begins (10.80 min)
t = 9.95 min
t = 11.67 min
incomplete closure
Vent Activation
Attic TC
VBD2
Activ
[°C]
[m/s]
time [min]
Peak shed HRR (12.68 min)
t = 12.68 min
t = 12.68 min
Peak Shed HRR
HRR
[kW]
time [min]

Vent Response: Partial Closure

EAVE_Phase_A_e10

Test ID: e10_SCh0-5-R1
Date: 4/23/2024

WUI Eave Vent ID: A
Eave Ignition: Yes

Shed Material: Steel
Shed Type: Closet (18 ft^2)

Fuel Loading: High (4 × [1-A wood cribs])
Combustible Mass: 93.1 kg (205.3 lb)

Wind Speed: 0 m/s
SSD: 5 ft

Objective: To assess the performance of WUI Eave Vent A and quantify the heat exposure from 4 wood cribs in the closet style steel shed. This is the 2nd experiment using these conditions (1st replicate), exactly the same configuration as e7, to compare the results to e7.

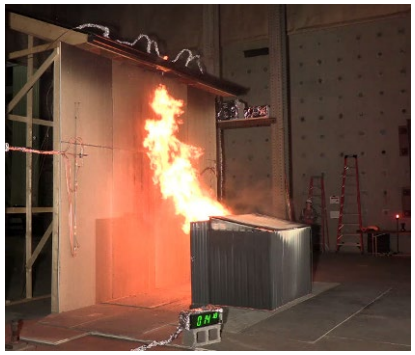

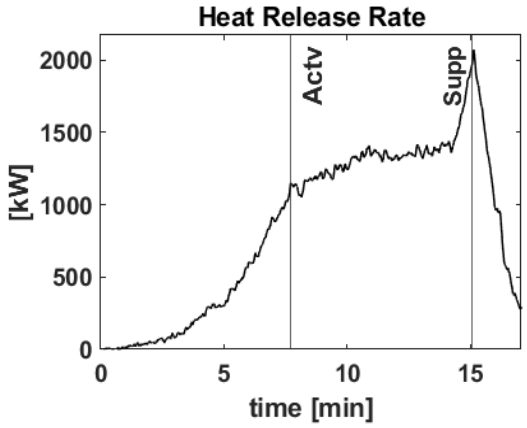

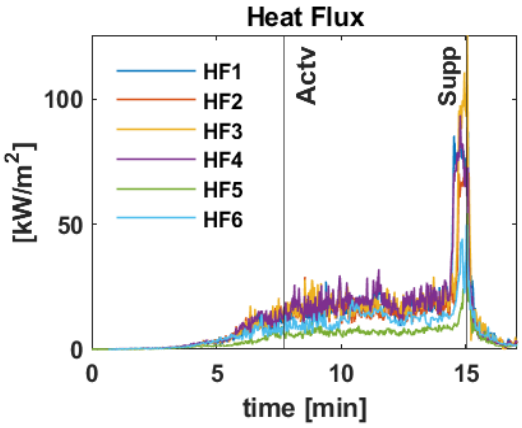

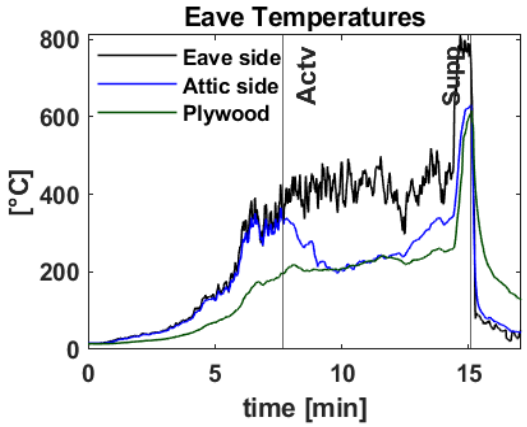

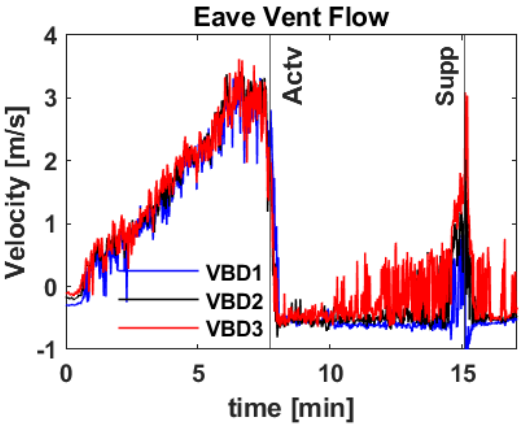

Temperature at Vent Activation

Location	(°C)
Vent – eave side	376
Vent – attic side	339
Attic plywood	197

Heat Flux at Vent Activation

Location	(kW/m^2)
HF 1 (S center, out)	13
HF 2 (N center, down)	14
HF 3 (N center, out)	14
HF 4 (S center, down)	14
HF 5 (N, out)	7
HF 6 (S, down)	9

Key Events (time after ignition)

Event	Time (min)
Vent activation begins	7.70
Peak shed HRR	12.85
Eave ignition	13.43
Flames through vent	14.40
Suppression	15.15

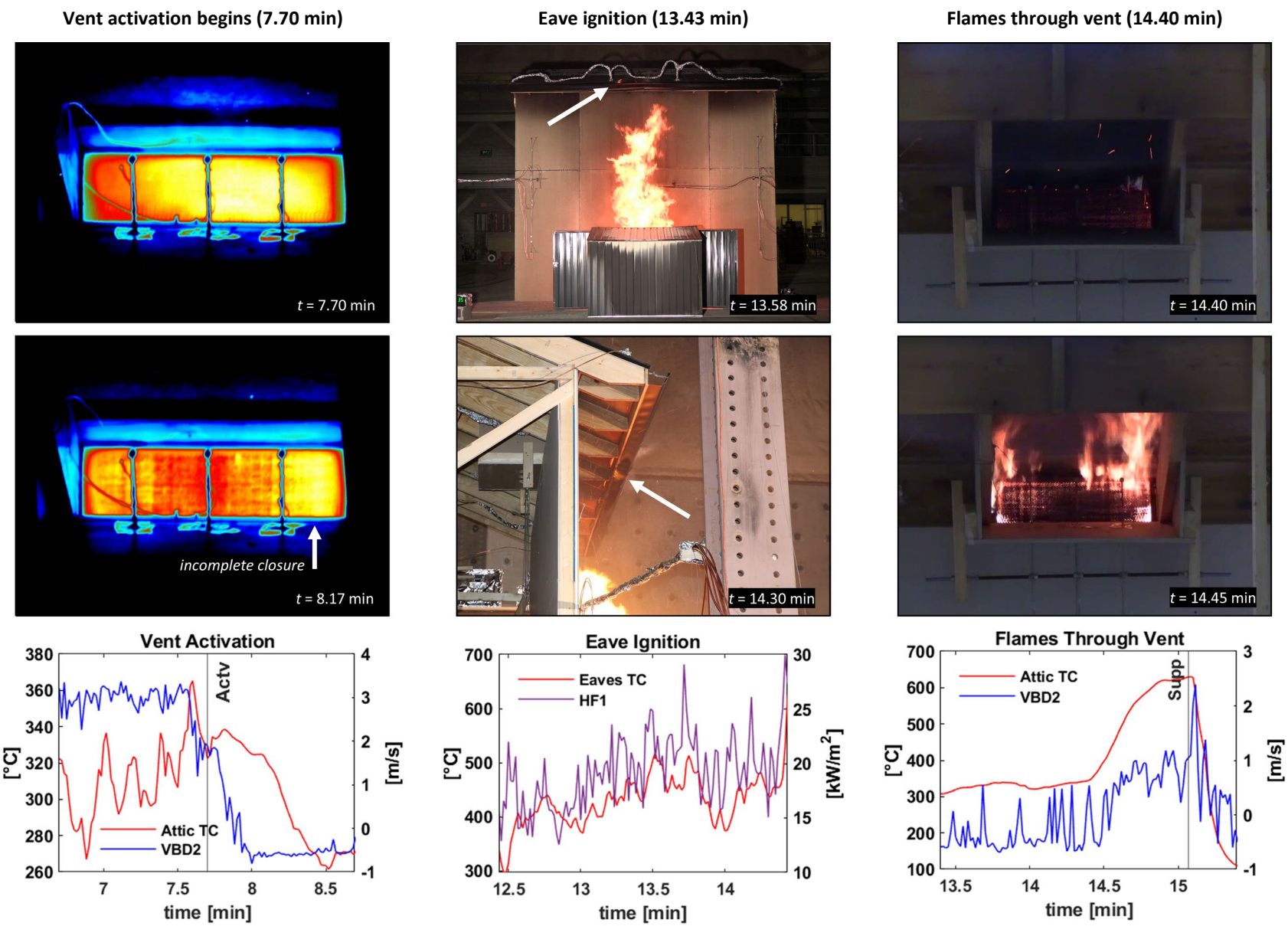
Vent activation begins (7.70 min)
Eave ignition (13.43 min)
Flames through vent (14.40 min)
t = 7.70 min
t = 13.58 min
t = 14.40 min
incomplete closure
t = 8.17 min
t = 14.30 min
t = 14.45 min
Vent Activation
Actv
Attic TC
VBD2
[°C]
[m/s]
time [min]
Eave Ignition
Eaves TC
HF1
[°C]
[kW/m²]
time [min]
Flames Through Vent
Supp
Attic TC
VBD2
[°C]
[m/s]
time [min]

Vent Response: Partial Closure

EAVE_Phase_A_e11

Test ID: e11_SCh0-5-R2
Date: 4/25/2024

WUI Eave Vent ID: A
Eave Ignition: Yes

Shed Material: Steel
Shed Type: Closet (18 ft^2)

Fuel Loading: High (4 × [1-A wood cribs])
Combustible Mass: 96.9 kg (213.6 lb)

Wind Speed: 0 m/s
SSD: 5 ft

Objective: This is the 3rd experiment using these conditions (2nd replicate), exactly the same configuration as e7 and e10. However, the exposed edges of the rafters and the lower two edges of the fascia board were routed. Red fire barrier caulk was used on all seams under the overhang.

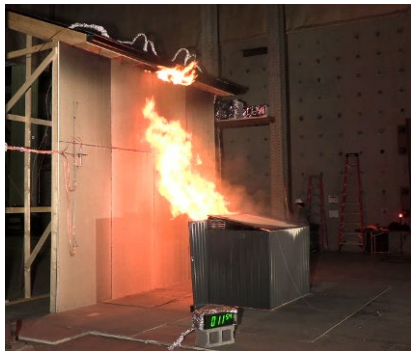

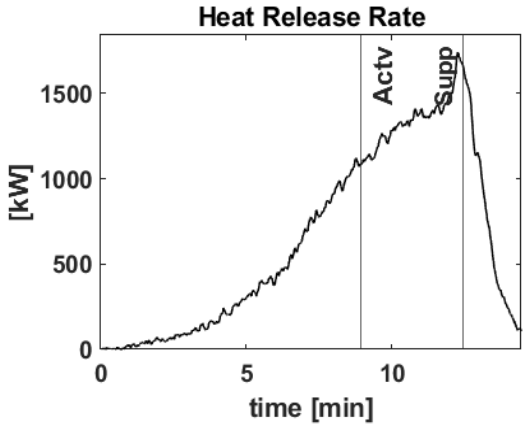

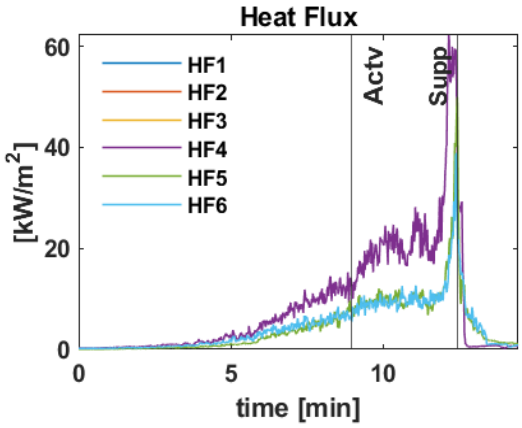

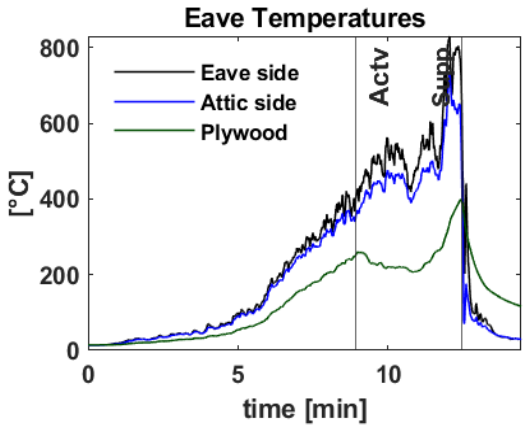

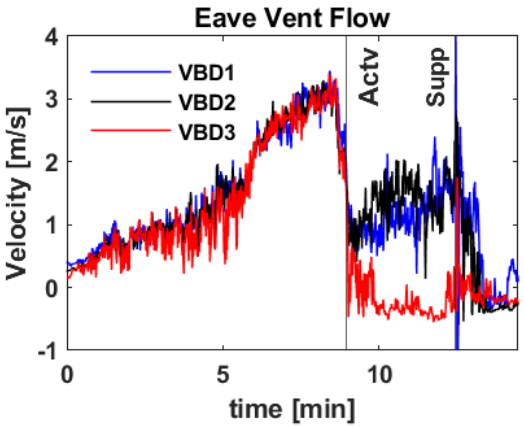

Temperature at Vent Activation

Location	(°C)
Vent – eave side	402
Vent – attic side	358
Attic plywood	253

Heat Flux at Vent Activation

Location	(kW/m^2)
HF 1 (S center, out)	n/d
HF 2 (N center, down)	n/d
HF 3 (N center, out)	n/d
HF 4 (S center, down)	13
HF 5 (N, out)	8
HF 6 (S, down)	7

Key Events (time after ignition)

Event	Time (min)
Vent activation begins	8.95
Peak shed HRR	11.02
Eave ignition	11.28
Flames through vent	11.27
Suppression	12.47

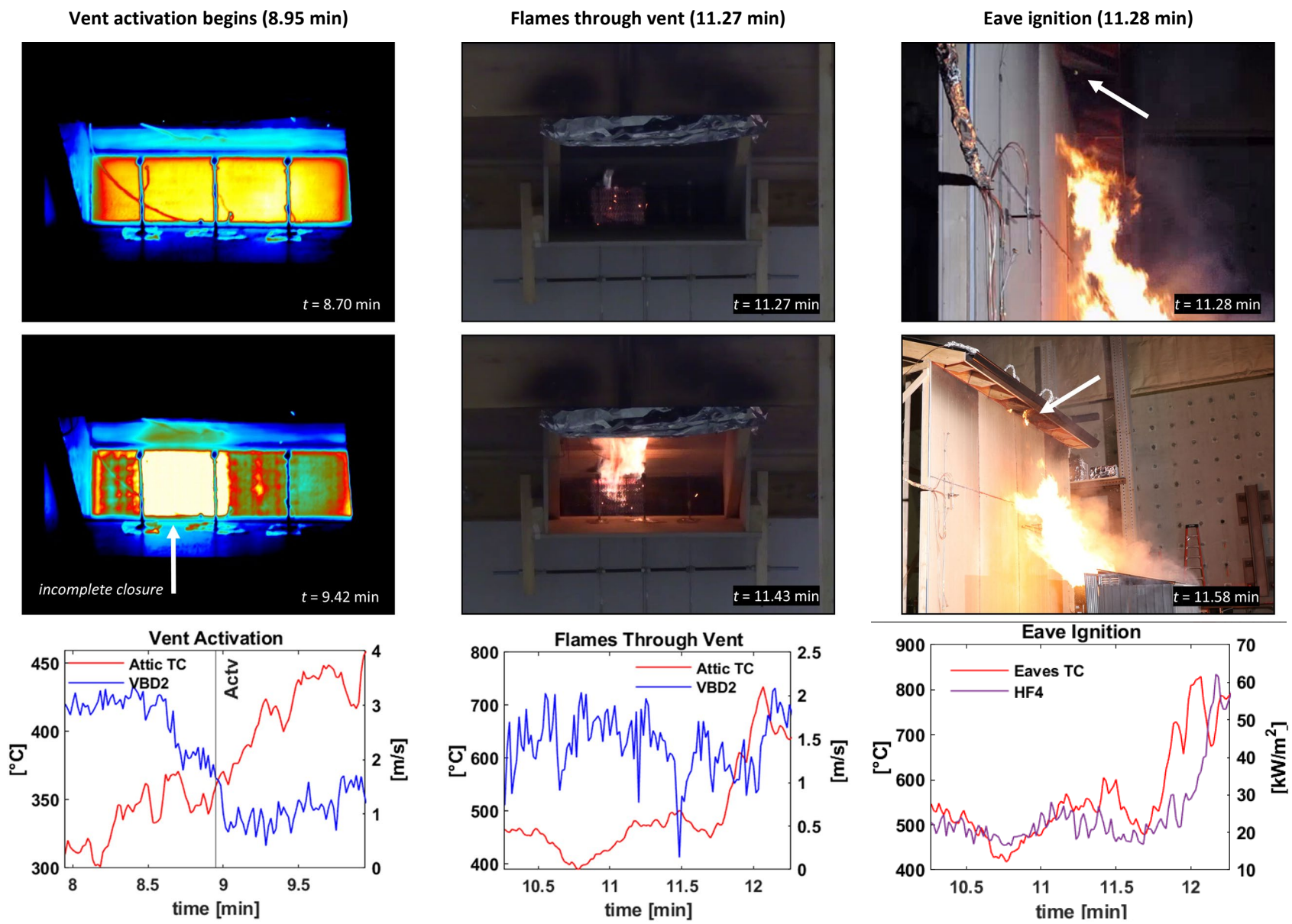
Vent activation begins (8.95 min)
Flames through vent (11.27 min)
Eave ignition (11.28 min)
t = 8.70 min
t = 11.27 min
t = 11.28 min
incomplete closure
t = 9.42 min
t = 11.43 min
t = 11.58 min
Vent Activation
Attic TC
VBD2
Actv
[°C]
[m/s]
time [min]
Flames Through Vent
Attic TC
VBD2
[°C]
[m/s]
time [min]
Eave Ignition
Eaves TC
HF4
[°C]
[kW/m2]
time [min]

Vent Response: No Closure

EAVE_Phase_A_e12

Test ID: e12_SNl0-0
Date: 4/30/2024

WUI Eave Vent ID: A
Eave Ignition: No

Shed Material: Steel
Shed Type: Narrow (26 ft^2)

Fuel Loading: Low (2 × [1-A wood cribs])
Combustible Mass: 48.9 kg (107.8 lb)

Wind Speed: 0 m/s
SSD: 0 ft

Objective: To assess the performance of WUI Eave Vent A and quantify the heat exposure from 2 wood cribs in the narrow style steel shed. This is the 1st experiment using the narrow shed. The low fuel was chosen first in order to potentially save time on rebuilding the roof.

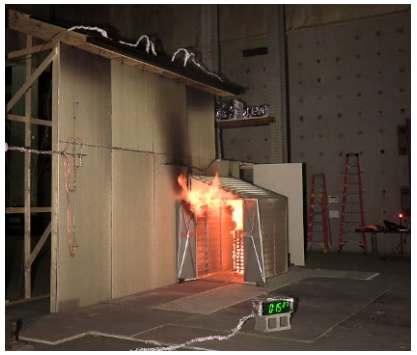

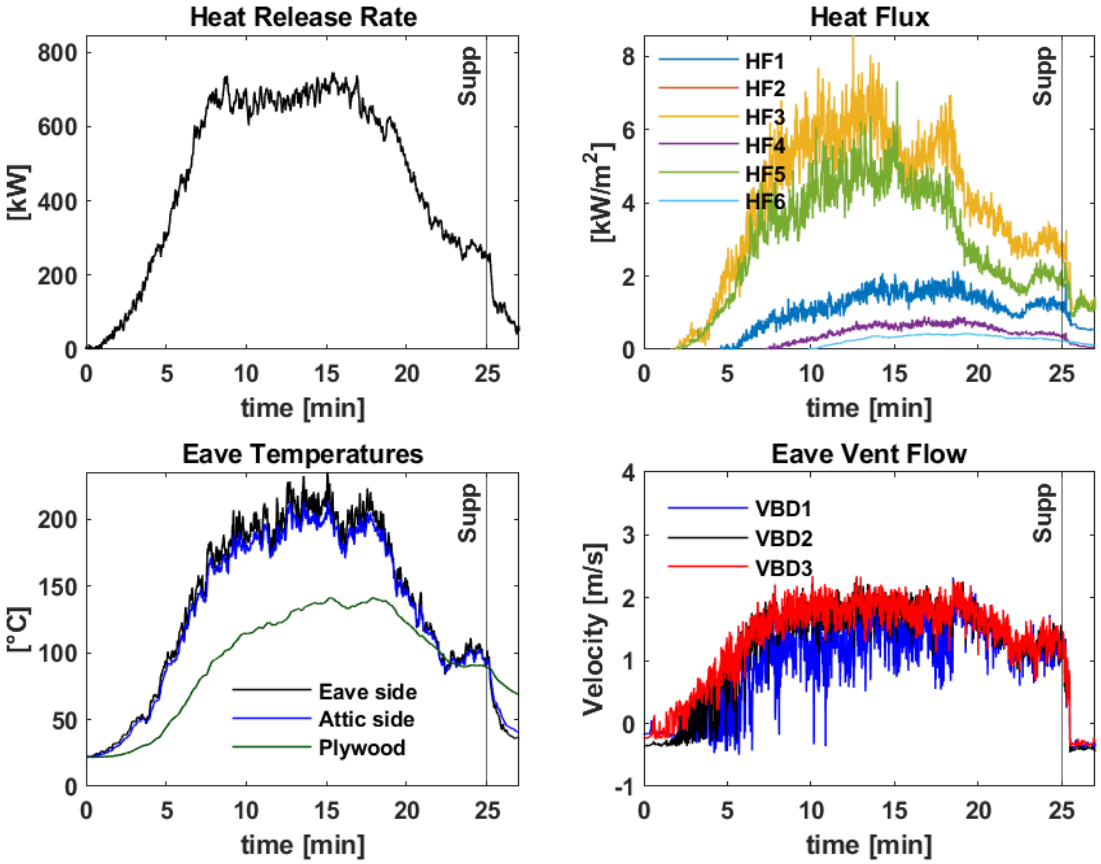

Maximum Temperature

Location	(°C)
Vent – eave side	235
Vent – attic side	214
Attic plywood	141

Maximum Heat Flux

Location	(kW/m^2)
HF 1 (S center, out)	n/d
HF 2 (N center, down)	n/d
HF 3 (N center, out)	7
HF 4 (S center, down)	1
HF 5 (N, out)	7
HF 6 (S, down)	0

Key Events (time after ignition)

Event	Time (min)
Vent activation begins	n/a
Peak shed HRR	15.45
Eave ignition	No
Flames through vent	n/a
Suppression	25.03

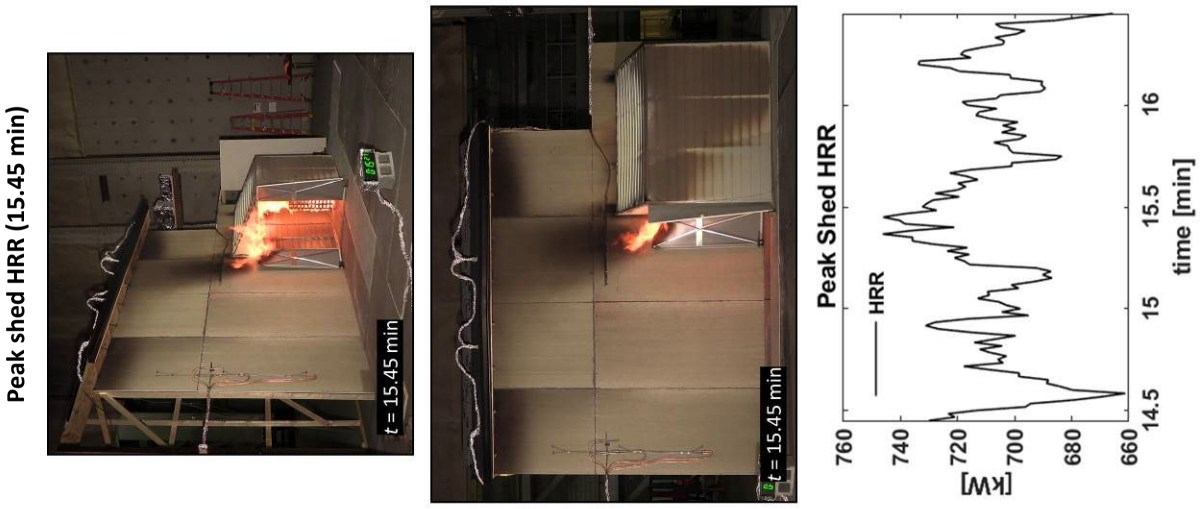
Peak shed HRR (15.45 min)
t = 15.45 min
t = 15.45 min
Peak Shed HRR
HRR
[kW]
time [min]
760
740
720
700
680
660
14.5
15
15.5
16

Vent Response: No Closure

EAVE_Phase_A_e13

Test ID: e13_SNi0-0
Date: 5/1/2024

WUI Eave Vent ID: A
Eave Ignition: No

Shed Material: Steel
Shed Type: Narrow (26 ft^2)

Fuel Loading: Intermed. (3 × [1-A wood cribs])
Combustible Mass: 59.7 kg (131.6 lb)

Wind Speed: 0 m/s
SSD: 0 ft

Objective: To assess the performance of WUI Eave Vent A and quantify the heat exposure from 3 wood cribs in the narrow style steel shed. This experiment used one additional crib in the narrow shed. The cribs were also placed close to the shed door.

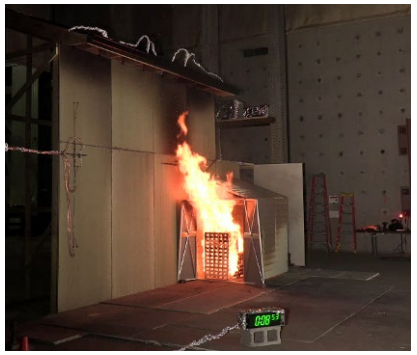

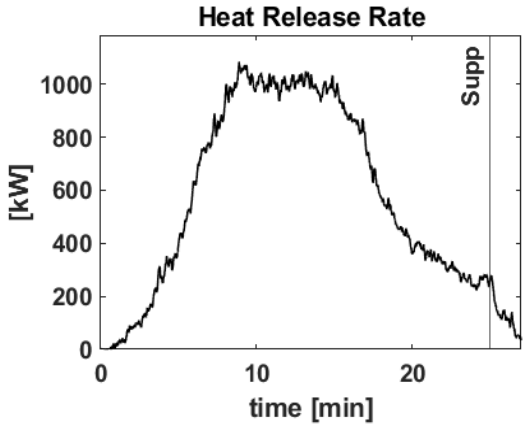

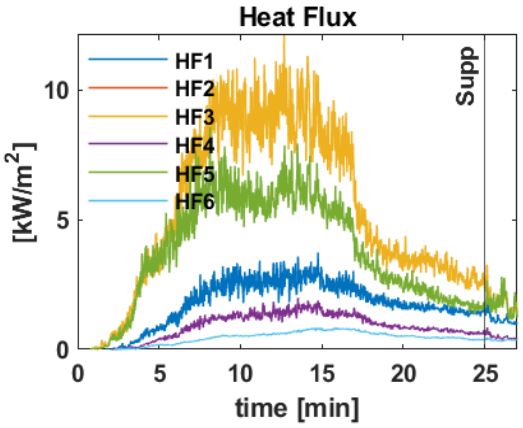

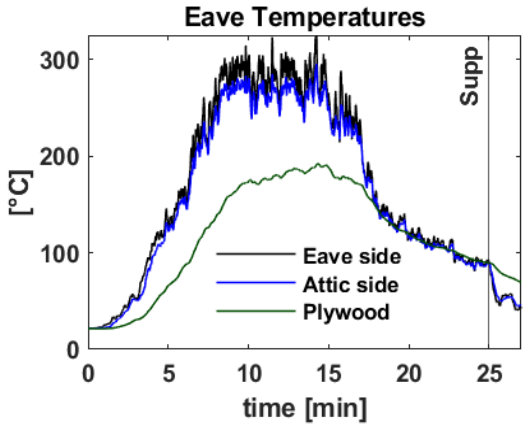

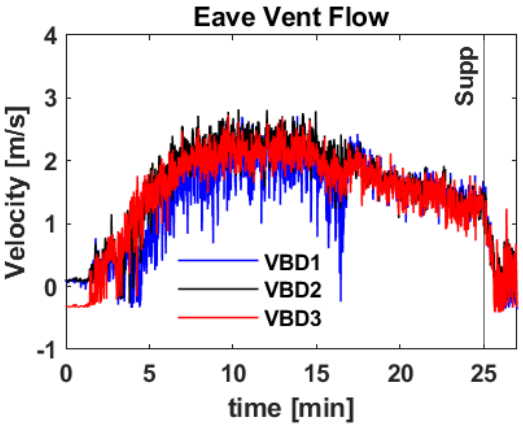

Maximum Temperature

Location	(°C)
Vent – eave side	325
Vent – attic side	295
Attic plywood	192

Maximum Heat Flux

Location	(kW/m^2)
HF 1 (S center, out)	4
HF 2 (N center, down)	n/d
HF 3 (N center, out)	12
HF 4 (S center, down)	2
HF 5 (N, out)	9
HF 6 (S, down)	1

Key Events (time after ignition)

Event	Time (min)
Vent activation begins	n/a
Peak shed HRR	8.88
Eave ignition	No
Flames through vent	n/a
Suppression	25.03

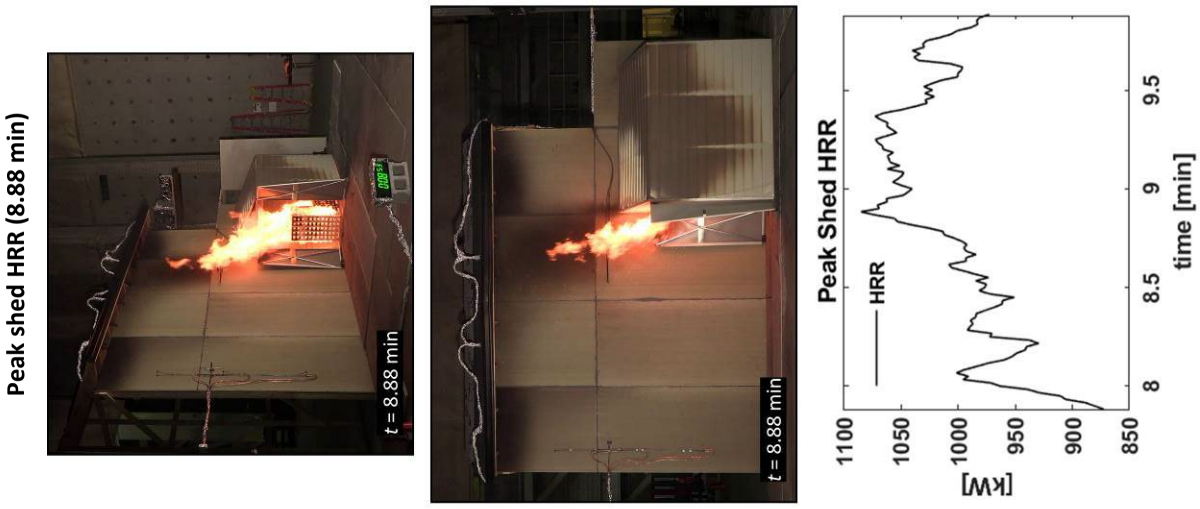
Peak shed HRR (8.88 min)
t = 8.88 min
t = 8.88 min
Peak Shed HRR
HRR
[kW]
time [min]
1100
1050
1000
950
900
850
8
8.5
9
9.5

Vent Response: No Closure

EAVE_Phase_A_e14

Test ID: e14_SNm0-0
Date: 5/6/2024

WUI Eave Vent ID: A
Eave Ignition: No

Shed Material: Steel
Shed Type: Narrow (26 ft^2)

Fuel Loading: Medium (4 × [1-A wood cribs])
Combustible Mass: 84.1 kg (185.4 lb)

Wind Speed: 0 m/s
SSD: 0 ft

Objective: To assess the performance of WUI Eave Vent A and quantify the heat exposure from 4 wood cribs in the narrow style steel shed. This experiment used one additional crib in the narrow shed. The cribs were also placed close to the shed door.

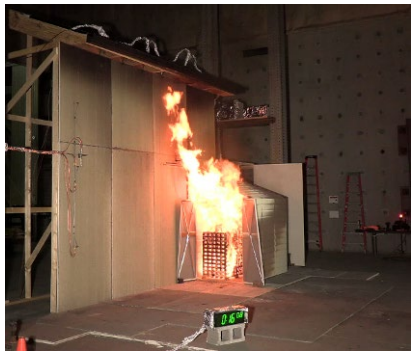

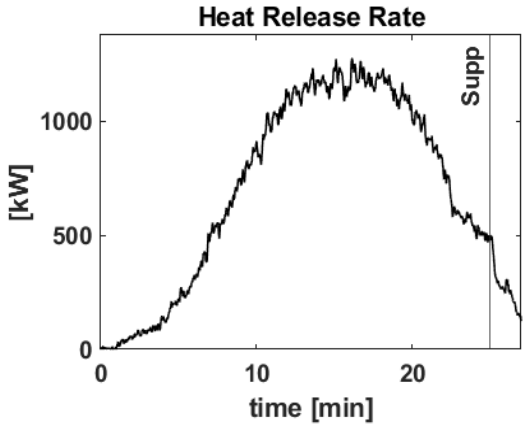

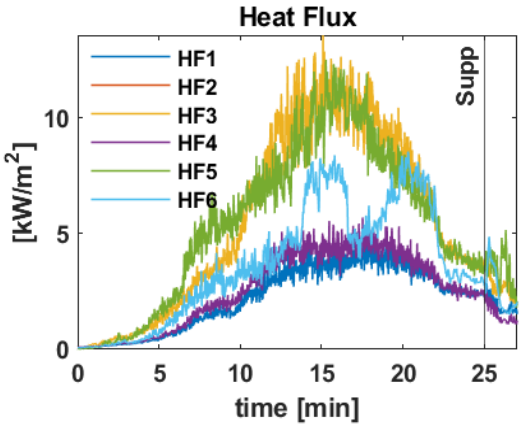

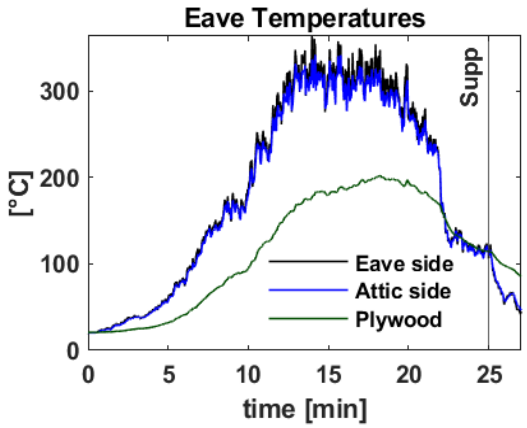

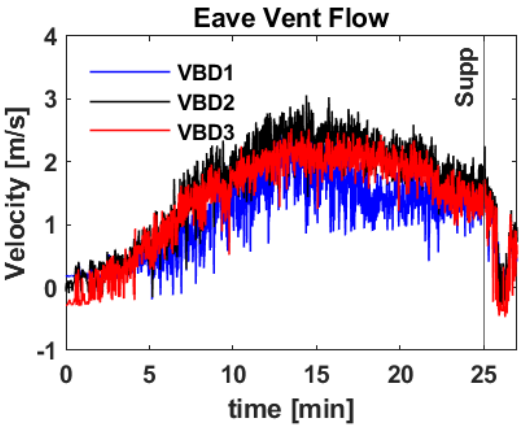

Maximum Temperature

Location	(°C)
Vent – eave side	363
Vent – attic side	342
Attic plywood	202

Maximum Heat Flux

Location	(kW/m^2)
HF 1 (S center, out)	5
HF 2 (N center, down)	n/d
HF 3 (N center, out)	14
HF 4 (S center, down)	6
HF 5 (N, out)	13
HF 6 (S, down)	9

Key Events (time after ignition)

Event	Time (min)
Vent activation begins	No
Peak shed HRR	16.15
Eave ignition	No
Flames through vent	n/a
Suppression	25.00

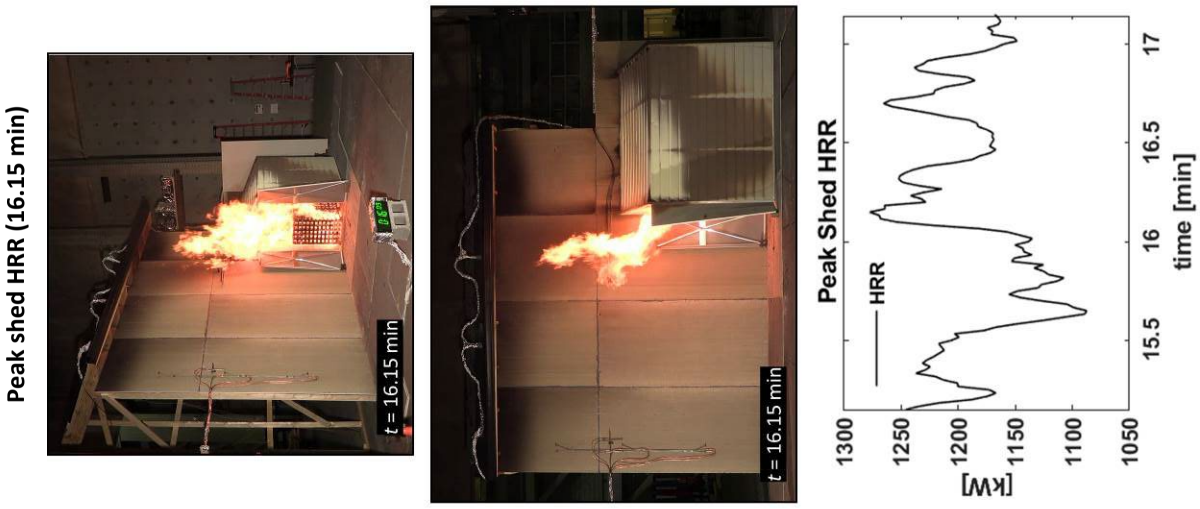
Peak shed HRR (16.15 min)
t = 16.15 min
t = 16.15 min
Peak Shed HRR
HRR
[kW]
time [min]
1300
1250
1200
1150
1100
1050
15.5
16
16.5
17

Vent Response: Partial Closure

EAVE_Phase_A_e15

Test ID: e15_SNh0-0
Date: 5/7/2024

WUI Eave Vent ID: A
Eave Ignition: Yes

Shed Material: Steel
Shed Type: Narrow (26 ft^2)

Fuel Loading: High (6 × [1-A wood cribs])
Combustible Mass: 137.5 kg (303.1 lb)

Wind Speed: 0 m/s
SSD: 0 ft

Objective: To assess the performance of WUI Eave Vent A and quantify the heat exposure from 6 wood cribs in the narrow style steel shed. This experiment used two additional cribs in the narrow shed. The cribs were centered within the shed door.

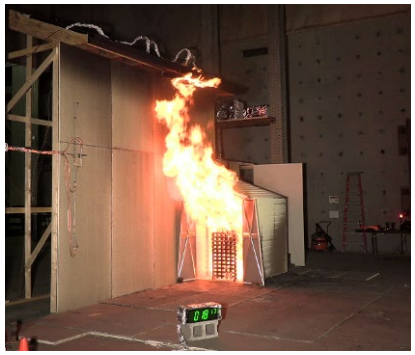

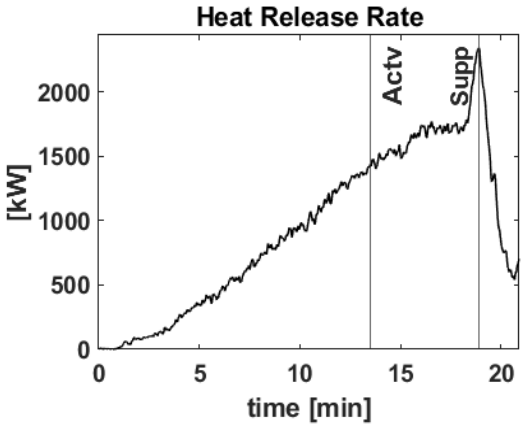

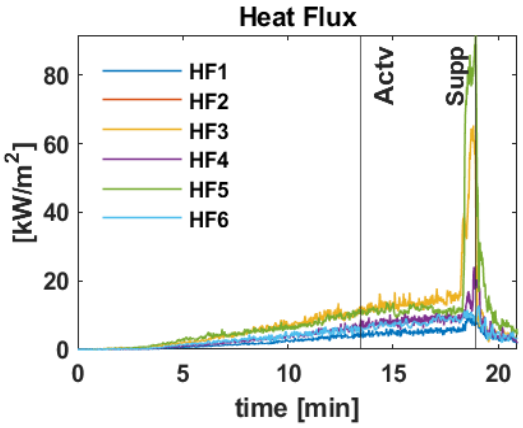

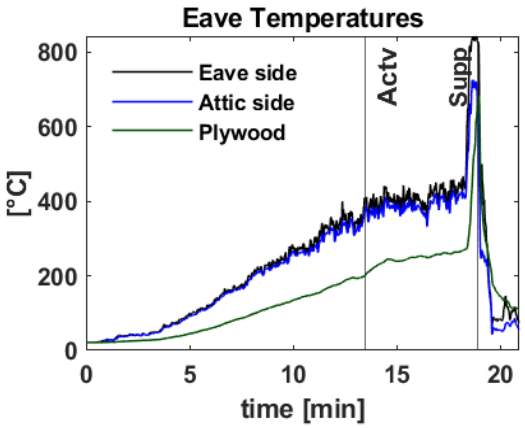

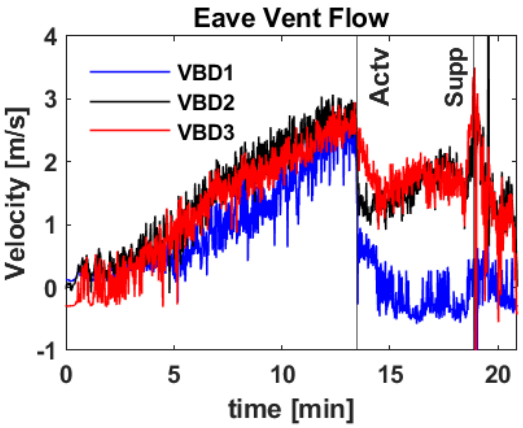

Temperature at Vent Activation

Location	(°C)
Vent – eave side	389
Vent – attic side	369
Attic plywood	203

Heat Flux at Vent Activation

Location	(kW/m^2)
HF 1 (S center, out)	4
HF 2 (N center, down)	n/d
HF 3 (N center, out)	12
HF 4 (S center, down)	7
HF 5 (N, out)	11
HF 6 (S, down)	6

Key Events (time after ignition)

Event	Time (min)
Vent activation begins	13.48
Peak shed HRR	16.55
Eave ignition	17.95
Flames through vent	18.35
Suppression	18.93

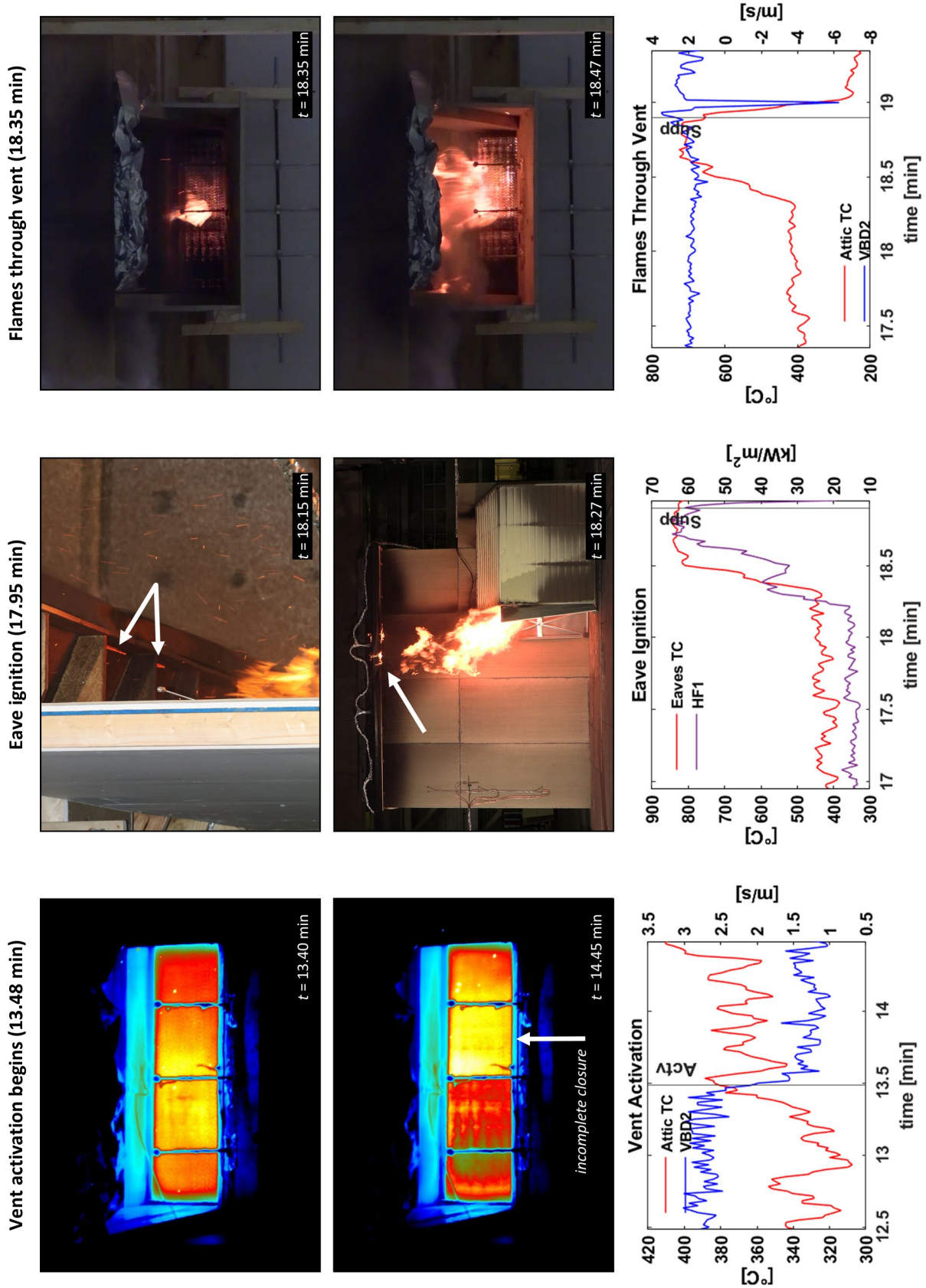
Vent activation begins (13.48 min)
t = 13.40 min
t = 14.45 min
incomplete closure
Vent Activation
Attic TC
VBD7
Actv
[°C]
[m/s]
time [min]
Eave ignition (17.95 min)
t = 18.15 min
t = 18.27 min
Eave Ignition
Eaves TC
HF1
Supp
[°C]
[kW/m²]
time [min]
Flames through vent (18.35 min)
t = 18.35 min
t = 18.47 min
Flames Through Vent
Attic TC
VBD2
Supp
[°C]
[m/s]
time [min]

Vent Response: Partial Closure

EAVE_Phase_A_e16

Test ID: e16_SNh0-0-R1
Date: 5/9/2024

WUI Eave Vent ID: A
Eave Ignition: Yes

Shed Material: Steel
Shed Type: Narrow (26 ft^2)

Fuel Loading: High (6 × [1-A wood cribs])
Combustible Mass: 131.6 kg (290.1 lb)

Wind Speed: 0 m/s
SSD: 0 ft

Objective: To assess the performance of WUI Eave Vent A and quantify the heat exposure from 6 wood cribs in the narrow style steel shed. This experiment is a repeat of e15.

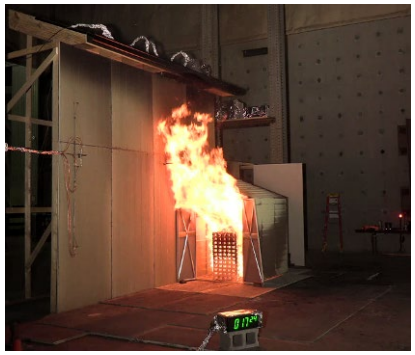

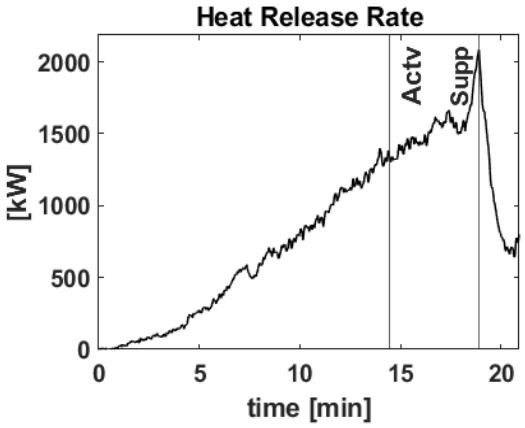

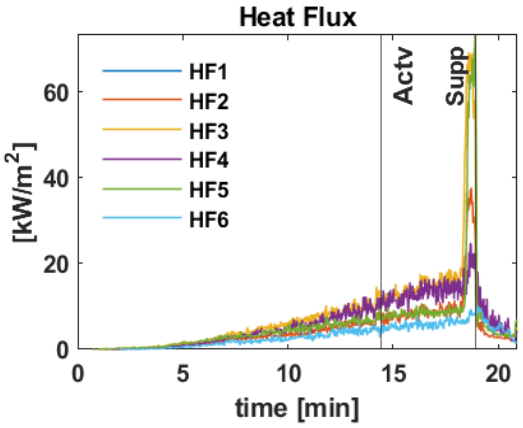

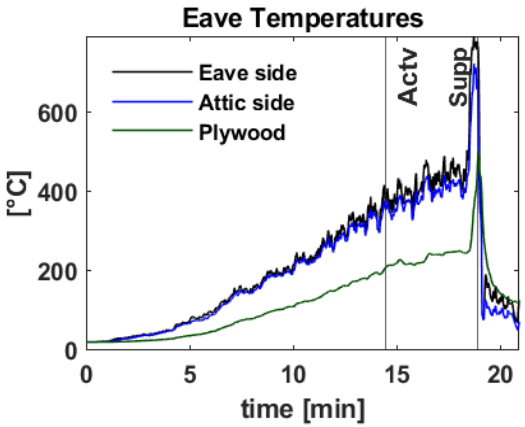

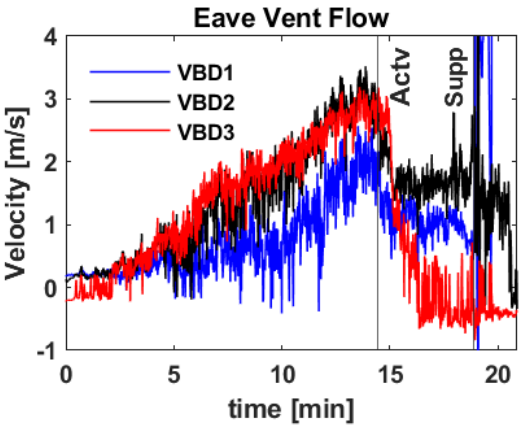

Temperature at Vent Activation

Location	(°C)
Vent – eave side	396
Vent – attic side	366
Attic plywood	207

Heat Flux at Vent Activation

Location	(kW/m^2)
HF 1 (S center, out)	n/d
HF 2 (N center, down)	8
HF 3 (N center, out)	12
HF 4 (S center, down)	11
HF 5 (N, out)	7
HF 6 (S, down)	4

Key Events (time after ignition)

Event	Time (min)
Vent activation begins	14.45
Peak shed HRR	17.40
Eave ignition	18.25
Flames through vent	18.45
Suppression	18.92

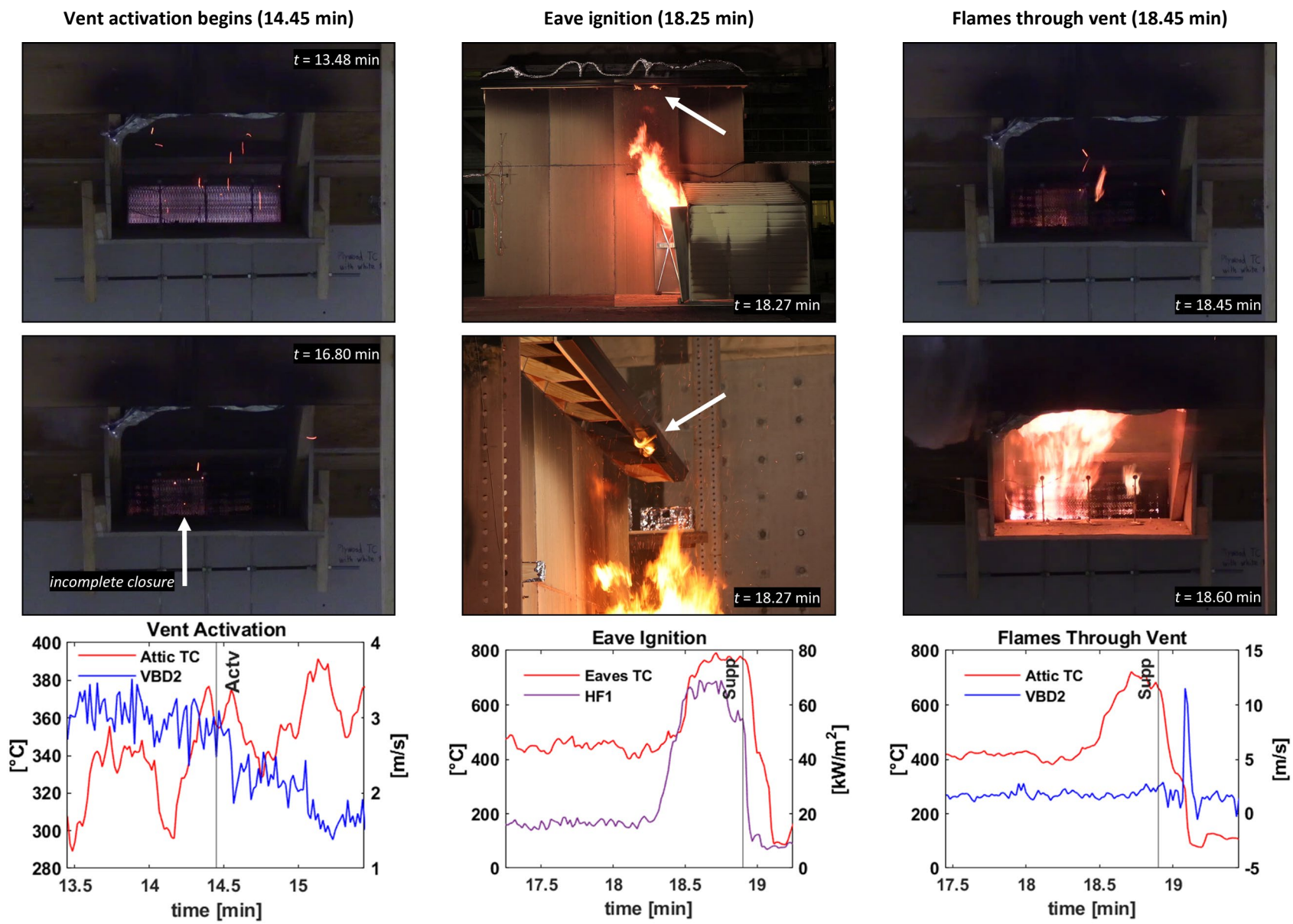
Vent activation begins (14.45 min)
Eave ignition (18.25 min)
Flames through vent (18.45 min)
t = 13.48 min
t = 18.27 min
t = 18.45 min
t = 16.80 min
incomplete closure
t = 18.27 min
t = 18.60 min
Vent Activation
Attic TC
VBD2
Actv
[°C]
[m/s]
time [min]
Eave Ignition
Eaves TC
HF1
Supp
[°C]
[kW/m²]
time [min]
Flames Through Vent
Attic TC
VBD2
Supp
[°C]
[m/s]
time [min]

Vent Response: Partial Closure

EAVE_Phase_A_e17

Test ID: e17_SVSl0-5
Date: 5/14/2024

WUI Eave Vent ID: A
Eave Ignition: No

Shed Material: Steel
Shed Type: Very Small (30 ft^2)

Fuel Loading: Low (4 × [1-A wood cribs])
Combustible Mass: 80.4 kg (177.3 lb)

Wind Speed: 0 m/s
SSD: 5 ft

Objective: To assess the performance of WUI Eave Vent A and quantify the heat exposure from 4 wood cribs in the very small style steel shed. This experiment is similar to preliminary experiment p6.

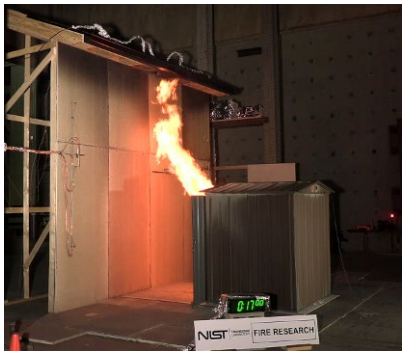

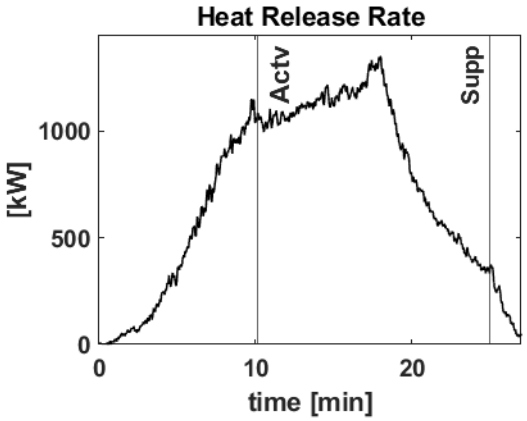

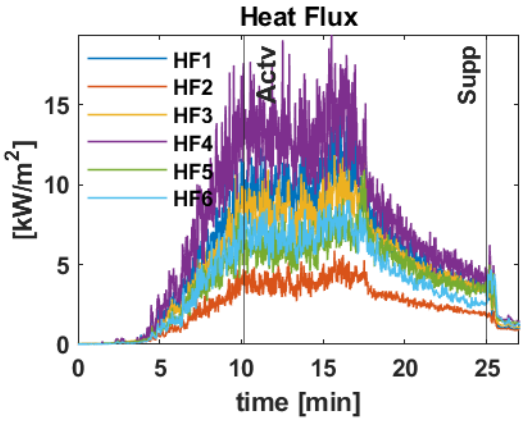

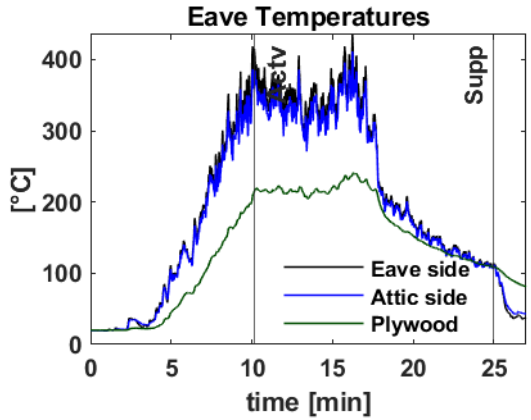

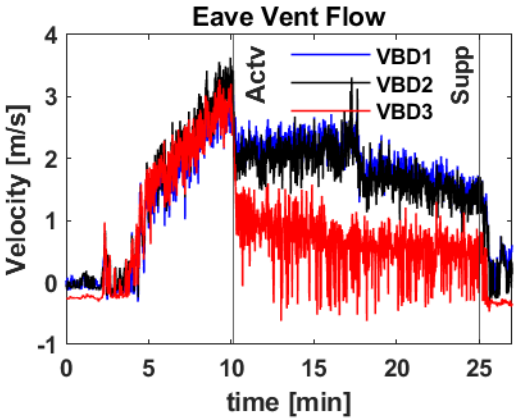

Temperature at Vent Activation

Location	(°C)
Vent – eave side	397
Vent – attic side	374
Attic plywood	214

Heat Flux at Vent Activation

Location	(kW/m^2)
HF 1 (S center, out)	6
HF 2 (N center, down)	5
HF 3 (N center, out)	9
HF 4 (S center, down)	14
HF 5 (N, out)	7
HF 6 (S, down)	7

Key Events (time after ignition)

Event	Time (min)
Vent activation begins	10.15
Peak shed HRR	18.00
Eave ignition	No
Flames through vent	n/a
Suppression	25.02

Vent activation begins (10.15 min)

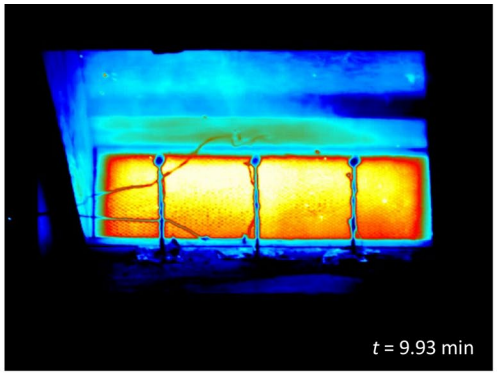

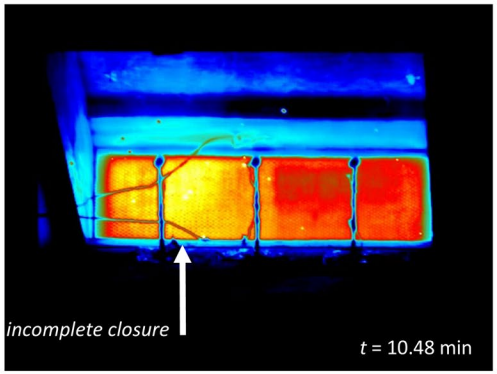

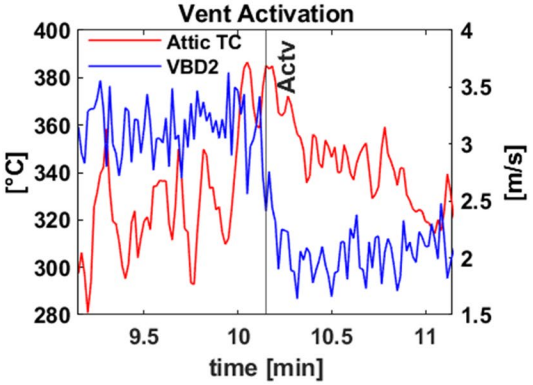

Peak shed HRR (18.00 min)

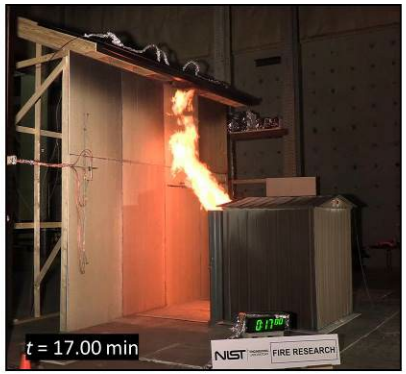

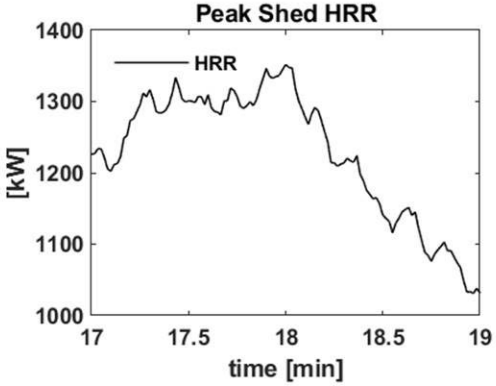

Vent Response: Partial Closure

EAVE_Phase_A_e18

Test ID: e18_SVSh0-5
Date: 5/15/2024

WUI Eave Vent ID: A
Eave Ignition: Yes

Shed Material: Steel
Shed Type: Very Small (30 ft^2)

Fuel Loading: High (6 × [1-A wood cribs])
Combustible Mass: 124 kg (273.4 lb)

Wind Speed: 0 m/s
SSD: 5 ft

Objective: To assess the performance of WUI Eave Vent A and quantify the heat exposure from 6 wood cribs in the very small style steel shed. This experiment is similar to preliminary experiment p2.

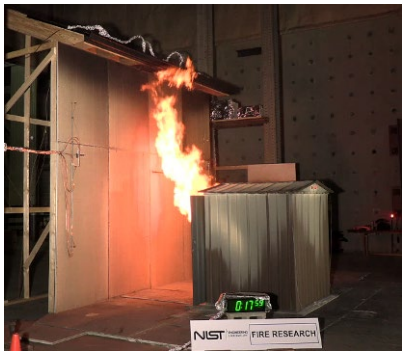

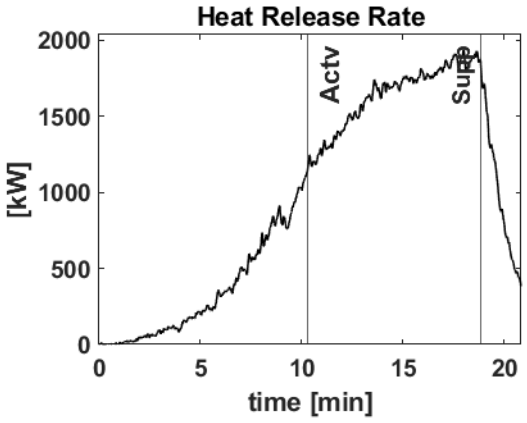

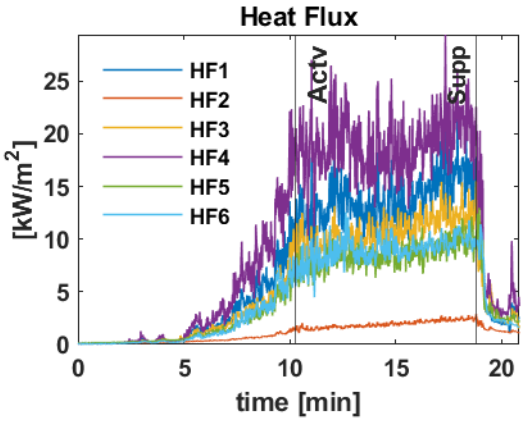

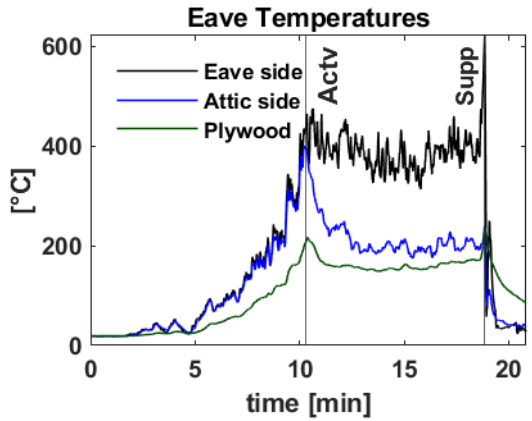

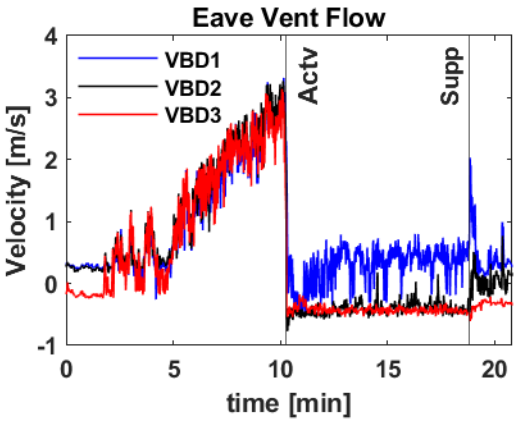

Temperature at Vent Activation

Location	(°C)
Vent – eave side	430
Vent – attic side	390
Attic plywood	204

Heat Flux at Vent Activation

Location	(kW/m^2)
HF 1 (S center, out)	7
HF 2 (N center, down)	2
HF 3 (N center, out)	10
HF 4 (S center, down)	18
HF 5 (N, out)	7
HF 6 (S, down)	7

Key Events (time after ignition)

Event	Time (min)
Vent activation begins	10.27
Peak shed HRR	17.98
Eave ignition	18.65
Flames through vent	18.63
Suppression	18.85

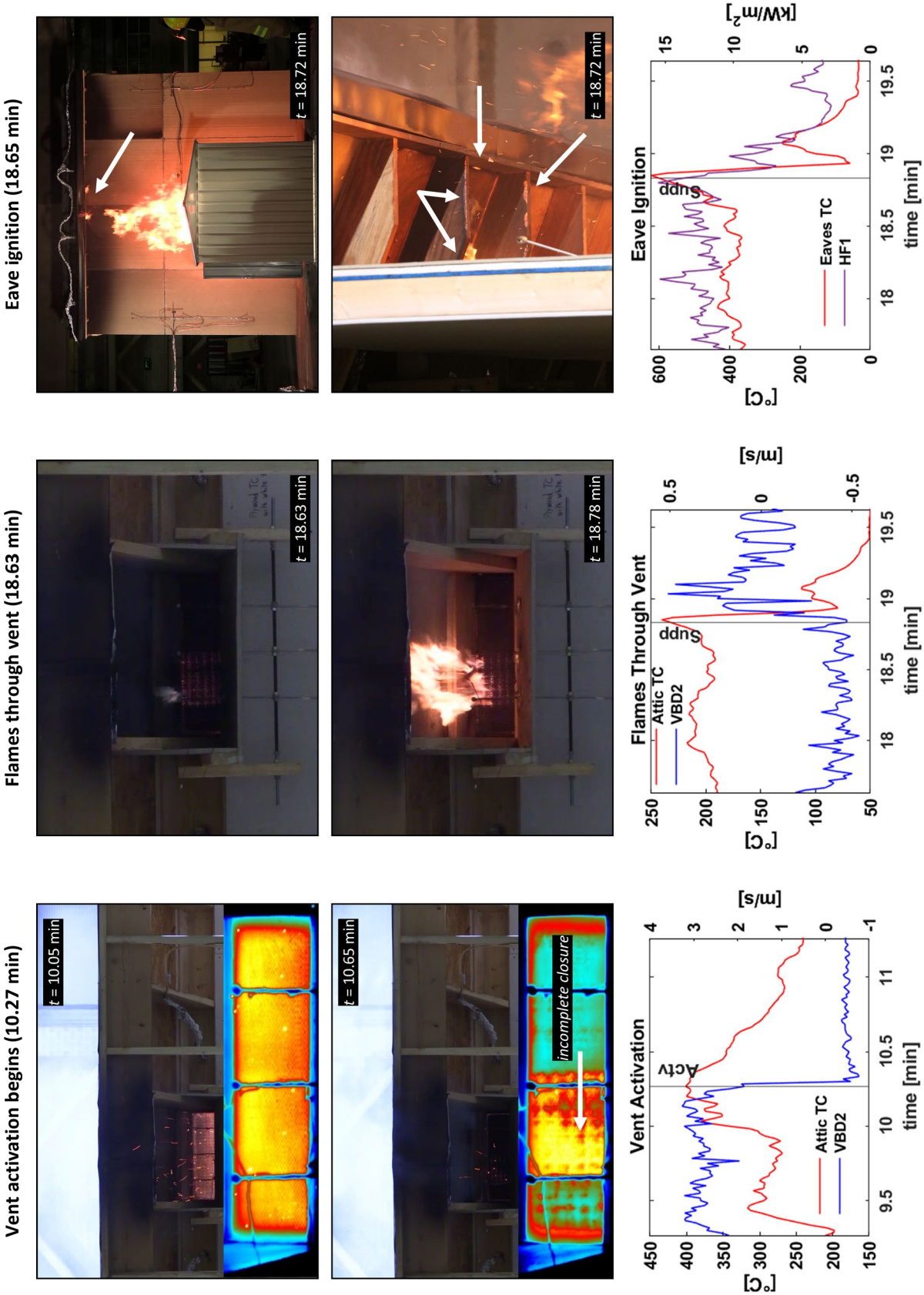
Eave ignition (18.65 min)
Flames through vent (18.63 min)
Vent activation begins (10.27 min)
t = 18.72 min
t = 18.72 min
t = 18.63 min
t = 18.78 min
t = 10.05 min
t = 10.65 min
incomplete closure
Eave Ignition
Eaves TC
HF1
Supp
[°C]
[kW/m²]
time [min]
Flames Through Vent
Attic TC
VBD2
Supp
[°C]
[m/s]
time [min]
Vent Activation
Attic TC
VBD2
Activ
[°C]
[m/s]
time [min]

Vent Response: Partial Closure

EAVE_Phase_A_e19

Test ID: e19_SVSh0-5-R1
Date: 5/21/2024

WUI Eave Vent ID: B
Eave Ignition: Yes

Shed Material: Steel
Shed Type: Very Small (30 ft^2)

Fuel Loading: High (6 × [1-A wood cribs])
Combustible Mass: 112.9 kg (248.9 lb)

Wind Speed: 0 m/s
SSD: 5 ft

Objective: To assess the performance of WUI Eave Vent B and quantify the heat exposure from 6 wood cribs in the very small style steel shed. This experiment is a replicate of the conditions for e18 but with Vent B.

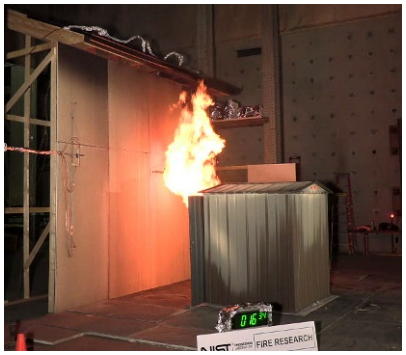

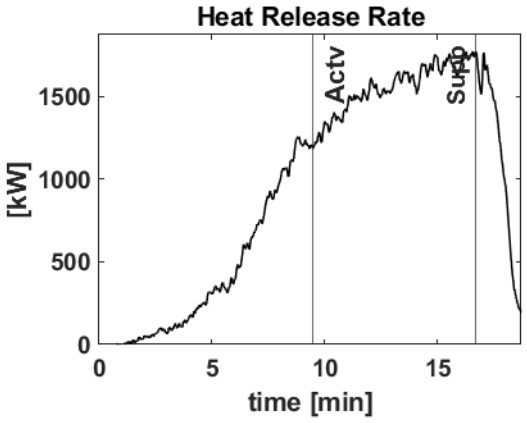

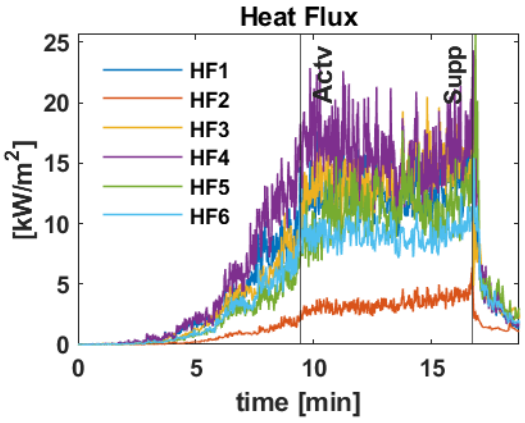

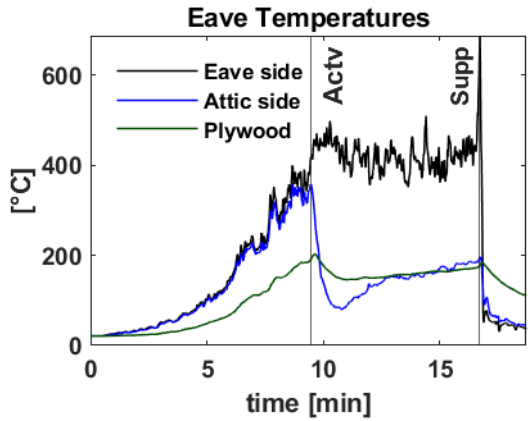

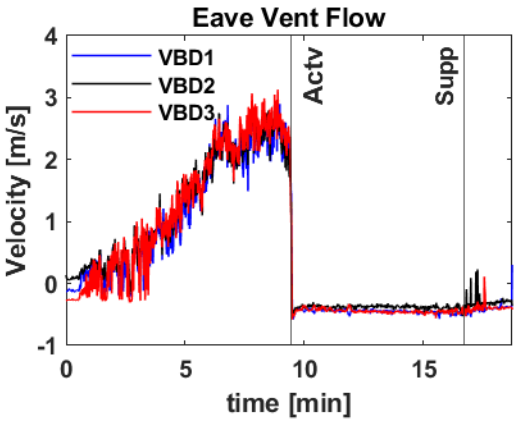

Temperature at Vent Activation

Location	(°C)
Vent – eave side	402
Vent – attic side	344
Attic plywood	191

Heat Flux at Vent Activation

Location	(kW/m^2)
HF 1 (S center, out)	7
HF 2 (N center, down)	3
HF 3 (N center, out)	11
HF 4 (S center, down)	16
HF 5 (N, out)	7
HF 6 (S, down)	9

Key Events (time after ignition)

Event	Time (min)
Vent activation begins	9.45
Peak shed HRR	15.53
Eave ignition	15.93
Flames through vent	16.73
Suppression	16.85

Vent activation begins (9.45 min)

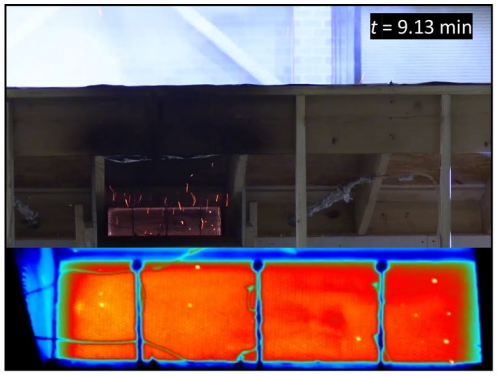

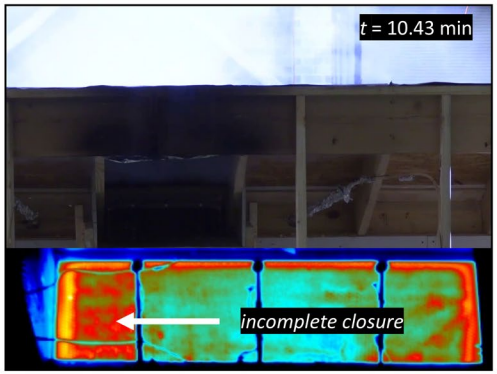

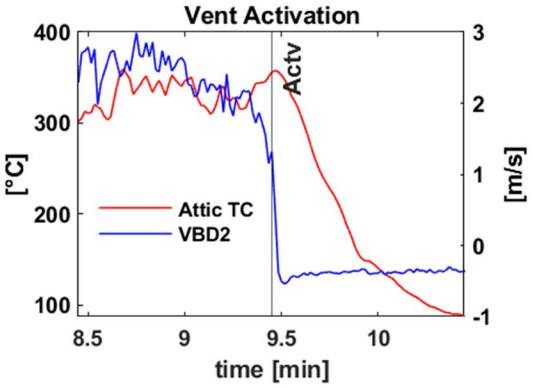

Eave ignition (15.93 min)

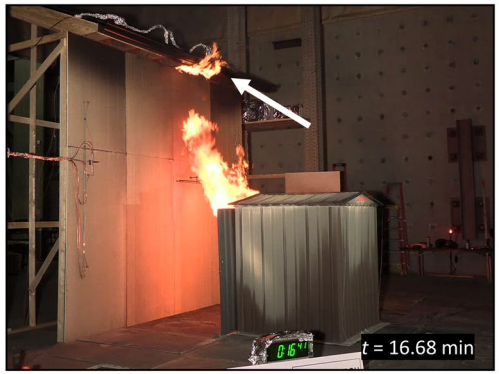

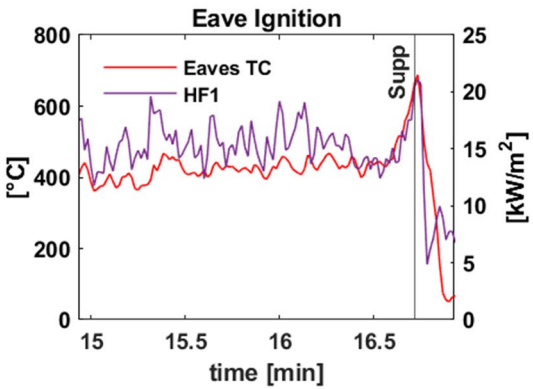

Flames through vent (16.73 min)

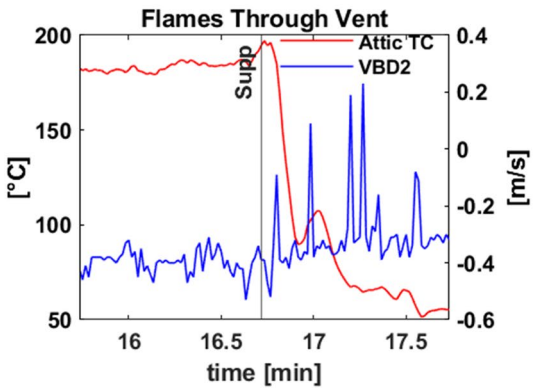

Vent Response: Closure

EAVE_Phase_A_e20

Test ID: e20_SCh0-5
Date: 5/22/2024

WUI Eave Vent ID: C
Eave Ignition: Yes

Shed Material: Steel
Shed Type: Closet (18 ft^2)

Fuel Loading: High (4 × [1-A wood cribs])
Combustible Mass: 76.2 kg (168 lb)

Wind Speed: 0 m/s
SSD: 5 ft

Objective: To assess the performance of WUI Eave Vent C and quantify the heat exposure from 4 wood cribs in the closet style steel shed. This experiment has the same conditions as e7, e10 and e11, except that the vent is from a different manufacturer (Vent C instead of Vent A).

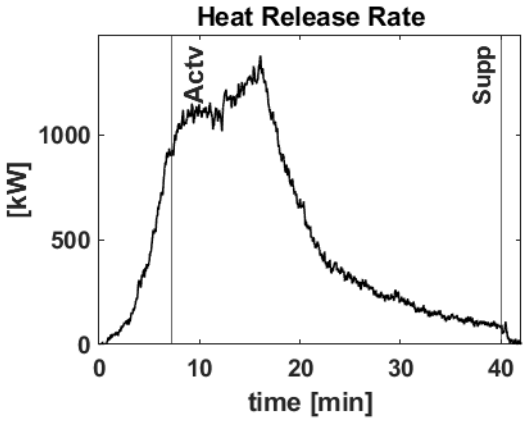

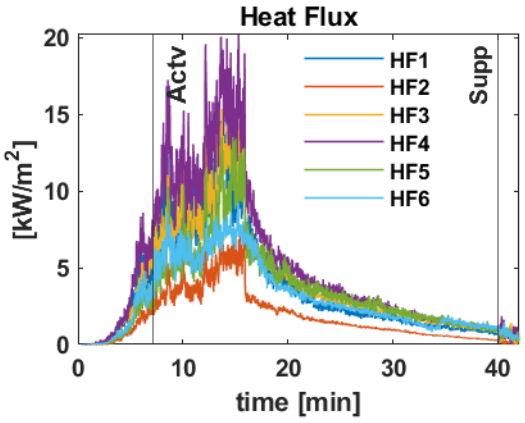

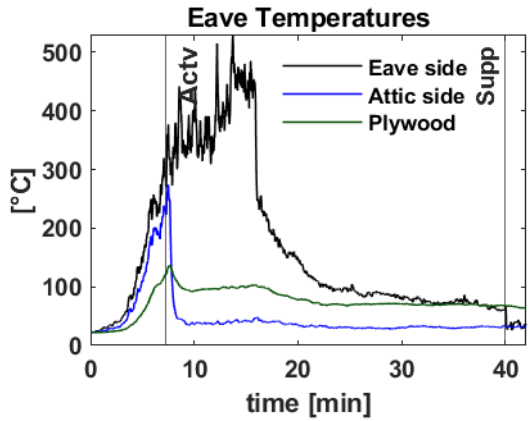

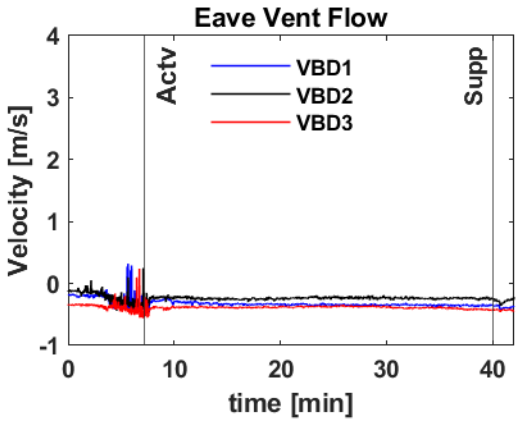

Temperature at Vent Activation

Location	(°C)
Vent – eave side	289
Vent – attic side	231
Attic plywood	120

Heat Flux at Vent Activation

Location	(kW/m^2)
HF 1 (S center, out)	4
HF 2 (N center, down)	3
HF 3 (N center, out)	6
HF 4 (S center, down)	8
HF 5 (N, out)	3
HF 6 (S, down)	4

Key Events (time after ignition)

Event	Time (min)
Vent activation begins	7.20
Peak shed HRR	16.07
Eave ignition	20.80
Flames through vent	No
Suppression	40.00

Vent activation begins (7.20 min)

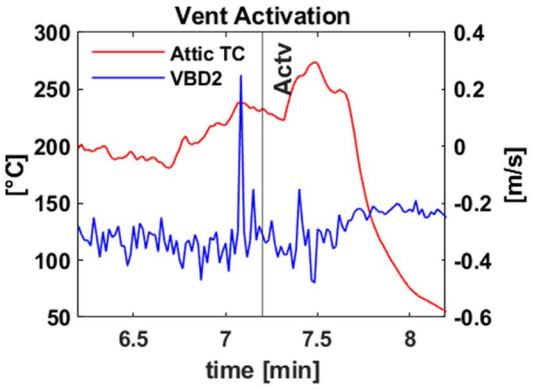

Peak shed HRR (16.07 min)

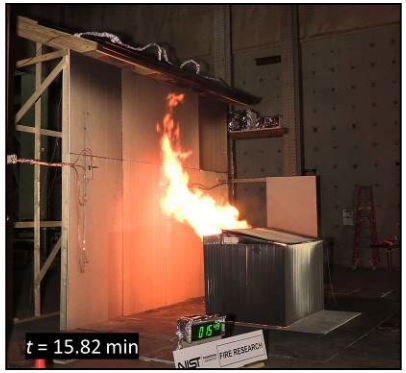

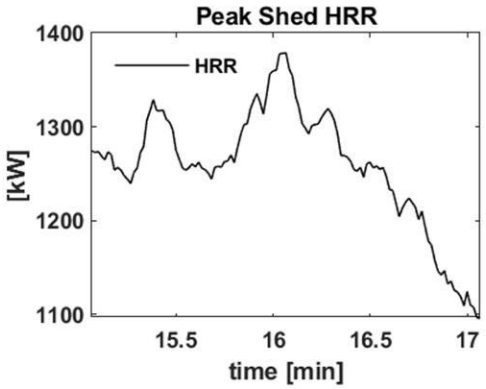

Eave ignition (20.80 min)

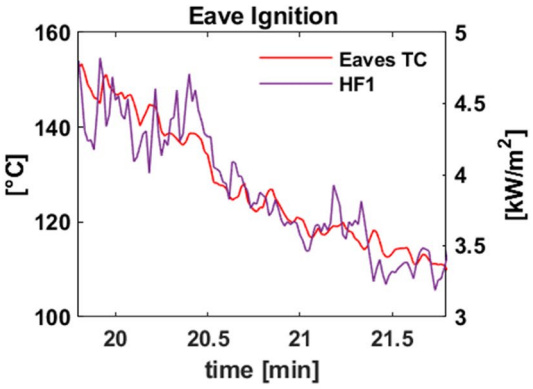

Vent Response: Closure

EAVE_Phase_A_e21

Test ID: e21_SCh0-5-R1
Date: 5/28/2024

WUI Eave Vent ID: C
Eave Ignition: Yes

Shed Material: Steel
Shed Type: Closet (18 ft^2)

Fuel Loading: High (4 × [1-A wood cribs])
Combustible Mass: 76.2 kg (168 lb)

Wind Speed: 0 m/s
SSD: 5 ft

Objective: To assess the performance of WUI Eave Vent C and quantify the heat exposure from 4 wood cribs in the closet style steel shed. This was a repeat of e20.

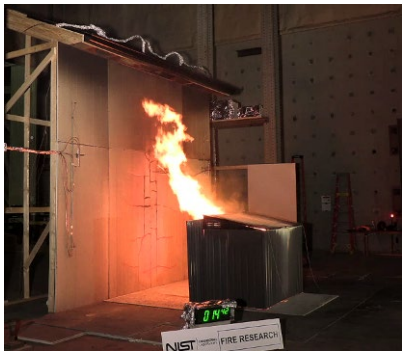

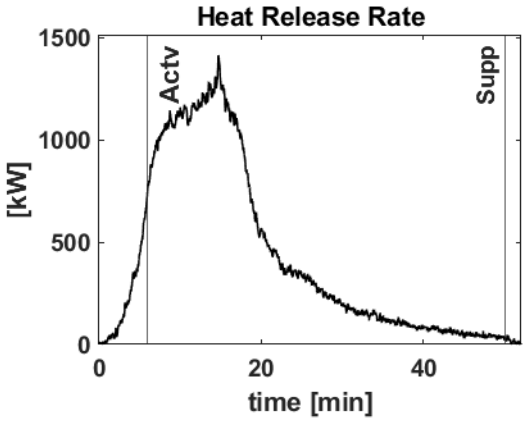

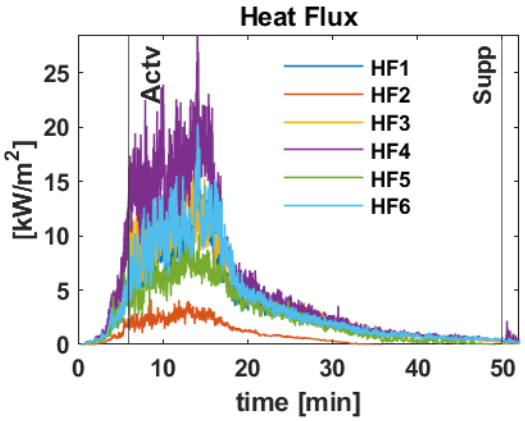

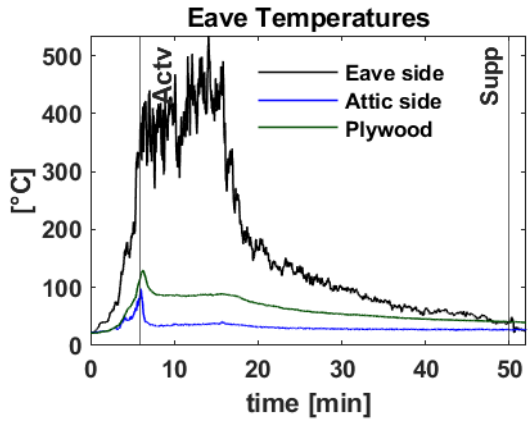

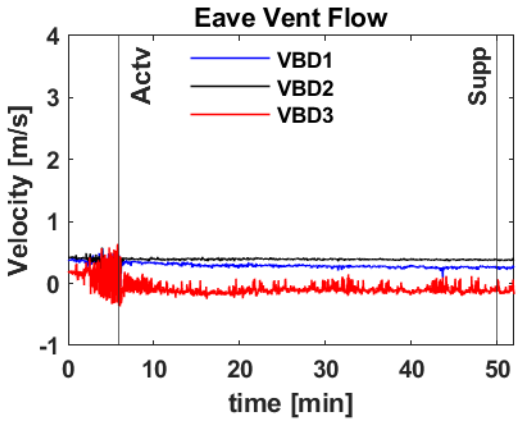

Temperature at Vent Activation

Location	(°C)
Vent – eave side	356
Vent – attic side	87
Attic plywood	117

Heat Flux at Vent Activation

Location	(kW/m^2)
HF 1 (S center, out)	4
HF 2 (N center, down)	2
HF 3 (N center, out)	9
HF 4 (S center, down)	13
HF 5 (N, out)	4
HF 6 (S, down)	5

Key Events (time after ignition)

Event	Time (min)
Vent activation begins	5.93
Peak shed HRR	14.72
Eave ignition	33.12
Flames through vent	No
Suppression	50.10

Vent activation begins (5.93 min)

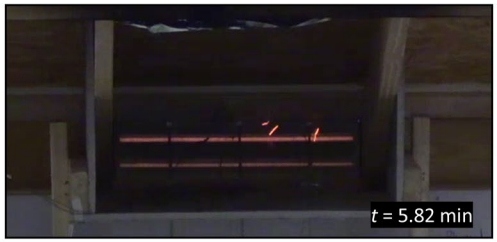

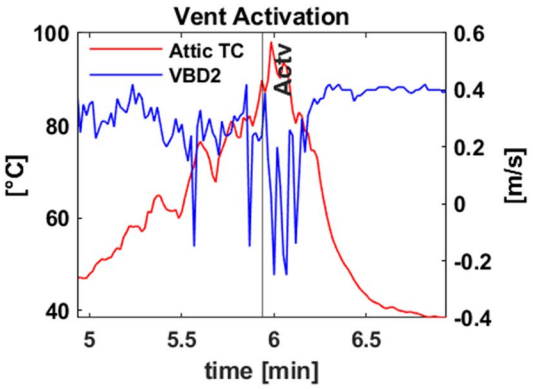

Peak shed HRR (14.72 min)

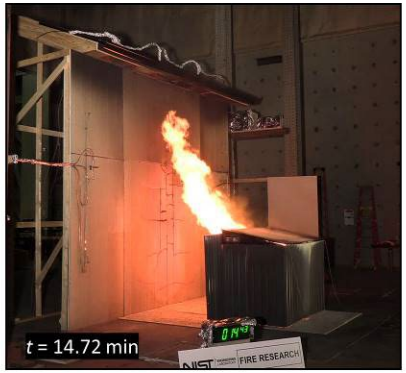

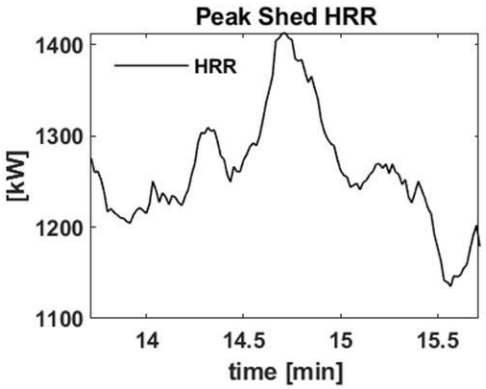

Eave ignition (33.12 min)

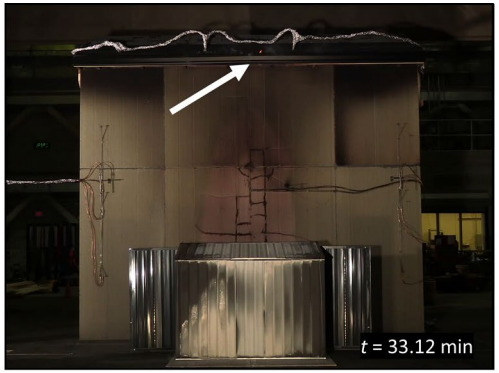

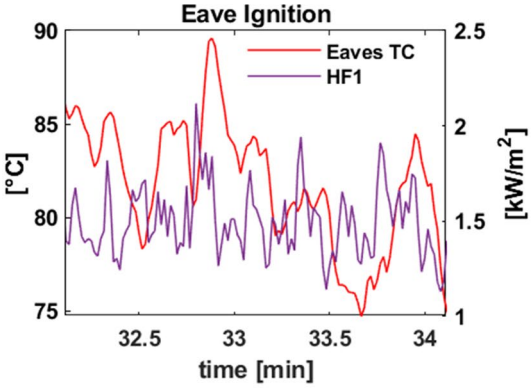

Vent Response: Partial Closure

EAVE_Phase_A_e22

Test ID: e22_SVSh0-5
Date: 6/3/2024

WUI Eave Vent ID: B
Eave Ignition: Yes

Shed Material: Steel
Shed Type: Very Small (30 ft^2)

Fuel Loading: High (6 × [1-A wood cribs])
Combustible Mass: 118.1 kg (260.4 lb)

Wind Speed: 0 m/s
SSD: 5 ft

Objective: To assess the absence of WUI eave vents directly above the heat exposure from 6 wood cribs in the very small style steel shed. Two WUI Eave Vent B's were placed in the furthest full rafter bays north and south while the very small shed remained centered to the wall. No heat flux gauges were used for this experiment.

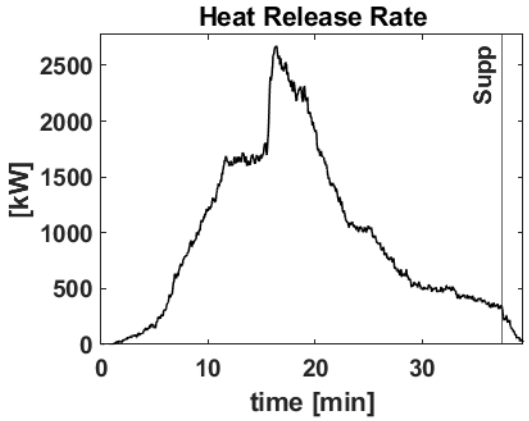

n/a

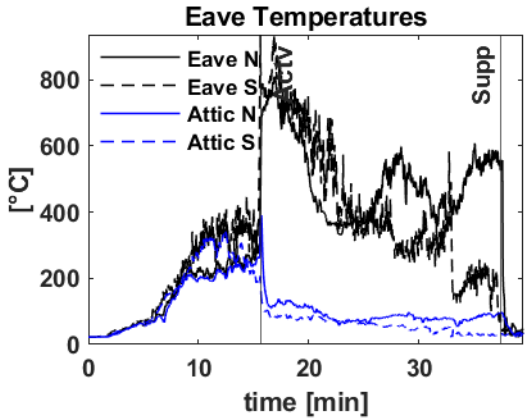

n/a

Temperature at Vent Activation

Location	N (°C)	S (°C)
Vent – eave side	606	756
Vent – attic side	334	180
Attic plywood	n/a	n/a

Heat Flux at Vent Activation

Location	(kW/m^2)
HF 1 (center, out)	n/a
HF 2 (center, down)	n/a
HF 3 (north, out)	n/a
HF 4 (north, down)	n/a
HF 5 (south, out)	n/a
HF 6 (south, down)	n/a

Key Events (time after ignition)

Event	N (min)	S (min)
Vent activation begins	15.60	15.70
Peak shed HRR	15.35	—
Eave ignition	15.37	—
Flames through vent	16.57	31.67
Suppression	37.45	—

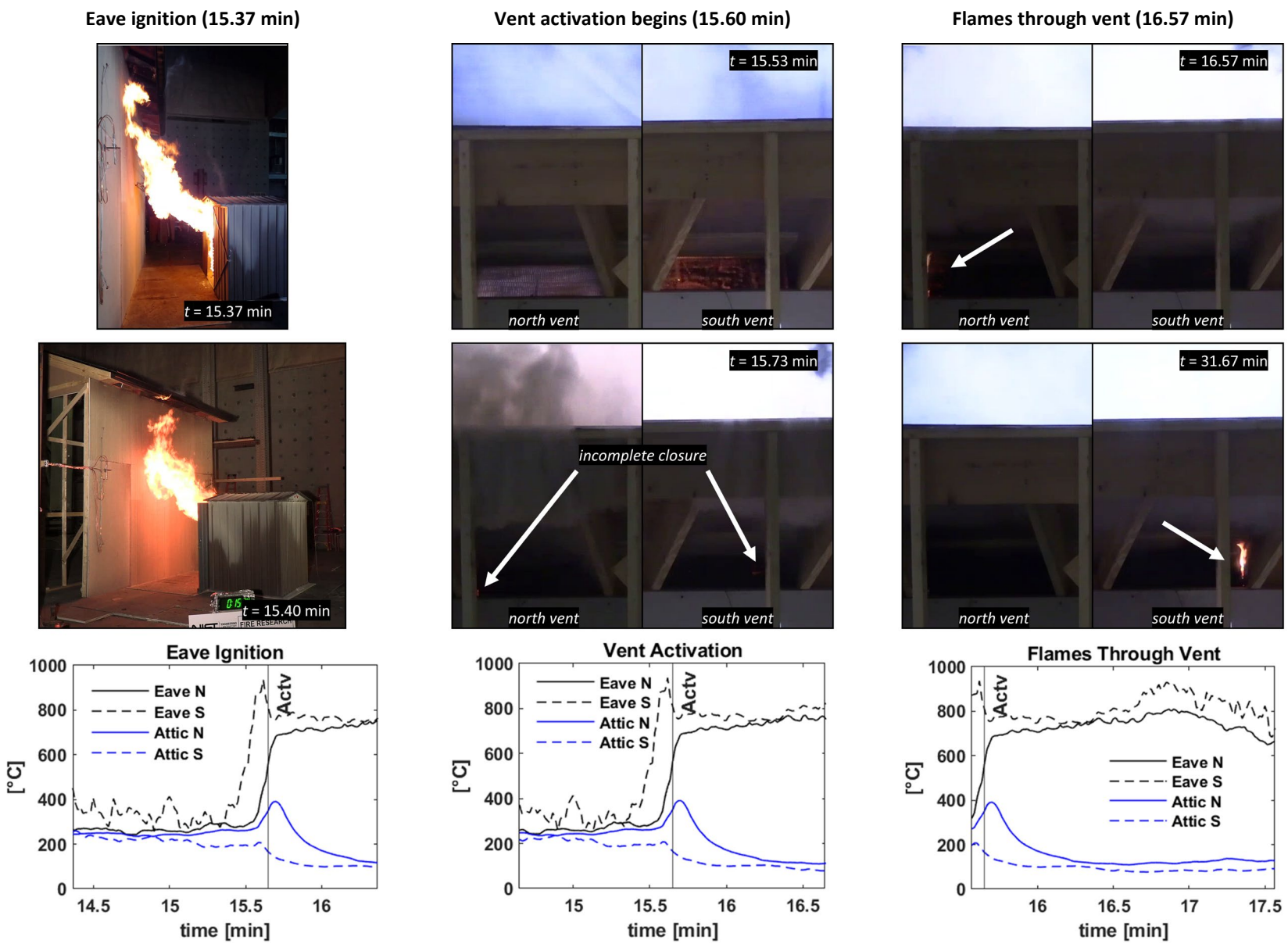
Eave ignition (15.37 min)
Vent activation begins (15.60 min)
Flames through vent (16.57 min)
t = 15.37 min
t = 15.53 min
t = 16.57 min
north vent
south vent
t = 15.40 min
t = 15.73 min
t = 31.67 min
incomplete closure
Eave Ignition
Vent Activation
Flames Through Vent
Eave N
Eave S
Attic N
Attic S
Actv
[°C]
time [min]

Appendix F. Flow Results

Various bi-directional velocity probes along the wall and behind the vent were utilized to assess the flow velocities and mass flow rates induced by the flames. The probes measure the total and static pressure at their upstream and downstream ports, respectively. The pressure differential between the two ports, ΔP, is measured utilizing a capacitance manometer (MKS 220CD Baratron). Data from the manometers was acquired using a networked data acquisition board (NI cDAQ-9188) containing inputs for voltage and temperature. The velocity is then calculated from the Bernoulli equation such that:

$$V = C_{bd}\sqrt{\frac{2\Delta P}{\rho}} \tag{F.1}$$

The air density, ρ, was calculated using the temperature, T, measured at the probe using a thermocouple (Omega Type K) and the ambient air static pressure, P_s:

$$\rho = \frac{P_s M}{RT} \tag{F.2}$$

where M is the molecular mass of air (28.96 g/mol) and R is the ideal gas constant (8.314 J/K*mol). C_{bd} represents the probe coefficient (0.9259).

F.1. Wall Flows

The peak flow velocities from experiments as measured by the center wall bi-directional velocity probe (WBD7, Instrumentation Schematic Fig. 7) for experiments 7 to 22 are shown in Fig. 55. The peak flow velocities are plotted against the respective experiment fuel mass.

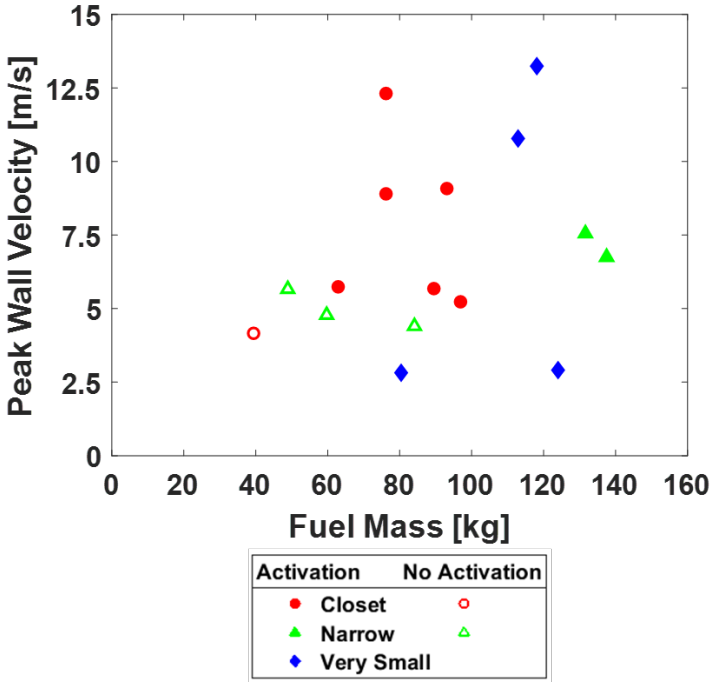

Fig. 55. Peak wall velocity for center wall bi-directional probe versus fuel mass.

Peak wall-center velocities ranged from approximately 2.5 m/s to 13 m/s. Although in general a higher fuel mass led to higher peak velocities, no real trend is observed. As the fuel inside the sheds burns, a jetting flame is formed through the opening which impinges on the wall, the induced air flow is then measured. The flame dynamics (which determine the induced flow velocities) such as the heat release rate (HRR), flame angle, and flame pulse frequency are strongly influenced by the fuel mass, the shed volume, and door opening area. Thus, it is important to note that the velocity probe measured the flow at a fixed location along the wall, but due to the factors outlined above, the flame angle changes are not accounted for. Interestingly, the four cases that did not see vent activation had very similar peak velocities, with an average of 4.75 m/s and only a 13 % relative standard deviation.

F.2. Vent Flows

An estimate of the mass flow through the vent was calculated using the following equation:

$$\dot{m} = \rho \bar{V} A \tag{F.3}$$

where ρ is the air density calculated using Eq. F.2, $\bar{V}$ is the average air flow velocity, and A is the vent area (0.1089 m^2). $\bar{V}$ was determined by averaging the measurement from the three velocity probes behind the vent. The peak mass flow from each experiment is shown in Fig. 56.

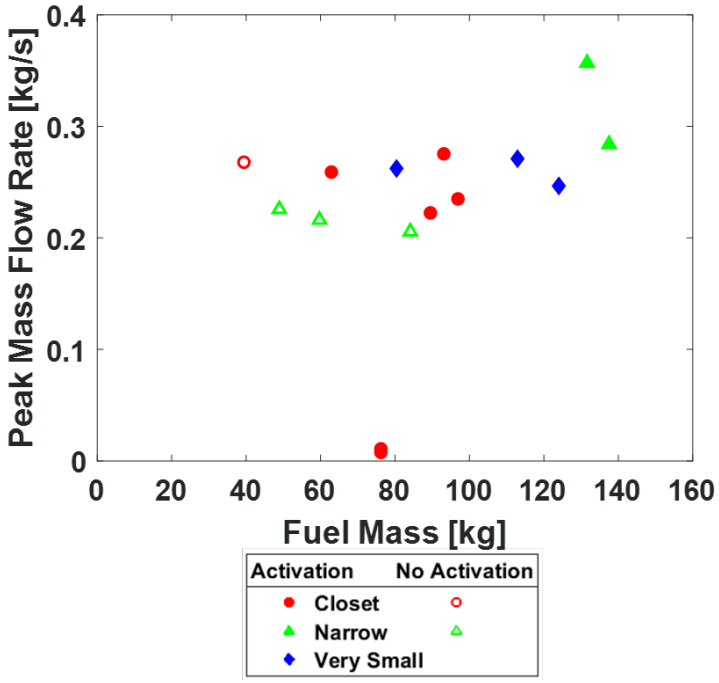

Fig. 56. Peak mass flow rate through the vent versus fuel mass.

The peak mass flow rates are very close together and invariant to the fuel mass. The two outliers with mass flow rates around 0.01 kg/s were from the experiments utilizing Vent B, which had interlocking louvers designed for air to be moved by a fan. The time traces of the vent air flow velocity measurements are contained in the Summary Sheets. With the outliers removed, the peak mass flow rate across the experiments was 0.26 kg/s.

The total air mass that flowed through the vent can be determined by integrating Eq. F.3 with respect to time from ignition (time = 0) to activation, these results are shown in Fig. 57. As a comparison, the total air mass for the non-activating cases is also shown, although the integration was performed up to the time of peak HRR. The average total air mass of the cases where the vent activated was 77.79 kg, and most of the activating cases lie within ± 20 % of the mean.

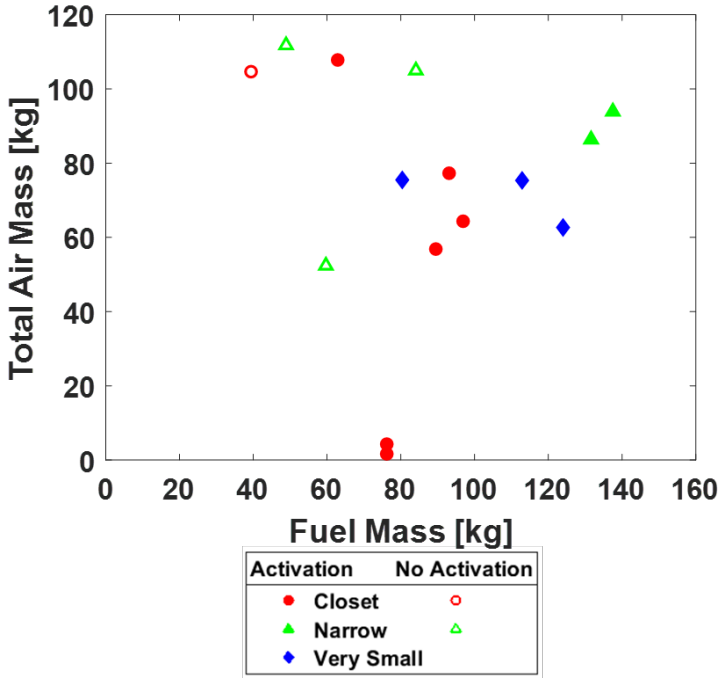

Fig. 57. Total air mass through the vent versus fuel mass.

Figure 56 and Fig. 57 show that neither the peak mass flow rate nor the total mass of air through the vent were strongly correlated with fuel mass (or shed type). This contrasts with the peak HRR_{shed} which was shown to be strongly correlated to the fuel mass (Fig. 27). In fact, when plotted against the peak wall velocities (Fig. 58), the peak mass flow rates (and total air mass) remain relatively steady across the entire spectrum of peak wall velocities.

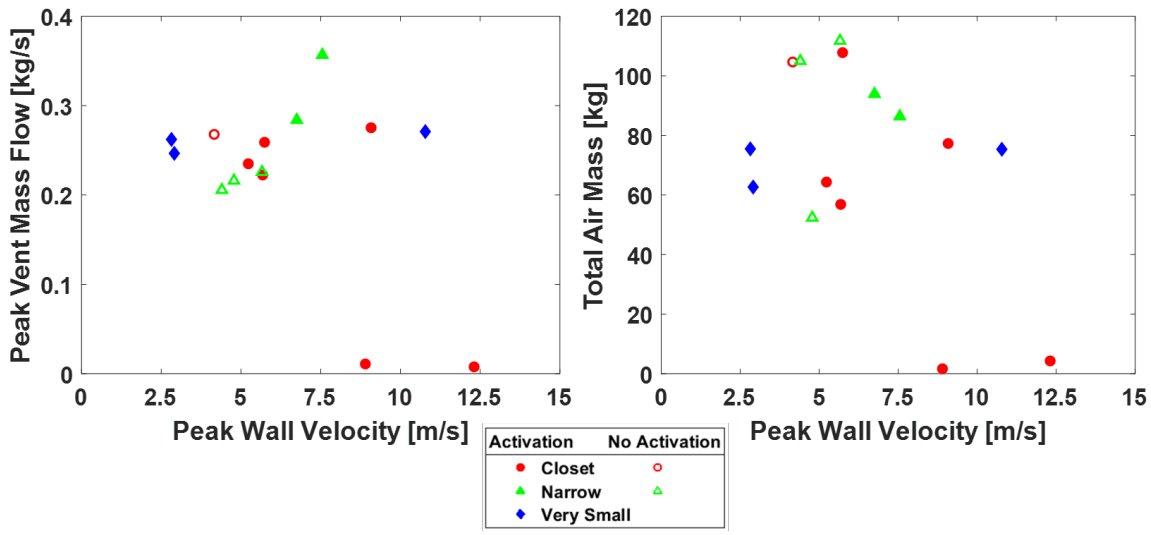

Fig. 58. Peak vent mass flow and total air mass versus peak wall velocity for all the sheds.

Increasing the fuel load, therefore, does not increase the flow through the vent but does increase the heat release rate. The vent is seemingly choked, i.e., reaching the maximum flow throughput. Increasing the fuel loading then increases the thermal exposure as hot gases build up in front of the vent because they cannot flow through the vent fast enough, and thus increase the risk of eave ignition. Of the experiments which had vent activation, only experiments 9 and 17 did not have the eaves ignite.

Appendix G. Repeatability Analysis

Fire behavior and exposure conditions are a function of both shed configuration (size and shape), door opening size, and fuel loading (mass and arrangement). Four exposure configurations were used in repeated experiments in the current series. Exposure sources demonstrated good qualitative repeatability among comparable configurations in terms of burning behavior and the thermal exposures measured at the target structure, as seen in Figs. 12 to 21. Peak heat release rate and time to ignition of the target structure were also repeatable among exposure groups.

A quantitative assessment of exposure repeatability was conducted for the growth period of the fire from ignition until peak heat release rate prior to ignition of the target structure. Experiments were grouped for each exposure condition and a mean exposure measurement was calculated at each time point for the timeseries data. The absolute error $|y_t - \hat{y}_t|$ and absolute percent error $|(y_t - \hat{y}_t)/y_t|$ were then calculated using the measured values y_t and mean values $\hat{y}_t$ at each time t. An overall metric was calculated using the mean of each of these values for each timeseries, yielding the mean absolute error (MAE) and mean absolute percent error (MAPE).

$$MAE = \frac{100}{n}\sum_{t=0}^{n}|y_t - \hat{y}_t| \tag{G.1}$$

$$MAPE = \frac{100}{n}\sum_{t=0}^{n}\left|\frac{y_t - \hat{y}_t}{y_t}\right| \tag{G.2}$$

In the case of MAPE, true values near zero result in infinite percent error. To avoid artificial inflation of the MAPE, the first 90 data points (90 s) were not included in the calculation. Data show that the mean absolute error within the first 90 s is 5 kW or less, small relative to the remainder of the time series. Overall, the MAE is not affected and was calculated including all data points.

Results of the repeatability analysis are tabulated in Table 12 regarding heat release rate and heat flux at the target. Overall, the maximum mean absolute percent error among all heat release rate timeseries was 12.6 %. Comparisons using heat flux resulted in larger MAPE values, ranging from 10.5 % to 48.5 %. This can be attributed to the larger variability and fluctuation in heat flux measurements. In absolute scale, the maximum MAE for heat flux was 1.4 kW/m^2.

Figure 59 shows an example of the workflow for the heat release measurements from three experiments using the closet shed loaded with four wood cribs (mean 93.2 kg) before ignition of the target structure. The full heat release rate measurements are shown in Fig. 12. Figure 59a shows the different experiment heat release rates with the group mean. Figure 59b shows the absolute error and Fig. 59c shows the absolute percent error. Note the extreme values of percent error before 1.5 min which correspond to relatively low absolute error. Figure 59d shows the calculated MAPE as a function of the delay in start time of the calculation. For instance, the vertical dashed line indicates 1.5 min. If the first 1.5 min of data are excluded from the MAPE calculation, the MAPE is 9.5 % for experiment e10. The graphs in Fig. 59c and 93d show why the first 1.5 min are excluded from the calculation.

Table 12. Repeatability metrics of heat release rate measurements for different exposure sources.

Exposure Source			Heat Release Rate		Heat Flux [a]	
Shed Type	Cribs (total mass)	Test ID	Max. MAE (kW)	Max. MAPE (%)	Max. MAE (kW/m^2)	Max. MAPE (%)
Closet	4 (76 kg, 76 kg)	e20, e21	15.5	4.16	1.0	29.9
Closet	4 (90 kg, 93 kg, 97 kg)	e7, e10, e11	47.0	9.48	1.4	24.4
Narrow	6 (137 kg, 131 kg)	e15, e16	58.5	11.4	0.45	17.6
Very Small	6 (124 kg, 113 kg)	e18, e19	62.6	13.6	0.33	48.5

[a] HF1, 2, 3, 2

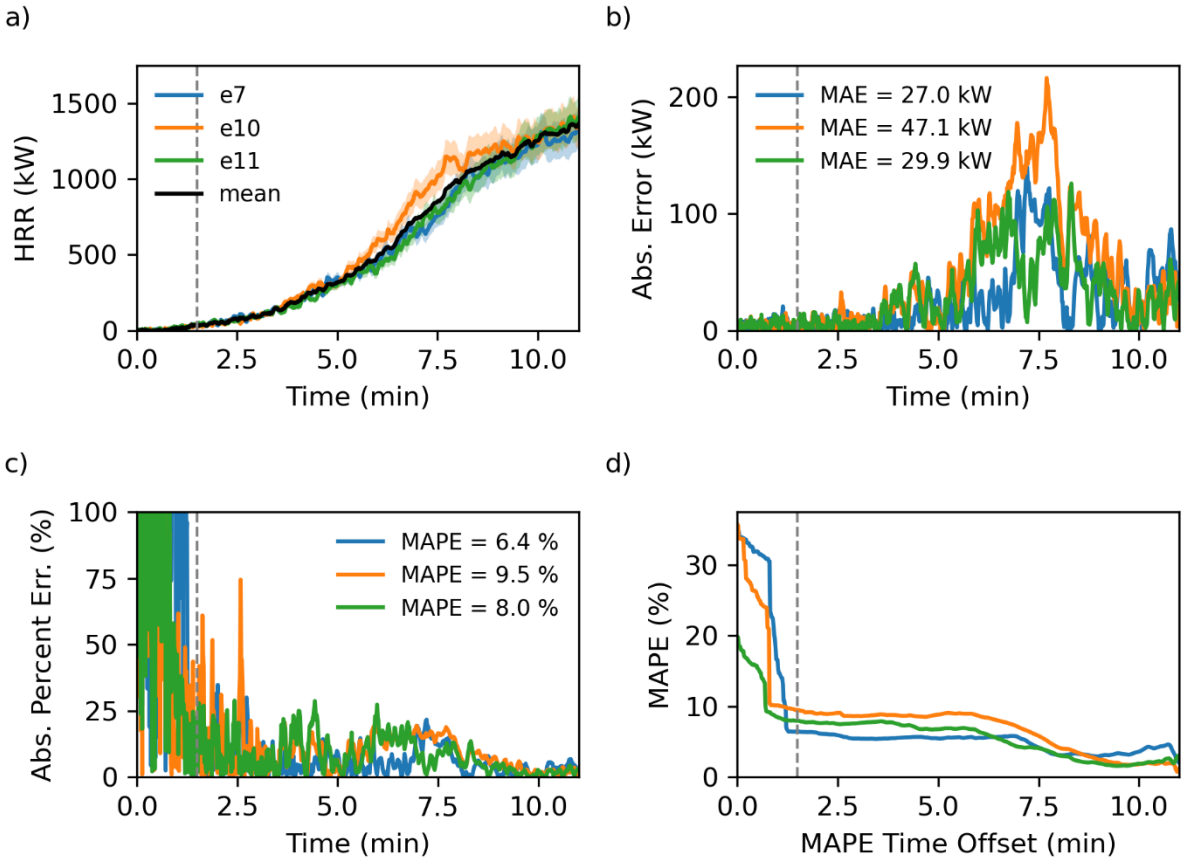

Fig. 59. Plots illustrating the repeatability of the HRR time series for e7, e10, and e11. a) HRR for each experiment and the mean value, b) the absolute error from each experiment to the mean, c) the absolute percent error from each experiment to the mean, d) the resulting MAPE for each experiment depending on the length of time excluded from the calculation. Legend values in b) and c) indicate the mean value for each experiment.